1996

Behavior of frames with partially restrained composite connections using the ATLSS connector

Kali E. Wyncott
Lehigh University

Wyncott,
Kali E.

Behavior of Frames with Partially Restrained Composite Connections...

January 14, 1995

Behavior of Frames with Partially Restrained Composite Connections Using the ATLSS Connector

by

Kali E. Wyncott

A Thesis

Presented to the Graduate Committee

of Lehigh University

in Candidacy for the Degree of

Master of Science

in

Civil Engineering

Lehigh University

January, 1996

Certificate of Approval

This thesis is accepted and approved in partial fulfillment of the requirements for the Master of Science Degree in Civil Engineering.

Dec. 7 '95
Date

Dr. Le-Wu Lu
Thesis Advisor and
Chairman of the Department
of Civil and Environmental
Engineering

Acknowledgments

This research project was conducted at the National Science Foundation sponsored Center for Advanced Technology for Large Structural Systems (ATLSS) in conjunction with the Department of Civil and Environmental Engineering at Lehigh University. Dr. John W. Fisher is director of ATLSS and Dr. Le-Wu Lu is chairman of the Department of Civil and Environmental Engineering.

First, I would like to thank the ATLSS Engineering Research Center and Dr. Le-Wu Lu for the opportunity to work on this research project. I also thank Dr. B. Vincent Viscomi and Dr. E. Sarah Slaughter for their proofreading help.

Special thanks go to graduate students John Abruzzo, Beth Dechant, Javier Escobedo, Mario Eraso Monzón, Perry Green, Kris Kanatharana, Abidin Kaya, Art Kney, George Krallis, Wayne Lawrence and Peter Lippert for their advice, support and time over the past two years.

I also would like to thank undergraduates Matt Aklan, Bill Bocchieri, Jason Cardone, John Daniels and Victor Stellakis for their help in the laboratory. Their hard work made my life much easier.

Further, I appreciate the technical support from the ATLSS and Fritz Lab staffs. Todd Anthony, Jack Bower, Peter Bryan, Bob Dales, John Fisher, Jack Gera, Ruth Grimes, Larry Heffner, Bud Hittinger, John Hoffner, Mark Kaczinski, Eric Kaufmann, Bruce Laub, Steve Leonard, Randy Lodzinski, Russ Longenbach, Betty MacAdam, Donna MacLean, Gene Matlock, Dawn McClay, Roger Moyer, Eleanor Nothelfer, Phyllis Pagel, John Pinter, Dave Schnalzer, Anna Silfies, Dick Sopko, Frank Stokes, Ed Tomlinson, Prisca Vidanage, Wayne

Wrona and Ben Yen made invaluable contributions to this project and to my academic growth.

The following organizations donated material to this project: Bethlehem Steel Corporation (Sparrows Point Division and Structural Shapes Division), Nicholas J. Bouras, Inc., TRW Nelson Stud, Inc. and United Steel Deck, Inc.

Finally, my parents deserve special recognition for their never-ending encouragement, advice and support.

Table of Contents

Title Page i
Certificate of Approval ii
Acknowledgments iii
Table of Contents v
List of Tables viii
List of Figures ix
Abstract 1

1. Introduction 3
   - 1.1 Introduction 3
   - 1.2 Purpose 3
   - 1.3 Objective 4
   - 1.4 Background 4
     - 1.4.1 Connections 5
     - 1.4.2 ATLSS Connector 6
     - 1.4.3 Construction Savings Using the ATLSS Connector 6
     - 1.4.4 Composite Construction 8
     - 1.4.5 Partially Restrained Connections 9
     - 1.4.6 Previous Research 10
     - 1.4.7 Exterior Partially Restrained Composite Connections 11
   - 1.5 Thesis Organization 12

2. Prototype Buildings: Design and Analysis 14
   - 2.1 Introduction 14
   - 2.2 Design Loads 14
     - 2.2.1 Gravity Loads 16
     - 2.2.2 Wind Loads 17
     - 2.2.3 Snow Loads 17
     - 2.2.4 Earthquake Loads 18
   - 2.3 Frame Analysis 18
     - 2.3.1 Rigid Frame 19
     - 2.3.2 Partially Restrained Composite Frame 19
     - 2.3.3 P-Delta Analysis 20
   - 2.4 Scale Model 21

3. Test Frame and Connections: Design and Predictions 23
   - 3.1 Introduction 23
   - 3.2 Exterior Connection Design 23
     - 3.2.1 Floor Beams 24

3.2.2 Columns 25
3.2.3 Composite Deck 26
3.2.4 ATLSS Connector 28
3.2.5 Seat Angle 29
3.3 Interior Connection Design 30
3.4 Analytical Models and Predictions 30
3.4.1 Exterior Connection 31
3.4.2 Interior Connection 32

4. Experimental Test: Setup, Instrumentation and Predictions 33
4.1 Introduction 33
4.2 Boundary Conditions 33
4.3 Test Fixture Design 34
4.3.1 Support Frame 34
4.3.2 Lateral Bracing System 35
4.3.3 Gravity Loading System 35
4.3.4 Lateral Loading System 36
4.4 Frame Designs 36
4.4.1 Monotonic Frame 37
4.4.2 Cyclic Frame 37
4.5 Comparison with University of Minnesota Test Specimens 37
4.6 Analytical Models and Predictions 38
4.6.1 Monotonic Frame 38
4.6.2 Cyclic Frame 40

5. Experimental Test: Construction, Procedures and Observations 42
5.1 Introduction 42
5.2 Construction Sequence 42
5.3 Material Properties 43
5.3.1 ATLSS Connectors 43
5.3.2 Seat Angles 44
5.3.3 Floor Beams 45
5.3.4 Columns 45
5.3.5 Composite Deck 45
5.4 Instrumentation 46
5.5 Data Acquisition System 48
5.6 Monotonic Test 48
5.6.1 Loading Procedure 48
5.6.2 Behavior 49
5.7 Gravity Load Tests 51
5.7.1 Loading Procedure 52
5.7.2 Behavior 52

5.8 Cyclic Test 53
5.8.1 Loading Procedure 54
5.8.2 Behavior 54

6. Experimental Test: Results and Comparison with Analytical Predictions 58
6.1 Introduction 58
6.2 Monotonic Test 58
6.2.1 Results 59
6.2.2 Comparison with Analytical Predictions 60
6.3 Gravity Load Tests 62
6.3.1 Results 62
6.3.2 Comparison with Analytical Predictions 64
6.4 Cyclic Test 65
6.4.1 Results 66
6.4.2 Comparison with Analytical Predictions 66
6.5 Comparison with University of Minnesota Test Results 67

7. Summary, Conclusions and Recommendations 69
7.1 Summary 69
7.2 Conclusions 69
7.3 Recommendations 70

Tables 71
Figures 83
List of References 155
Nomenclature 160
Vita 163

List of Tables

Table 1.1 Construction Savings Using the ATLSS Connector

Table 2.1 Prototype Building P-Delta Analysis Comparison
Table 2.2 Basic Scale Factors

Table 3.1 4000 PSI Concrete Mix Design

Table 4.1 Frame Scale Comparison With University of Minnesota Test Specimen
Table 4.2 Monotonic Test Predictions
Table 4.3 Cyclic Test Predictions

Table 5.1 ATLSS Connector Chemical Composition
Table 5.2 ATLSS Connector Weldability
Table 5.3 ATLSS Connector Material Properties
Table 5.4 ATLSS Connector Charpy V Notch Results
Table 5.5 Frame Material Properties
Table 5.6 Concrete Cylinder Strengths-Monotonic Frame
Table 5.7 Concrete Cylinder Strengths-Cyclic Frame
Table 5.8 Rebar Material Properties
Table 5.9 Instrumentation for Frame Tests
Table 5.10 Behavior Summary-Monotonic Test
Table 5.11 Behavior Summary-West Bay Gravity Load Test
Table 5.12 Behavior Summary-East Bay Gravity Load Test
Table 5.13 Lateral Loading Procedure-Cyclic Test
Table 5.14 Behavior Summary-Cyclic Test

Table 6.1 Monotonic Test Results

List of Figures

Figure 1.1 Connection Classification
Figure 1.2 ATLSS Connector Components (6/94/33-2)
Figure 1.3 ATLSS Connector (6/94/33-10)
Figure 1.4 ATLSS Connector Dimensions
Figure 1.5 Typical Partially Restrained Connections
Figure 1.6 Flexible Partially Restrained Composite Connection
Figure 1.7 Stiff Partially Restrained Composite Connection
Figure 1.8 Moment-Rotation Comparison
Figure 1.9 University of Minnesota Typical Connections
Figure 1.10 University of Minnesota Frame Test
Figure 1.11 Exterior Partially Restrained Composite Connection -Monotonic Frame
Figure 1.12 Exterior Partially Restrained Composite Connection -Cyclic Frame

Figure 2.1 Prototype Building Plan and Elevation
Figure 2.2 Prototype Building with Rigid Connections
Figure 2.3 Prototype Building with Partially Restrained Composite Connections

Figure 3.1 Overall View of Monotonic Frame
Figure 3.2 End View of Monotonic Frame
Figure 3.3 Photograph of Monotonic Frame (6/95/15-3)
Figure 3.4 Composite Deck
Figure 3.5 Concrete Deck Shoring (6/95/21-11)
Figure 3.6 General Reinforcement Layout
Figure 3.7 Detailed Reinforcement Layout
Figure 3.8 Exterior Connection Rebar Pattern (8/95/5-1)
Figure 3.9 Frame Prior to Concrete Pour (6/95/20-8)
Figure 3.10 Reinforcement Lap Splices
Figure 3.11 Placing Concrete Deck (6/95/26-10)
Figure 3.12 Leveling Concrete Deck (6/95/26-2)
Figure 3.13 Exterior PRCC Moment-Rotation Prediction-Monotonic Frame

Figure 4.1 Support Frame
Figure 4.2 Frame with Wooden Work Platform (6/95/19-12)
Figure 4.3 Lateral Bracing System (10/95/10-5A)
Figure 4.4 Gravity Loading System
Figure 4.5 East Bay with Gravity Load Simulator (6/95/15-1)

Figure 4.6 Actuator Wall Plate
Figure 4.7 Lateral Loading System (7/95/13-5)
Figure 4.8 Monotonic Frame Lateral Load-Lateral Displacement Prediction

Figure 5.1 East Bay Steel Frame (5/95/33-9)
Figure 5.2 Steel Frame (5/95/33-11)
Figure 5.3 Monotonic Frame Instrumentation-Plan
Figure 5.4 Monotonic Frame Instrumentation-Elevation
Figure 5.5 Cyclic Frame Instrumentation-Plan
Figure 5.6 Cyclic Frame Instrumentation-Elevation
Figure 5.7 Concrete Blockouts for Clip Gages (6/95/25-5A)
Figure 5.8 Clip Gages (7/95/6-4)
Figure 5.9 Exterior Connection (7/95/6-1)
Figure 5.10 Monotonic Frame Lateral Load-Lateral Displacement Curve
Figure 5.11 Seat Angle Separation at Exterior Connection 1 at East Peak (7/95/22-3A)
Figure 5.12 Concrete Crushing at Exterior Connection 1 (7/95/16-3)
Figure 5.13 Exterior Connection 1 at East Peak (7/95/22-14A)
Figure 5.14 Concrete Cracking at Interior Connection 1 at East Peak (7/95/22-13A)
Figure 5.15 Concrete Cracking at Exterior Connection 1 at West Peak (7/95/16-1)
Figure 5.16 Exterior Connection 1 at West Peak (7/95/14-2)
Figure 5.17 Exterior Connection 1 (7/95/14-3)
Figure 5.18 Rotation at Exterior Connection 1 (7/95/16-4)
Figure 5.19 Interior Connection 2 at West Peak (7/95/15-8)
Figure 5.20 Exterior Connection 2 at West Peak (7/95/22-11A)
Figure 5.21 West Bay Gravity Load Test Load-Deflection Curve
Figure 5.22 West Bay--Start of Plastic Hinge (7/95/22-21A)
Figure 5.23 West Bay--Plastic Hinge Formation (7/95/26-2)
Figure 5.24 During West Bay Test (7/95/26-12)
Figure 5.25 West Bay--Plastic Hinge (7/95/20-6)
Figure 5.26 West Bay--Plastic Hinge (7/95/20-8)
Figure 5.27 East Bay Gravity Load Test Load-Deflection Curve
Figure 5.28 East Bay Concrete Deck Crushing (7/95/28-11)
Figure 5.29 Interior Connections after Failure (7/95/28-5)
Figure 5.30 Interior Connection 2 (7/95/21-7)
Figure 5.31 ATLSS Connector Fracture (7/95/25-4)
Figure 5.32 Cyclic Frame Lateral Load-Lateral Displacement Curve
Figure 5.33 Overall Deformation of Frame after Cyclic Test (11/95/2-7A)

Figure 6.1 Monotonic Frame Lateral Load-Lateral Displacement Curve
Figure 6.2 Exterior Connection 1 Moment-Rotation Relationship
Figure 6.3 Exterior Connection 1 Moment/M_p-Rotation Relationship
Figure 6.4 Interior Connection 1 Moment-Rotation Relationship
Figure 6.5 Interior Connection 1 Moment/M_p-Rotation Relationship
Figure 6.6 Interior Connection 2 Moment-Rotation Relationship
Figure 6.7 Interior Connection 2 Moment/M_p-Rotation Relationship
Figure 6.8 Exterior Connection 2 Moment-Rotation Relationship
Figure 6.9 Exterior Connection 2 Moment/M_p-Rotation Relationship
Figure 6.10 Monotonic Frame Lateral Load-Lateral Displacement Prediction
Figure 6.11 Exterior Connection 1 Moment-Rotation Prediction
Figure 6.12 Interior Connection 1 Moment-Rotation Prediction
Figure 6.13 Interior Connection 2 Moment-Rotation Prediction
Figure 6.14 Exterior Connection 2 Moment-Rotation Prediction
Figure 6.15 West Bay Gravity Load Test Load-Deflection Curve
Figure 6.16 Exterior Connection 1 Moment-Rotation Relationship
Figure 6.17 Interior Connection 1 Moment-Rotation Relationship
Figure 6.18 East Bay Gravity Load Test Load-Deflection Curve
Figure 6.19 Interior Connection 2 Moment-Rotation Relationship
Figure 6.20 Exterior Connection 2 Moment-Rotation Relationship
Figure 6.21 West Bay Plastic Hinge Moment with Exterior Connection 1
Figure 6.22 West Bay Plastic Hinge Moment with Interior Connection 1
Figure 6.23 East Bay Plastic Hinge Moment with Interior Connection 2
Figure 6.24 East Bay Plastic Hinge Moment with Exterior Connection 2
Figure 6.25 Cyclic Test Lateral Load-Story Drift Curve
Figure 6.26 Comparison of Monotonic Test Curve with Cyclic Test Curve
Figure 6.27 Lateral Load History for Cyclic Test
Figure 6.28 Lateral Load History for University of Minnesota Test
Figure 6.29 Lateral Deflection History for Cyclic Test
Figure 6.30 Lateral Deflection History for University of Minnesota Test

Abstract

The 1993 *AISC LRFD Specification* classifies connections as either fully restrained (Type FR) or partially restrained (Type PR). Type PR connections may be used "upon evidence that the connections to be used are capable of furnishing, as a minimum, a predictable percentage of full end restraint." Therefore, partially restrained connections can be used in lateral load resisting frames.

Frames with PR connections are not used widely because analysis is difficult and PR connections tend to behave non-linearly in the service load region. However, previous research has shown that the behavior of partially restrained composite connections (PRCCs) is relatively easy to predict and that PRCCs behave linearly in the service load region. The objective of this thesis is to design, test and analyze a low-rise frame with partially restrained composite connections using a new type of steel beam-to-column connector known as the ATLSS Connector.

Research results are presented which show that frames with partially restrained composite connections can be used to resist lateral loads and that the frame behavior can be predicted relatively accurately from the behavior of the individual connections. Also, the same basic connection configuration may be used for exterior as well as interior partially restrained composite connections

with a few adjustments. Finally, the ATLSS Connector performs satisfactorily when used as a component in partially restrained composite connections.

Chapter 1

Introduction

1.1 Introduction

This chapter describes the purpose and objective of the thesis. It also provides a summary of related background material about connections, the ATLSS Connector, possible construction savings by using the ATLSS Connector, composite construction, partially restrained composite connections and previous research.

1.2 Purpose

The majority of new construction projects in the United States are low-rise buildings. A 1992 report from AISC Marketing, Inc. states that over 60% of the steel volume is used in one-story buildings, almost 90% in four-story or lower buildings and less than 2% in high-rise buildings over 20 stories (Griffis, 1994). Therefore, new connections and framing systems for low-rise buildings have a ready market. The purpose of this thesis is to address these needs by designing, testing and analyzing a low-rise frame with partially restrained composite connections using a new type of steel beam-to-column connector known as the ATLSS Connector (described in Section 1.4.2).

1.3 Objective

The objective of this research is to study the behavior of frames with partially restrained composite connections using the ATLSS Connector which are designed to resist gravity and lateral loads. The specific objectives are to:

1. Apply a previously designed interior partially restrained composite connection to a planar frame (Rosa, 1993).

2. Extend previous research results for interior partially restrained composite connections to exterior partially restrained composite connections.

3. Develop analytical tools for predicting the behavior of frames with partially restrained composite connections.

4. Provide experimental verification of the predicted frame behavior, assuming that the behavior of the individual connections is known.

5. Determine the behavior of the ATLSS Connector when used as a component in partially restrained composite connections.

To meet these objectives, two test frames were designed, tested and analyzed during this research project. The first frame was subjected to combined gravity and monotonic lateral loads whereas the second frame was subjected to combined gravity and cyclic lateral loads.

1.4 Background

The main purpose of the ATLSS Engineering Research Center is to conduct research which will increase the global competitiveness of the U.S. construction industry. Since structural connections often account for a relatively

large portion of both the time and the cost associated with the design, fabrication and erection of large structural systems, research that focuses on designing connections which are amenable to fabrication/construction automation and on designing composite beam connections with slab reinforcement are being explored (ATLSS, 1995).

Previous research in the areas of new connections and framing systems has focused on the behavior of interior beam-to-column composite connections for low-rise unbraced buildings in moderate seismic zones. Much of this work was conducted by testing cruciform-shaped subassemblages. A summary of previous research results is provided in Section 1.4.6. This project extends this type of research to planar frames.

1.4.1 Connections

The 1993 *AISC LRFD Specification* classifies connections as either fully restrained (Type FR) or partially restrained (Type PR). Restraint refers to the rotational resistance against relative angle change between intersecting members. Shear connections, although usually assumed to provide no end restraint, are included in the Type PR classification to recognize that some restraint is always present. Shear connections are defined as providing less than 20% restraint. Fully restrained connections must provide at least 90% restraint. All connections whose characteristics are between these two extremes

are partially restrained connections (Salmon and Johnson, 1990). Figure 1.1 defines these classifications graphically.

1.4.2 ATLSS Connector

The ATLSS Connector (AC) is a new steel beam-to-column shear connector that consists of two interlocking components known as the mortise and the tenon. The mortise is shop welded to the column flange and the tenon is field bolted to the beam web. Also, a seating bolt serves as a physical connection between the two elements. By preloading the connection, it also prevents rigid body motion between the mortise and the tenon during initial loading. The ATLSS Connector is shown in Figures 1.2 to 1.4.

The connector also serves as a construction aid as the tapered tenon slides into the wedge shaped mortise during beam erection--a concept known as keystone coupling. The AC is self-aligning and self-guiding which makes it an ideal candidate for automated and semi-automated erection techniques. Erection tolerances are met partially by the short slotted holes on the tenon. The connector then resists both positive and negative shear forces through wedging of the two elements, frictional forces and the seating bolt (Fleischman, 1995).

1.4.3 Construction Savings Using the ATLSS Connector

Two economic assessments of the ATLSS Connector have been performed. The first, a related research project at ATLSS, Project ADC-11 "Economic Assessment of an Integrated Building System," has developed a new

methodology to assess the impacts on construction productivity, cost, safety and utilization of resources when using new construction technologies (Eraso, 1995). The ATLSS Connector is one of the new construction technologies that has been evaluated.

The time, cost, safety and worker resources required to erect the prototype building described in Chapter 2 were evaluated using dynamic process simulation models (Slaughter and Eraso, 1995). As the baseline for comparison, the erection of the building was simulated with standard bolted connections. The simulation was repeated assuming that the building was erected and connected using ATLSS Connectors.

The time required to erect the prototype building decreased by 12% when using the ATLSS Connectors. This savings was due to the increased rate at which members could be erected and to a significant reduction in the number of bolts. The decrease in time spent erecting and bolting allowed the labor resources to be reassigned to other activities, thereby increasing overall project productivity. The decrease in erection time translated directly to an 11% cost savings. Worker safety improved by 28% as the number and duration of activities above ground were reduced. This fact is shown in Table 1.1 by the danger index that relates worker activities to worker safety risks. The number of workers used to erect the prototype building was not changed to use the ATLSS Connector to highlight the impacts of the connector on duration, cost and safety

given a specific set of resources. Idle time for the workers was minimized in all simulation runs. Table 1.1 summarizes these results.

The second economic assessment compared industry cost estimates for fabricating and erecting a prototype building with three different erection scenarios (Viscomi et. al., 1995). Case 1 was a standard composite frame using standard erection, Case 2 was a composite frame with ATLSS Connectors using standard erection and Case 3 was a composite frame with ATLSS Connectors using automated crane erection. A cost savings of 9% to 12% was projected by using the ATLSS Connector and a cost savings of 12% to 18% was estimated by using the ATLSS Connector with an automated crane system.

1.4.4 Composite Construction

As used in this thesis, a composite section is defined as a concrete slab supported on a steel beam with shear studs to provide shear transfer between the two elements. The use of composite floor systems has many advantages. First, the concrete slab increases the strength of the steel beam since it acts like a large cover plate on the top flange. As such, it raises the location of the neutral axis which allows a larger percentage of the steel beam to be in tension while most or all of the concrete slab is in compression. This can result in the use of smaller steel sections that may reduce floor heights. Next, composite sections have larger stiffnesses and thus smaller deflections than noncomposite sections and are better able to resist overload.

Composite construction is classified as either shored or unshored depending upon whether the formwork, wet concrete and other construction loads are supported by temporary shores or solely by the steel beams. Unshored construction is more common because it is cheaper, simpler and it does not affect the ultimate strength of the composite section. However, shored construction can result in smaller deflections, eliminate the need to check the strength of the bare steel beams and make it possible to use lighter steel sections. Typically, all loads applied after the concrete has reached 75% of its 28-day strength are assumed to be resisted by the composite section regardless of construction method (McCormac, 1995).

1.4.5 Partially Restrained Connections

Several typical partially restrained steel connections are shown in Figure 1.5 (Chen, 1993). Frames with PR connections are not used widely because analysis is difficult and PR connections tend to behave non-linearly in the service load region (Leon, 1992).

An interior partially restrained composite connection (PRCC) is shown in Figure 1.6 (Rosa, 1993). This type of connection provides positive moment resistance through a combination of the concrete slab bearing against the column flange, the slab reinforcing bars acting in compression and the ATLSS Connector acting in tension. Negative moment resistance is provided by the slab reinforcing bars in tension and the ATLSS Connector in compression against the

column flange. The design procedure used for this connection is discussed in more detail in Chapter 3.

The use of partially restrained composite connections in general provides many advantages. First, the connections tend to behave linearly in the service load region (Leon, 1992). Also, steel beam sizes may be reduced as moments are more evenly distributed over the entire length of the beam due to end restraint. Lateral bracing requirements are reduced as the concrete deck provides continuous lateral bracing to the top flange of the steel beam. Both connection details and construction are simplified as the need to connect the top flange of the beam to the column is eliminated. Further, the post-elastic energy dissipation required of a structure subjected to earthquake loads is achieved through excellent PRCC rotational capacities (ASCE, 1993).

1.4.6 Previous Research

Previous research at Lehigh University in this area has focused on the design and testing of partially restrained composite connections for interior beam-to-column joints. One such connection that has been developed for wide flange columns is shown in Figure 1.6 (Rosa, 1993). This connection is considered flexible as it can develop only 94% of the plastic moment strength of the bare beam in negative bending. Also, a stiff PRCC designed for use with either wide flange or tubular columns is shown in Figure 1.7 (Lawrence, 1994). It has been shown to develop 173% of the plastic moment strength of the bare

beam in negative bending. Figure 1.8 provides a comparison of the negative moment-rotation curves for the two connections.

Much of the research conducted at Lehigh University makes use of work which was done under the supervision of Dr. Roberto T. Leon at the University of Minnesota. Since many comparisons between work at the two universities will be made in this thesis, Figure 1.8 also illustrates the negative moment-rotation curves for Leon's connections that are shown in Figure 1.9 (Leon, 1992). Figure 1.10 provides a sketch of Leon and Ammerman's two-bay frame test from which the frame tests of this study were modeled (Ammerman, 1988). The Type 4 connection with rebar and web angles is comparable to Rosa's connection (Rosa, 1993). The Type 2 connection with rebar, web angles and a bottom plate is comparable to Lawrence's connection (Lawrence, 1994). The Type 1 connection with rebar, web angles and a seat angle is comparable to the new exterior connection that is developed in this thesis.

1.4.7 Exterior Partially Restrained Composite Connections

Two types of exterior partially restrained composite connections were designed and used in this study. Initially, it was believed that Rosa's connection, shown in Figure 1.6, was too flexible for use at exterior columns. Thus, the connection shown in Figure 1.11 was developed based on tests of similar connections at the University of Minnesota (Leon, 1992). However, the results from the monotonic test indicated that Rosa's connection could be used directly

without the seat angle. The cyclic frame contained the same connection, shown in Figure 1.12, for both the interior and the exterior connections.

1.5 Thesis Organization

This thesis is divided into seven chapters. Chapter 1 describes the purpose and objective of the thesis. It also provides a summary of related background material about connections, the ATLSS Connector, possible construction savings by using the ATLSS Connector, composite construction and previous research.

Chapter 2 describes the design and analysis of two full-scale prototype buildings. The process which was used to scale down the prototype frames for the test specimens also is discussed.

Chapter 3 discusses the connection design processes. Analytical models for the connection moment-rotation responses are presented as well as predictions for the connection behavior of the frame tests.

Chapter 4 explains the test frame and support frame designs. Also, an analytical model for the frame behavior is presented along with predictions for the frame experimental behavior. Comparisons to similar tests that were performed at the University of Minnesota are also provided.

Chapter 5 discusses the experimentation of the frames. Information about the test construction sequence, material properties, instrumentation, data acquisition system, loading procedures and general test behavior is given.

Chapter 6 summarizes the experimental results of the frame tests. Also, comparisons are provided between the analytical predictions and the experimental results. Further comparisons are given to similar test results that were obtained at the University of Minnesota.

Chapter 7 provides the summary, conclusions and recommendations from this research project.

Chapter 2

Prototype Buildings: Design and Analysis

2.1 Introduction

The purpose of this chapter is to describe the design and analysis of two full-scale prototype structures. Both structures are two bay by six bay four-story office buildings (Rosa, 1993). The unbraced buildings resist wind and earthquake loads through lateral load resisting frames. Plan and elevation views of the building frames are given in Figure 2.1. The story heights and bay dimensions used in these prototype buildings are identical to those used by Leon et. al. at the University of Minnesota (Forcier, 1990).

Both buildings were designed and analyzed in the transverse direction. The first building was designed using fully rigid beam-to-column connections with non-composite floor beams. The second building was designed with the type of partially restrained composite connections studied. Special provisions that were used to simulate the partially restrained composite connections are discussed in Section 2.3.2.

2.2 Design Loads

All design loads for the prototype buildings were taken from *ASCE 7-93: Minimum Design Loads for Buildings and Other Structures* (ASCE, 1993). The buildings were considered Category I in determining wind, snow and earthquake

loads. An importance factor, I, of 1.05 was used for wind load determination since the buildings were designed for eastern Pennsylvania which is within 100 miles of a hurricane oceanline. The buildings also were considered to have Exposure Category B which is for urban and suburban areas. The buildings were classified in Seismic Performance Category C.

The following nine load combinations were considered (AISC, 1993):

1. 1.0D + 1.0L + 1.0W
2. 1.4D
3. 1.2D + 1.6L + 0.5S
4. 1.2D + 1.6S + 0.5L
5. 1.2D + 1.6S + 0.8W
6. 1.2D + 1.3W + 0.5L + 0.5S
7. 1.2D + 1.0E + 0.5L + 0.2S
8. 0.9D - 1.3W
9. 1.2D + 1.0E

where D = dead load
E = earthquake load
L = live load
S = snow load
W = wind load

Several building design constraints were modeled. First, the design goal was to minimize the overall structure weight subject to the constraint that the same steel section (A36) be used for all six floor beams and the same steel section (A36) be used for the two roof beams. Also, columns (A572 Gr. 50) were considered to be at least two stories high to minimize connection splices and the exterior columns were to be the same on both sides of the building. Finally,

service level displacement constraints were set which corresponded to 0.25% interstory drift (0.39 inches).

2.2.1 Gravity Loads

The methods used to calculate dead loads, live loads and construction loads are discussed in this section.

2.2.1a Dead Loads

ASCE 7-93 defines dead loads as consisting of "...the weight of all permanent construction, including walls, floors, roofs, ceilings, stairways and fixed service equipment..." The weights of common materials and constructions as given in *ASCE 7-93* were used to determine the floor and roof dead loads for the prototype buildings. Uniformly distributed dead loads of 70 psf and 18 psf were calculated for the floor and roof beams, respectively. As input to the models, the floor dead load was 1.80 klf and the roof dead load was 0.46 klf.

2.2.1b Live Loads

Building live loads, as defined by *ASCE 7-93*, are "...those loads produced by the use and occupancy of the building...and do not include environmental loads such as wind load, snow load, rain load, earthquake load or dead load. Live loads on a roof are those produced (1) during maintenance by workers, equipment and materials and (2) during the life of the structure by movable objects such as planters and by people." The minimum specified uniformly distributed live load for office buildings of 50 psf was used. A special provision of

4 psf for movable office partitions was required since the specified live load was less then 80 psf. The final uniformly distributed floor live load was 1.39 klf.

2.2.1c Construction Loads

Construction loads for unshored construction include the weight of formwork, wet concrete, other construction materials and workers. Values for construction loads were required by Step 3 of the frame analysis procedure described in Section 2.3. A floor construction load of 2.52 klf and a roof construction load of 0.64 klf were calculated from Load Combination 2 from Section 2.2.

2.2.2 Wind Loads

Design wind loads were determined using the analytical procedure outlined in *ASCE 7-93* for main wind-force resisting systems. A basic wind speed of 80 mph for eastern Pennsylvania was used to determine wind forces at each story of the prototype buildings. Final wind loads were 5.24 kips at the first story, 5.92 kips at the second story, 6.53 kips at the third story and 3.54 kips at the fourth story.

2.2.3 Snow Loads

The ground snow load for eastern Pennsylvania was estimated as 35 psf. This value of ground snow load translated to a flat-roof snow load of 0.63 klf.

2.2.4 Earthquake Loads

Earthquake loads were calculated using the Equivalent Lateral Force Procedure described in *ASCE 7-93*. For eastern Pennsylvania, the effective peak acceleration, A_a, was 0.10 and the effective peak velocity-related acceleration, A_v, was 0.10. The structural framing system was considered an special moment frame; thus, the response modification factor, R, was 8 and the deflection amplification factor, C_d, was 5.5. Also, the prototype building configuration was classified as having no irregularities. Final distribution of earthquake loads resulted in 2.16 kips at the first story, 4.33 kips at the second story, 6.5 kips at the third story and 7.0 kips at the fourth story.

2.3 Frame Analysis

The following composite frame design process was used (Forcier, 1990):

1. Design the frame as rigid non-composite.
2. Keep the same column sizes.
3. Replace the steel girders by steel girders which are capable of resisting the factored construction loads without yielding (if necessary).
4. Detail the composite girder to carry all the factored dead and live loads.
5. Provide enough shear connectors for 100% composite action in the negative moment regions.
6. Replace the rigid connections by partially restrained composite connections.

A commercially available PC program, *Structural Optimization Design and Analysis (SODA)*, was used as an aid to design and analyze both buildings based upon the 1993 *AISC LRFD Specification*.

2.3.1 Rigid Frame

Using the design constraints from Section 2.2 and following the design recommendations from Section 2.3, the first frame was designed using fully rigid beam-to-column connections with non-composite floor beams. The building design was controlled by Load Combination 6 (1.2D + 1.3W + 0.5L + 0.5S) from Section 2.2. Member sizes based upon this analysis are shown in Figure 2.2.

2.3.2 Partially Restrained Composite Frame

As recommended by Forcier in Section 2.3, the same column sizes were used for the partially restrained composite frame as were determined from the design of the rigid frame. Additionally, since unshored construction was assumed for the building, the steel girders were designed to carry the factored construction loads discussed in Section 2.2.1c as simply supported beams without yielding. Fully composite girders were modeled in SODA by using a steel section with a flexural stiffness, EI, near that of the composite girder. As composite girders are not symmetric about the main axis, a weighted moment of inertia, I_B, was calculated. Since, under normal loading conditions, 60% of the beam is in positive bending and 40% of the beam is in negative bending, I_B was calculated as follows (Forcier, 1990):

$$I_B = 0.6I_{LBp} + 0.4I_{LBn} \qquad \text{(Eq. 2.1)}$$

where I_B = weighted moment of inertia
I_{LBp} = LRFD lower bound moment of inertia for positive bending
I_{LBn} = LRFD lower bound moment of inertia for negative bending

SODA did not have the capability to model partially restrained connections directly. Therefore, a special linear spring element was developed for this purpose (Lawrence, 1994). The element consisted of two parallel one inch long beam segments. The short length was chosen to minimize rotational influences from shear loads on the element. The first segment was chosen to provide a flexural stiffness, EI, consistent with the initial secant stiffness of the connections. The second segment had a flexural stiffness, EI, which was 10,000 times greater than the first to simulate a propped cantilever which prevented any transverse movement of the end of the element due to shear (Meyer, 1987). When used in parallel, these two segments adequately modeled the behavior of the PR connections. The building design again was controlled by Load Combination 6 (1.2D + 1.3W + 0.5L + 0.5S) from Section 2.2 due to service level displacement constraints. Member sizes based upon this analysis are shown in Figure 2.3.

2.3.3 P-Delta Analysis

A P-delta analysis of the partially restrained composite frame was important since frames with PR connections sway more than those with FR connections. However, use of the linear spring models prohibited a P-delta analysis using SODA. Therefore, the iterative P-delta method and the direct P-delta method, both approximate P-delta analysis procedures, were used.

The iterative P-delta method corrects first-order displacements by adding the P-delta shears to the applied story shears. Usually this type of analysis

converges after one or two cycles of iteration (Naeim, 1989). After two cycles of iteration, the displacement was 0.270 inches at the first story, 0.572 inches at the second story, 0.808 inches at the third story and 0.917 inches at the fourth story.

The direct P-delta method is a simplification of the iterative method. The story drift at each level is assumed to be proportional only to the applied story shear at that level (Naeim, 1989). This method resulted in displacements of 0.257 inches at the first story, 0.546 inches at the second story, 0.791 inches at the third story and 0.910 inches at the fourth story. These results are summarized in Table 2.1.

2.4 Scale Model

A scaled down model of the partially restrained composite frame from the column inflection points just below the first floor to those just above the first floor was necessary to accommodate laboratory floor space restrictions and to use existing laboratory floor bolt locations. A length scale factor, S_l, was necessary to determine the size-related properties of the scale model. A value of 0.58 was calculated for S_l by dividing the 25'-8" bay dimension of the prototype building by the comparable 15'-0" bay dimension of the scale model. Since the same construction materials were used in the prototype frame as in the scale model the elasticity scale factor, S_E, was one.

Table 2.2 lists some of the basic scale factors that were used to scale down the structural properties and the loads of the prototype frame. In general,

sections which had the closest property values to the values obtained after applying the scaling factors to the prototype building were chosen for the specimens. Section 4.5 provides further comparisons between the prototype frame and the lab specimen.

Chapter 3

Test Frame and Connections: Design and Predictions

3.1 Introduction

The frames and connections discussed in this chapter are scaled down from the partially restrained composite frame discussed in Chapter 2. They represent the prototype building from the column inflection points just below the first floor to those just above the first floor. This chapter describes the design processes for the partially restrained composite connections. In addition, the analytical models for the connection moment-rotation responses are presented as well as the predictions for the connection behaviors during the frame tests. Figures 3.1 to 3.3 show overall views of the frame setup.

3.2 Exterior Connection Design

Two types of exterior partially restrained composite connections were used in this study. Initially, it was believed that Rosa's connection, shown in Figure 1.6, was too flexible for use at exterior columns. Thus, the connection shown in Figures 1.11 and 1.12 was developed based on tests of similar connections at the University of Minnesota (Leon, 1992). However, the results from the monotonic test indicated that Rosa's connection could be used directly without the seat angle. The cyclic frame contained the same connection for both

the interior and the exterior columns. The design process for the initial exterior connection follows.

3.2.1 Floor Beams

Two 14'-0 3/4" long W12x19 (A36) steel sections were used as floor beams for each frame. The W12x19 section was chosen from scaled down properties of the partially restrained prototype building and was the same section used in Rosa's research (Rosa, 1993). The yield strength, F_y, of the beams was 51 ksi as determined by testing standard tensile coupons; therefore, the yield moment capacity, M_y, was 1,086 k-in and the plastic moment capacity, M_p, was 1,260 k-in.

Since unshored construction was used to erect the specimens, the steel girders were designed to carry the factored construction loads discussed in Section 2.2.1c as simply supported beams without yielding. In addition, gravity loads were applied directly to the bottom flange of the W12x19s as shown in Figure 3.2. To prevent local failure of the beams due to these concentrated loads, two 1/4" x 1 1/2" x 11 1/2" (A36) stiffeners were used at each gravity load attachment point.

Four 3/4" standard bolt holes were drilled at each end of the W12x19 beams to attach the tenon of the ATLSS Connector. The centerline of the bolt hole pattern for the exterior connection was 5" below the top flange of the beam for reasons to be discussed in Section 3.2.4. Calculations were made for gross

area yield, net area fracture and block shear rupture of the W12x19 at the bolt hole locations.

3.2.2 Columns

The strong column-weak beam philosophy was followed for the connection design. Two W8x35 (A572 Gr. 50) sections served as the exterior columns and one W8x48 (A588 Gr. 50) section served as the interior column. Again, these column sections were chosen from scaled down properties of the partially restrained prototype building and were consistent with the interior column which was used in Rosa's research (Rosa, 1993). All columns were 6'-7 1/2" long which, when combined with the lengths of the top and bottom pin supports, was 7'-7" or the distance between column inflection points.

Both column sections were checked for compactness, local and global bending strength to insure failure in the beams. The yield strength, F_y, of the W8x35 was 60 ksi as determined by testing standard tensile coupons; therefore, the yield moment capacity, M_y, was 1,872 k-in and the plastic moment capacity, M_p, was 2,082 k-in. Similarly, the yield strength, F_y, of the W8x48 was 61 ksi which was again determined by testing standard tensile coupons; therefore, the yield moment capacity, M_y, was 2,641 k-in and the plastic moment capacity, M_p, was 2,989 k-in.

3.2.3 Composite Deck

This section describes the design of the composite deck. Concrete deck size, concrete strength, concrete deck shoring, reinforcement layout and shear stud layout are discussed.

3.2.3a Concrete Deck Size

The effective width, b_E, of the concrete slab is the width within which all slab steel must be placed to be considered as acting to resist moments in the composite beam. From the 1993 *AISC LRFD Specification*, the effective width of the concrete slab for this project was determined to be 3'-9". The overall dimensions for the slab were 3" x 3'-9" x 33'-2". The steel deck ribs over the W12x19 beams were split longitudinally and separated to form a concrete haunch. This provided a larger concrete area to bear against the column flange for positive moment resistance (AISC, 1993). An elevation view of the composite deck is shown in Figure 3.4.

3.2.3b Concrete Strength

Normal weight concrete with a specified compressive strength, f'_c, of 4000 psi was used. The concrete mix design is provided in Table 3.1.

3.2.3c Concrete Deck Shoring

Unshored construction was assumed for the prototype building. However, some shoring was required for the test specimens to simulate the infill beams which would be present in the standard building frame. The concrete deck

shoring scheme is pictured in Figure 3.5. Eight 4" x 4" x 1/4" x 1'-8" (A36) angles were welded to each beam. Two foot long pieces of lumber then were attached to each of these angles to support the concrete formwork. Additional support was provided from the wooden work platform, the support columns and the laboratory floor to level the concrete formwork.

3.2.3d Reinforcement Layout

The reinforcement layout is shown in Figures 3.6 to 3.9. A sufficient amount of longitudinal reinforcement was provided to resist the maximum beam end moment from the prototype building and was consistent with the amount of reinforcement used in Rosa's research (Rosa, 1993). Provisions from *ACI 318-89* were used to check the distribution of flexural reinforcement for this one-way slab. The slab was designed as under-reinforced to ensure a ductile failure.

Since much of the connection performance depended upon attaining the full yield strength of the reinforcing bars at the column face, special attention was given to assuring proper anchorage of the bars. As shown in these figures, 180° #3 hoops were used around the exterior columns to insure that the bars were able to develop their full yield strength at the inner flange of the exterior columns.

The longitudinal bars were spliced with Class B lap splices as shown in Figure 3.10. All splices were at least 1'-3 1/2" long to meet the minimum tension lap splice length requirement to assure full load transfer. The splices were staggered a distance at least equal to the minimum clear spacing between the

bars. Also, the splices were lightly wired with reinforcement ties to avoid movement during concrete pours (ACI, 1989).

ACI 318-89 requires that shrinkage and temperature reinforcement be provided transverse to the main longitudinal reinforcement. Use of ACI calculations determined that a minimum of one #3 bar every 1'-3" along the length of the deck was required as shrinkage and temperature reinforcement. For ease of construction, one #3 bar was placed at each shear stud location.

Figures 3.11 and 3.12 are photographs taken during the concrete pour for the monotonic frame.

3.2.3e Shear Stud Layout

Shear stud design recommendations from the AISC seminar, "Innovative Practices in Structural Steel" were used both to size and to distribute the studs (AISC, 1994). Thirty-eight 3/8" x 2 1/2" headed shear studs were used on each beam as shown in Figures 3.4, 3.6 and 3.7. These studs were designed to provide 100% composite action between the W12x19 and the concrete deck. However, previous research has shown that, due to moment redistribution, 100% composite action is not required in the positive moment regions (Leon, 1995).

3.2.4 ATLSS Connector

All shear forces were assumed to be carried by the ATLSS Connector. The ATLSS Connector was positioned just above the composite neutral axis for the exterior connections. This placement was intended to aid the reinforcing

bars in resisting tensile forces due to negative moments since rebar anchorage had been a problem for past researchers due to the short length of the deck extension past the exterior columns (Ammerman, 1988). Another reason for placing the ATLSS Connector near the composite neutral axis was to limit the tensile forces along its net section.

Each ATLSS Connector required two 1/16" shim plates to fill in the gap between the 1/4" beam web and the 3/8" standard opening of the tenon plates. Each shim plate had four 3/4" standard bolt holes to match those of the beam web. The shim plates were not attached to either the AC or the beam web.

3.2.5 Seat Angle

A beam flange seat angle was used only on the exterior connections and was sized according to recommendations from the AISC seminar, "Innovative Practices in Structural Steel" (AISC, 1994). First, the required area of the top leg was determined by equating the yield stress and area of the rebar with the yield stress and unknown area of the seat angle. This required angle leg area was then increased by a 1.50 overstrength factor to insure full yielding of the longitudinal rebars before yielding of the seat angle. A 7" x 4" x 3/8" x 0'-8" (A36) seat angle was used at each exterior connection. Usual bolt hole gage distances were used for the six 3/4" diameter A-325 bolts as recommended by AISC (AISC, 1993). All bolts were designed as slip-critical and were used with oversized holes to minimize erection problems.

3.3 Interior Connection Design

A sketch of the interior partially restrained composite connection is shown in Figure 1.6 (Rosa, 1993). This PRCC was used for the two interior connections of the monotonic frame. It was then used for all four connections of the cyclic frame.

This connection was designed, tested and analyzed previously at Lehigh University using cruciform specimens (Rosa, 1993). Three modifications were made to the basic connection design for use in the frame tests of this research project. First, the single row of 1/2" x 2 1/2" headed shear studs was changed to a double row of 3/8" x 2 1/2" headed shear studs to improve the shear stud ductility. In addition, the clear cover of the longitudinal reinforcing bars was increased from 1/2" to 3/4" to permit the longitudinal reinforcing bars to be located below the top of the shear studs. This change was intended to enhance the strength of the concrete failure cone around the headed shear studs. Finally, the concrete haunch which was described in Section 3.2.3a was not present in the original design of the interior connection (Rosa, 1993).

3.4 Analytical Models and Predictions

This section provides detailed information about the analytical models which were used to predict the connection moment-rotation behavior for both the exterior and the interior connections. A conservative bilinear approximation for the negative moment-rotation response of each connection is included. The first

linear segment represents the elastic response of the connection to 4 mrad. The second linear segment represents the inelastic response from 4 mrad to 20 mrad. The connections were assumed to maintain a constant moment for all rotations greater than 20 mrad (Leon and Ammerman, 1990a).

3.4.1 Exterior Connection

The equation which was used to model the negative moment-rotation behavior of the exterior connections described in Section 3.2 was developed by J. Lin at the University of Minnesota (Lin, 1986 and Leon and Ammerman, 1990a). It is defined as follows:

$$M = C_1 (1 - e^{- C_2\theta}) + C_3\theta \qquad \text{(Eq. 3.1)}$$

$$C_1 = A_r F_{yr} (d + Y_3) \qquad \text{(Eq. 3.2)}$$

$$C_2 = 32.9 (A_1/A_r)^{0.15} (d + Y_3) \qquad \text{(Eq. 3.3)}$$

$$C_3 = 24 F_y A_1 (d + Y_3) \qquad \text{(Eq. 3.4)}$$

where M = moment (k-in)
θ = rotation (radians)
A_r = area of reinforcing bars (in^2)
F_{yr} = yield stress of reinforcing bars (ksi)
A_1 = area of seat angle (in^2)
F_y = yield stress of seat angle (ksi)
d = depth of steel beam (in)
Y_3 = distance from top of steel beam to centroid of rebar (in)

Based on the design values for these variables which were developed in Section 3.2, Equation 3.1 then becomes:

$$M = 648 (1 - e^{-585\theta}) + 42100\,\theta \qquad \text{(Eq. 3.1)}$$

where moment is measured in kip-inches and rotation is measured in radians. This negative moment-rotation relationship is presented in Figure 3.13. The initial secant stiffness of the exterior connection, K_i, was 170 k-in/mrad. The inelastic stiffness of the connection was 46 k-in/mrad.

3.4.2 Interior Connection

The predicted moment-rotation relationship in negative bending for the interior connections was taken directly from past experimental research of this connection. This relationship is labeled "Rosa" in Figure 1.8 (Rosa, 1993). The initial secant stiffness of the interior connection, K_i, was 117 k-in/mrad. The inelastic stiffness of the connection was 27 k-in/mrad.

Chapter 4

Experimental Test:

Setup, Instrumentation and Predictions

4.1 Introduction

Laboratory testing of structures which are permitted to sway requires the use of special loading and lateral bracing systems which do not inhibit the sidesway movement of the test specimens. This chapter describes the design of the planar frames and the test fixtures which were used for the laboratory tests. Also, an analytical model for the frame behavior is presented along with predictions for the frame experimental behavior. Comparisons to similar tests that were performed at the University of Minnesota are also given.

4.2 Boundary Conditions

In order to model correctly the prototype building behavior, several boundary conditions were introduced for the laboratory test specimens. First, the top and bottom of each test column were designed to simulate the behavior at inflection points of the prototype building; thus, to assure zero moment at these locations, a pinned bearing was used to support the bottom of each column and a pinned connection was created between the top of each column and the lateral load tube. A lateral bracing system was used to simulate the support from parallel frames in the prototype building and this is addressed in Section 4.3.2.

Also, as discussed further in Section 4.3.3, pinned connections were provided between the bottom flanges of the test specimens and the gravity loading system to prevent the introduction of axial loads into the beams.

4.3 Test Fixture Design

The test fixtures which were used in this project consisted of a support frame, a lateral bracing system, a gravity loading system and a lateral loading system. Each of these components is described below.

4.3.1 Support Frame

The support frame fixtures, shown in Figures 3.2, 4.1 and 4.2, consisted of the following items:

1. 2 - PL 2" x 6'-6" x 8'-0" (A36)
2. 1 - PL 2" x 8'-0" x 10'-6" (A36)
3. 6 - W12x190 columns
4. Wooden work platform
5. 3 - L 4" x 4" x 1/4" x 7'-0" (A36)
6. 6 - Stub columns
7. Miscellaneous lateral bracing angles

Items 1 and 2 were bolted to the concrete laboratory floor via existing tie down points to provide a means to anchor the stub columns and the gravity-load simulators. The stub columns were welded to and the gravity-load simulators were bolted to these plates.

The W12x190 columns were bolted to the lab floor through the floor plates. They acted to support the wooden work platform along the south side of

the specimen, to shore the wet concrete deck and to support the lateral bracing fixtures.

4.3.2 Lateral Bracing System

Lateral bracing was required to prevent out-of-plane movement of the test specimens. Each column top was braced laterally by angles which were bolted to the support frame as pictured in Figures 3.2 and 4.3. These guides also served to maintain the alignment of the lateral load tube. Grease was applied to the contact surfaces between the lateral bracing and the lateral load tube to minimize frictional forces.

Similarly, the top flange of each beam was braced continuously by the composite deck (AISC, 1993). No other lateral bracing was used for either test specimen.

4.3.3 Gravity Loading System

Previously designed loading devices known as gravity-load simulators were used to apply gravity loads to the floor beams (Yarimci, Yura and Lu, 1966). These simulators were used to maintain the vertical alignment of load even as the test frames swayed; thus, the introduction of restraining horizontal load components was eliminated. Two gravity-load simulators were used for each frame test.

Each gravity-load simulator was used in conjunction with an 80 kip capacity hydraulic actuator, a spreader beam and two load cells as shown in

Figures 4.4 and 4.5. The connections between each of these components and with the floor beams was pinned to maintain the vertical alignment of load. The horizontal displacement capacity of the system was ± 16" (Yarimci, Yura and Lu, 1966).

4.3.4 Lateral Loading System

The lateral loading system was designed to apply the same displacement increment to each of the three column tops. This was accomplished using a hydraulic actuator mounted on the laboratory reaction wall and a rigid horizontal loading tube. General views of the lateral loading system are shown in Figures 3.1 and 3.2.

The hydraulic actuator was attached to the laboratory reaction wall as shown in Figure 4.6. Its zero load position was located at the center of its ± 12" displacement capacity to assure enough stroke in both the positive and negative drift directions. The 50 kip capacity load cell limited the load range of the ± 120 kip jack. The lateral load tube was pinned to the tops of the columns as shown in Figure 4.7. This photo also shows the pinned connection between the actuator and the lateral load tube.

4.4 Frame Designs

This section describes the design processes which were used for the monotonic and the cyclic frames. Both frames were designed to represent the

first floor (between column inflection points) of the partially restrained composite frame which was described in Section 2.3.2.

4.4.1 Monotonic Frame

The monotonic frame was designed to represent a scaled down version of the partially restrained composite frame which was described in Chapter 2. As such, it also was designed to resist the scaled down loads from the prototype structure. The member sizes for the beams and the interior column were the same as those used by Rosa to facilitate comparisons between the behavior of the interior connections in cruciform-shaped tests and in the planar frame tests (Rosa, 1993). The frame was designed to reach its service wind load of 7.25 kips before reaching its service level story drift of 0.223 inches.

4.4.2 Cyclic Frame

The same design process was used for the cyclic frame as for the monotonic frame.

4.5 Comparison with University of Minnesota Test Specimens

As mentioned in Chapter 2, the test specimens described in this thesis are scaled down by approximately 58% from a similar specimen tested at the University of Minnesota. Thus, an attempt was made to use standard scaling factors to convert the sizes of the beams and the columns. Special attention was paid to accurate conversions of section dimensions, moments of inertia, weights, etc. However, the member sizes for the beams and the interior column

were the same as those used by Rosa to facilitate comparisons between the behavior of the interior connections in cruciform-shaped tests and in the planar frame tests (Rosa, 1993). Table 4.1 summarizes the member size changes which were made between the two sets of tests.

In addition to these member size changes, several other noteworthy differences existed between the Lehigh University test frames and the University of Minnesota test frame. First, traditional shear connections were used at the University of Minnesota whereas the ATLSS Connector was used at Lehigh University. Also, the same connection was used at both the interior and the exterior columns at the University of Minnesota. However, this was true only for the cyclic frame at Lehigh University since two separate connections were used at the interior and the exterior columns for the monotonic frame. Next, the formed metal deck was perpendicular to the floor beams at the University of Minnesota while it was parallel at Lehigh University.

4.6 Analytical Models and Predictions

This section provides detailed information about the analytical models which were used to predict the load-displacement behavior of the test frames under both monotonic and cyclic lateral loads.

4.6.1 Monotonic Frame

The overall load-displacement behavior of the monotonic frame was predicted based on the anticipated moment-rotation response for each of the

four connections. Actual test data was used to determine both the negative and the positive bending responses for the interior connections (Rosa, 1993). Similarly, analytical predictions were used for the exterior connections. These responses were summarized in Section 3.4.

The model accounted for the initial rotations of the individual connections due to gravity loads. This is not readily evident from Figure 4.8 since this figure only relates lateral load and lateral displacement. Also, the model assumed that a given displacement, applied at one end of the rigid lateral load tube, would be transferred equally to the top of each of the three columns. Further, this displacement would cause rotation at each connections relative to its stiffness. Thus for a given rotation the moment at each connection was determined from the appropriate moment-rotation model. Then the moment at each connection was converted to a column top lateral load. This process was repeated in 0.1 inch displacement increments from 0 inches to 2.73 inches. Figure 4.8 illustrates the predicted load-displacement response of the monotonic frame. The predicted lateral displacement for the service wind load of 7.25 kips is 0.15 inches whereas a predicted lateral displacement of 2.73 inches corresponds to the ultimate frame lateral load of 41.5 kips. These results are summarized in Table 4.2.

The slope of the lateral load-lateral displacement curve changes several times as each of the connections reaches its service rotation of 4 mrad and thus

changes from its elastic stiffness to its inelastic stiffness. These changes in slope correspond to each of the connections reaching its 4 mrad service rotation. Exterior Connection 1, in positive bending due to the applied lateral load, was the first to reach 4 mrad at a lateral displacement of 0.16 inches with a corresponding lateral load of 12 kips. Next, Exterior Connection 2, in negative bending due to the applied lateral load, arrived at 4 mrad at 0.56 inches and 15.5 kips. Third, Interior Connection 2, in positive bending from the applied lateral load, reached 4 mrad at a lateral displacement of 0.71 inches and a lateral load of 19 kips. Finally, Interior Connection 1, initially in negative bending, reached its service rotation at 1.36 inches with 24 kips. The final constant load portion of the plot which begins at 2.36 inches and 41.5 kips, signifies that all four connections have reached their ultimate rotation of 20 mrad and are no longer able to carry additional load.

4.6.2 Cyclic Frame

The analytical model described in Section 4.6.1 for the monotonic frame was modified to predict the behavior of the cyclic frame at the excursion peaks. The moment-rotation models for the exterior connections were updated since the exterior connections were changed from those which were used in the monotonic frame. Note that this model does not account for strength degradation due to damage from previous loading cycles.

Loading for the cyclic frame test was controlled by percent story drift. The allowable story drift for this frame was 0.5% (UBC, 1991). The cycles at 0.25%, 0.5% and 0.75% story drift were considered to be the elastic cycles of loading. Table 4.3 provides a summary of the load-displacement predictions for the cyclic frame at certain cycles.

Chapter 5

Experimental Test:

Construction, Procedures and Observations

5.1 Introduction

This chapter describes the experimentation for the monotonic and cyclic test frames. Information about the test construction sequence, material properties, instrumentation, data acquisition system, loading procedures and general test behavior is given.

5.2 Construction Sequence

Both frames, shown in Figures 5.1 and 5.2, were fabricated and erected using this construction sequence:

1. Shop welded mortises to column flanges and drilled bolt holes for seat angle (if required).
2. Erected columns.
3. Field bolted seat angles to column flanges with loose bolts (if required).
4. Installed tenons on beam webs with loose bolts.
5. Lowered beams into place.
6. Installed ATLSS Connector seating bolts and torqued to minimum specified pretension.
7. Torqued ATLSS Connector tenon bolts to minimum specified pretension.
8. Installed metal deck, shear studs, reinforcing bars and concrete formwork.
9. Poured concrete deck.
10. Re-torqued seating bolts at least one day after the concrete set.
11. Installed and torqued to minimum specified pretension seat angle-beam flange bolts (if required).

12. Torqued seat angle-column bolts to minimum specified pretension (if required).

All bolt holes for the seat angles of the monotonic frame were oversized to minimize erection problems. In addition, the ATLSS Connectors contained short-slotted holes to minimize erection problems and to aid the self-aligning, self-guiding features of the connector. To take advantage of the short-slotted holes, the ATLSS Connector was attached to the beam web with loose bolts. These tenon bolts were tightened after the beams were erected. At this point, the connections were considered to be simply supported.

The ATLSS Connector seating bolts were pretensioned before the concrete deck was poured to eliminate any rigid body motion between the mortises and the tenons due to the additional weight of the concrete. The seating bolts were re-torqued at least one day after the concrete deck set. Lastly, all seat angle bolts were tightened. At this point the connections were considered to be partially restrained composite connections.

5.3 Material Properties

This section details the material properties of the frame tests.

5.3.1 ATLSS Connectors

Two batches of ATLSS Connectors were used for the frame tests. Batch C-12 was used for the monotonic frame and batch C-10 was used for the cyclic frame. The weldability of each group was evaluated using the following formulas to calculate carbon equivalence, C_{eq}:

$$C + Mn/6 \qquad \text{(Eq. 5.1)}$$

$$C + (Mn + Si)/6 + (Cr + Mo + V)/5 + (Ni + Cu)/15 \qquad \text{(Eq. 5.2)}$$

$$C + Mn/6 + Ni/20 + (Cr + Mo)/10 + Cu/40 \qquad \text{(Eq. 5.3)}$$

Carbon equivalence is used to measure the effect of various elements on weld cracking by the formation of hardness zones. The tendency for crack growth increases with larger values of C_{eq}, thus a maximum acceptable value for C_{eq} is often 0.40. The chemical composition for each batch of connectors is provided in Table 5.1 (Kaufmann, 1994). Preheat requirements were calculated using the *AWS Structural Welding Code* (AWS,1994). Weldability and preheat requirements for each batch of connectors are shown in Table 5.2. Material properties for each batch of ATLSS Connectors is given in Table 5.3 and Charpy V Notch test results are presented in Table 5.4 (Kaufmann, 1994). This information is provided for completeness and is not related directly to this research project.

5.3.2 Seat Angles

The 7" x 4" x 3/8" (A36) seat angles had a yield strength, F_y, of 41.3 ksi and a tensile strength, F_u, of 61.7 ksi as reported on the manufacturer mill report. This information is summarized in Table 5.5.

5.3.3 Floor Beams

The W12x19 (A36) floor beams had a yield strength, F_y, of 51 ksi and a tensile strength, F_u, of 72.5 ksi as determined by testing standard tensile coupons. This information is summarized in Table 5.5.

5.3.4 Columns

The W8x35 (A572 Gr. 50) exterior columns had a flange yield strength, F_{yf}, of 56 ksi, a web yield strength, F_{yw}, of 64.3 ksi and a tensile strength, F_u, of 80.8 ksi as determined by testing standard tensile coupons. This information is summarized in Table 5.5.

5.3.5 Composite Deck

Material properties for the shear studs, concrete and reinforcing bars of the composite deck are discussed in this section.

5.3.5a Shear Studs

The yield strength, F_y, of the 3/8" x 2 1/2" headed shear studs was 50.1 ksi and the tensile strength, F_u, was 60.1 ksi (TRW, 1977). This information is shown in Table 5.5.

5.3.5b Concrete

Standard 6 inch by 12 inch concrete cylinders were cast for each test frame. All cylinders were field cured near the test frames. A total of 9 standard concrete cylinder compression tests were performed for each frame; three each at seven, fourteen and twenty-eight days after casting the deck. The average

28-day concrete compressive strength, f'_c, for the monotonic frame was 4367 psi. A comparable result for the cyclic frame was f'_c of 5275 psi. All cylinder strength test results are summarized in Tables 5.6 and 5.7.

5.3.5c Reinforcing Bars

This information is summarized in Table 5.8.

5.4 Instrumentation

The six types of transducers used in each test were: clip gages, linear voltage displacement transducers (LVDTs), load cells, strain gages, tiltmeters and trim pots. Figures 5.3 and 5.4 show the instrumentation layout for the monotonic frame test. Similarly, Figures 5.5 and 5.6 show the instrumentation layout for the cyclic frame test. Table 5.9 provides a summary of the transducers for the frame tests.

A total of 12 clip gages were used for each test to monitor the post-yielding stress-strain behavior of some of the reinforcing bars after the strain gages became ineffective. Styrofoam blocks were placed around the reinforcing bars at the desired clip gage locations prior to pouring the concrete deck as shown in Figure 5.7. These Styrofoam blocks then were removed after the concrete hardened to expose the reinforcing bars for mounting the clip gages. Figures 5.8 and 5.9 show the clip gages in-situ.

LVDTs were used for two purposes. First, a pair of LVDTs was utilized at two of the connections to measure the relative rotation between the beam and

the column. These results were used to check the rotation measurements which were obtained with the tiltmeters. Also, although no slip was expected between the pinned supports and the stub columns, an LVDT was used to monitor any such movement at the base of each of the three columns.

Five load cells were used for each test. One load cell monitored the lateral load. Each gravity load simulator contained a load cell between the spreader beam and each of the two beam attachment points.

Strain gages were used in many locations. First, pairs of strain gages were mounted on the columns above and below each connection. Similarly, pairs of strain gages were attached at several locations along each beam. Thus, it was possible to determine the moment at each connection. Also, strain gages were positioned on each reinforcing bar near the column flanges to monitor the stress-strain behavior of the bars. The ATLSS Connectors were instrumented with a pair of strain gages to measure the moment which each AC carried. Finally, the lateral load tube was gaged to monitor the load distribution among the three columns.

Tiltmeters were used to measure the beam and column rotations at each connection. Measurements from the individual tiltmeters were compared to obtain the relative rotation between the beam and column at each connection.

Trim pots were used to measure displacements at five locations. First, they were used to monitor the midspan deflection of the two beams. Also, they were used to measure the lateral displacement of each of the three column tops.

5.5 Data Acquisition System

The MegaDAC Data Acquisition System was used to record 127 channels of data for the monotonic test and 110 channels of data for the cyclic test.

5.6 Monotonic Test

The objectives of testing the monotonic frame were to:

1. Evaluate the lateral load-lateral displacement behavior of the frame.

2. Assess the moment-rotation response of both the exterior and the interior partially restrained composite connections due to combined gravity and lateral loads.

3. Determine the behavior of the ATLSS Connector when used as a component in partially restrained composite connections.

Section 5.6.1 describes the loading procedure which was used for the monotonic frame. Then Section 5.6.2 details the experimental behavior of the monotonic frame.

5.6.1 Loading Procedure

Load application for the monotonic frame test occurred in three phases. Initially, gravity loads were applied to both floor beams simultaneously in the zero drift position. Load was applied in one kip increments until each beam carried 28 kips. The gravity load levels were monitored during the application of the lateral

load and were adjusted as needed to maintain the 28 kip load. At this point, lateral load was applied in 0.015 inch displacement increments to a maximum eastward displacement of 2.73 inches. The loading direction then was reversed and load was applied at 0.1 inch displacement increments to a maximum westward displacement of 2.73 inches. Again the loading direction was reversed and the test was continued to the zero load position. Finally, the gravity loads were released and the test ended. A plot of lateral load versus lateral displacement is shown in Figure 5.10 with key loading parameters noted.

5.6.2 Behavior

The final moment and the final rotation of each connection due to the initial application of gravity load are provided in Table 5.10. No cracking of the concrete deck was observed during this stage of loading.

As lateral load was applied, cracking of the concrete deck began near Interior Connection 1 and Exterior Connection 2 at 9.7 kips. The moment and the rotation for each connection at this stage are reported in Table 5.10. Most cracks started either at the column or at one of the clip gage blockouts and propagated across the width of the deck to the edge of the concrete slab.

At 39.7 kips, the seat angle at Exterior Connection 1 had pulled away from the column flange approximately 1/8 inch. Concrete crushing against the column flanges was first noticed at Exterior Connection 1 at 41.0 kips. Again, the corresponding connection moment and rotation are reported in Table 5.10.

The first of several load drops due to the release of frictional forces between the lateral load tube and the lateral bracing occurred when the load dropped from 42.0 kips to 35.9 kips with a corresponding displacement increase of 0.08 inches. All lateral load plots have been adjusted to account for these frictional forces. Also, more severe concrete crushing was noticed at Exterior Connection 1 at this point as well as larger cracks at Interior Connection 1 and Exterior Connection 2.

Frictional forces built up as loading continued and another load drop occurred from 39.1 kips to 34.7 kips with a coinciding 0.05 inch displacement increase. The peak eastward displacement of 2.73 inches was reached at a load of 36.1 kips. Figure 5.11 shows the 3/16 inch gap between the seat angle and the column flange while Figures 5.12 and 5.13 depict the concrete crushing against the column flange at Exterior Connection 1. Similarly, Figure 5.14 shows the gap between the column flange and the concrete deck as well as the general crack pattern at Interior Connection 1. The moment and the rotation for each connection is provided in Table 5.10.

At this point the loading direction was reversed. Concrete cracks first were noticed at Exterior Connection 1 and Interior Connection 2 at -35.3 kips. The moment and the rotation for each connection at this stage are reported in Table 5.10.

Another load drop occurred from -37.0 kips to -26.1 kips due to frictional forces between the lateral load tube and the lateral bracing. Figures 5.15 to 5.17 show the crack pattern on the concrete deck near Exterior Connection 1. Figure 5.18 shows the 35.4 mrad rotation of Exterior Connection 1. Note that the previous gap between the seat angle and the column flange has closed since this connection is in negative bending. The whitewash which had flaked away above the first bolt row on the ATLSS Connector indicates that the AC was carrying tensile force. Figures 5.19 and 5.20 show both Interior Connection 2 and Exterior Connection 2 at peak westward displacement. Again, all relevant moments and rotations are summarized in Table 5.10.

The frame was returned to its zero load state. This position no longer corresponded to zero displacement due to inelastic rotations of the connections. The floor gravity loads were released and the test was terminated. Final moments and rotations for the four connections are provided in Table 5.10.

5.7 Gravity Load Tests

At the conclusion of the monotonic frame test, it was decided to test each of the two bays individually subjected to gravity load only. The objectives of the two gravity load tests were to:

1. Assess the moment-rotation response of both the exterior and the interior partially restrained composite connections due to gravity load only.

2. Evaluate the failure mechanisms of the bays.

Section 5.7.1 details the loading procedure while Sections 5.7.2a and 5.7.2b relate the experimental behavior of the West Bay and the East Bay, respectively.

5.7.1 Loading Procedure

Gravity load was applied to the floor beam under investigation in roughly one kip increments. Each test was terminated when the floor beam in question failed locally and lost its load-carrying capacity. The gravity load versus beam midspan deflection relationship was monitored during each test.

5.7.2 Behavior

The behavior of the two bay tests are summarized individually in this section. Note that all rotations are plotted relative to the start of the original monotonic frame test to emphasize the decreased stiffness at these large rotations.

5.7.2a West Bay

A plot of gravity load versus midspan deflection is provided in Figure 5.21. New cracks at both connections were noticed first at 39.4 kips. Also, the W12x19 beam started to yield between L2 and L3. Corresponding connection moments and rotations are summarized in Table 5.11. Then, even though no lateral load was being applied to the specimen, 11.0 kips of load were lost due to friction forces between the lateral load tube and the lateral bracing since the tube was still connected to the test frame. The W12x19 began to yield at L4 at this point also as shown in Figure 5.22. Further local deformations were noticed near

L4 at 36.6 kips, 36.2 kips and 37.3 kips when shear studs broke. Figures 5.23 to 5.26 detail the formation of a plastic hinge near L4. The test ended at 32.5 kips with a corresponding midspan deflection of 6.7 inches when the top flange of the W12x19 locally buckled with a corresponding crippling of the web. No crushing of the concrete deck was noticed near the location of the plastic hinge.

5.7.2b East Bay

A plot of gravity load versus midspan deflection is provided in Figure 5.27. The W12x19 beam started to yield between L6 and L7 at the peak load of 44.8 kips. Corresponding connection moments and rotations are summarized in Table 5.12. Then, even though no lateral load was being applied to the specimen, 5.9 kips of load were lost due to friction forces between the lateral load tube and the lateral bracing since the tube was still connected to the test frame. Further local deformations were noticed near L6 at 39.2 kips and 40.0 kips when shear studs broke. The test ended at 40.4 kips with a corresponding midspan deflection of 4.6 inches when the top flange of the W12x19 locally buckled with a corresponding crippling of the web. Slight crushing of the concrete deck was noticed near the location of the plastic hinge as shown in Figure 5.28. In addition, Figures 5.29 to 5.31 show the fracture of the ATLSS Connector at Interior Connection 2.

5.8 Cyclic Test

The objectives of testing the cyclic frame were to:

1. Evaluate the lateral load-lateral displacement behavior of the frame.

2. Assess the moment-rotation response of both the exterior and the interior partially restrained composite connections due to combined gravity and cyclic loads.

3. Determine the behavior of the ATLSS Connector when used as a component in partially restrained composite connections.

5.8.1 Loading Procedure

Load application for the cyclic frame test occurred in three phases. Initially, gravity loads were applied to both floor beams simultaneously in the zero drift position. Load was applied in one kip increments until each beam carried 28 kips. The gravity load levels were monitored during the application of the lateral load and were adjusted as needed to maintain the 28 kip load. At this point, lateral load was applied initially in 0.02 inch displacement increments. Table 5.13 summarizes the lateral loading procedure for this test. The lateral load cycles at 0.25%, 0.50% and 0.75% story drift were considered the elastic cycles of the test. Lateral loading was terminated when the specimen exhibited significant strength deterioration. Finally, the gravity loads were released and the test ended. A plot of lateral load versus story drift is shown in Figure 5.32.

5.8.2 Behavior

After the initial application of the gravity loads, several small cracks were detected near the connections. These cracks were not present in the monotonic test frame.

During the first cycle at 0.25% story drift, the concrete deck separated slightly from the metal deck at the two ends of the slab. The maximum crack width at Exterior Connection 2 was 0.025 inches. Also, one of the innermost reinforcing bars at Exterior Connection 2 and at Interior Connection 1 began to yield just before the peak of 1^+ was reached. The starting displacement, peak displacement and load at peak displacement for each excursion are summarized in Table 5.14. No significant events occurred during the remaining two cycles at 0.25% story drift.

During the first cycle at 0.50% story drift, one of the innermost reinforcing bars at Exterior Connection 1 and at Interior Connection 2 began to yield just before the peak of 4^-. Again, no other significant events occurred during the remaining two cycles at 0.50% story drift.

During the first cycle at 0.75% story drift, the maximum crack width at Exterior Connection 1 was 0.03 inches. One of the innermost reinforcing bars at Interior Connection 2 began to yield again just before the peak of 7^-. The remaining two cycles at 0.75% story drift were rather uneventful. The end of the ninth cycle signified the conclusion to the elastic loading cycles.

The displacement increment was increased to 0.30 inches at the beginning of the 1.0% story drift cycles. At the peak 10^+, a significant number of reinforcing bars at Interior Connection 1 and at Exterior Connection 2 had

yielded. At the peak of 10^-, the maximum crack width at Exterior Connection 1 was 0.04 inches.

During the 1.5% story drift cycles, the maximum crack width at Exterior Connection 2 was 0.2 inches. Just 12^-, several small bangs were heard. Since these noises could be attributed to frictional forces between the lateral load tube and the lateral bracing, grease was reapplied to the interface. No sudden load drops due to the release of these frictional forces were noticed at any time during the cyclic test.

During the 2.0% story drift cycles, concrete crushing against the column flanges was first noticed. This first occurred at Interior Connection 1 and at Exterior Connection 2 at 15^-. By the peak of 16^-, the ATLSS Connector at Exterior Connection 2 had slipped into bearing. Also, small yield lines were noted on the beam flanges near each of the ATLSS Connectors. Significant concrete crushing at all connections was noticed by the peak of 17^+. The load at the peak of 17^+ had degraded to approximately 56% of the peak positive load which was obtained at 14^+. Similarly, the load at the peak of 17^- had degraded to approximately 12% of the peak negative load which was obtained at 14^-. Therefore, the lateral loading was ended at this point.

The frame was returned to its zero load state. This position no longer corresponded to zero displacement due to inelastic rotations of the connections.

The floor gravity loads were released and the test was terminated. Figure 5.33 shows the frame after the conclusion of the cyclic test.

Chapter 6

Experimental Test:

Results and Comparison with Analytical Predictions

6.1 Introduction

This chapter summarizes the experimental results of the frame tests. Also, comparisons are provided between the analytical predictions and the experimental results. Further comparisons are given to similar test results that were obtained at the University of Minnesota.

6.2 Monotonic Test

As described in Section 5.6, the objectives of testing the monotonic frame were to:

1. Evaluate the lateral load-lateral displacement behavior of the frame.

2. Assess the moment-rotation response of both the exterior and the interior partially restrained composite connections due to combined gravity and lateral loads.

3. Determine the behavior of the ATLSS Connector when used as a component in partially restrained composite connections.

The moment-rotation response of the connections was evaluated using the following parameters:

1. Maximum Strength Ratio, R:
   R is defined as the ratio M_{max}/M_p. The maximum moment, M_{max}, is obtained from the experimental moment-rotation curve. M_p is the plastic moment capacity of the steel beam.

2. Initial and Secant Stiffnesses, K_i and K_{sec}:
   K_i is the initial slope of the experimental moment-rotation curve from the zero load position. K_{sec} is the slope of the experimental moment-rotation curve at 4 mrad.

3. Rotational Ductility Ratio, μ_θ:
   μ_θ is defined as θ_{max}/θ_y. θ_{max} is the rotation at M_{max} and θ_y is the rotation at M_y. μ_θ measures the ability of a structure to undergo increasing deformation beyond first significant yield while still sustaining load.

These four parameters were defined only in the initial direction of loading for each connection. The experimental results for each objective are discussed in Section 6.2.1. Then comparisons between the experimental results and the analytical predictions are provided in Section 6.2.2.

6.2.1 Results

A plot of lateral load versus lateral displacement is shown in Figure 6.1. The loads at the peak displacements were 36.1 kips and -25.6 kips which were approximately 5.0 and 3.5 times the service wind load of 7.25 kips. Similarly, the peak displacements both were 2.73 inches which corresponded to 6.0 times the allowable story drift of 0.455 inches. The moment-rotation curves for the connections due to combined gravity and lateral loads are given in Figures 6.2 to 6.9. Note that Figures 6.8 and 6.9 depict partial curves due to instrumentation problems at Exterior Connection 2. The experimental behavior of the

connections was described in detail in Section 5.6.2. All significant events such as first cracking or first crushing are noted on the graphs.

The ATLSS Connectors satisfactorily provided resistance against both positive and negative shear forces at each of the connections. No noticeable deformations of the ATLSS Connectors occurred during the monotonic test.

6.2.2 Comparison with Analytical Predictions

Figure 6.10 compares the experimental lateral load-lateral displacement behavior with the analytical prediction. This comparison was made only for the initial portion of the curve up to the east peak. As shown, the experimental value for the initial stiffness of the frame was closely predicted by the analytical model. The central portion of the lateral load-lateral displacement curve was underestimated by the prediction. The load at the peak displacement was overestimated by approximately 15%. Since the model is based solely on the moment-rotation responses of the connections, this discrepancy could be due to a redistribution of moments away from the connections toward the midspan of the beams (Leon, 1995).

The predicted moment-rotation response for each connection is superimposed on its experimental moment-rotation curve in Figures 6.11 to 6.14. The predicted responses for the interior connections were taken directly from Rosa's experimental results (Rosa, 1993). The predicted responses for the exterior connections were analytically determined as described in Chapter 3. All

four connections originally were in negative bending due to the initial application of the gravity loads; therefore, the predicted moment-rotation responses were revised to account for this initial preload. This initial resistance to the applied gravity loads resulted in consistently lower positive moments at the connections than would have been required without the preload.

Table 6.1 summarizes the values for the parameters R, K_i, K_{sec} and μ_θ which were described in Section 6.2. Again, these four parameters were defined only in the initial direction of loading for each connection. The maximum strength ratio, R, was overestimated by the predictions for each connection. In other words, none of the connections ever reached its ultimate predicted moment. This may be due to redistribution of moments away from the connections towards the midspan of the beams. This effect could not be predicted from the results of tests on isolated connections in cruciform-shaped subassemblages. The initial stiffness, K_i, for each connection was overestimated by the prediction. This could be due to the fact that the predictions did not take into account the reduced stiffness due to cracked concrete. The secant stiffness, K_{sec}, used more often than K_i, was also overestimated by the predictions for all connections. Again, this could be attributed to decreased stiffness due to cracked concrete or to redistribution of moments away from the connections into the midspan of the beams. The rotational ductility ratio, μ_θ, was overestimated for all connections except Interior Connection 1. This is due to the fact that neither of the

connections which started in positive bending (Exterior Connection 1 and Interior Connection 2) ever reached the ultimate rotation of 20 mrad in the initial direction of loading.

The fixed end moment for the beams under gravity load only was 525 k-in. Under the same loading condition, the exterior connections showed an average moment of 258 k-in and the interior connections showed an average moment of 187 k-in. Thus, the degree of end restraint was 49.1% and 35.6% for the exterior and the interior connections respectively.

6.3 Gravity Load Tests

As discussed in Section 5.7, the objectives of the two gravity load tests were to:

1. Assess the moment-rotation response of both the exterior and the interior partially restrained composite connections due to gravity load only.

2. Evaluate the failure mechanisms of the bays.

The experimental results for each objective are discussed in Section 6.3.1. Comparisons between these experimental results and the analytical predictions are provided in Section 6.3.2.

6.3.1 Results

The experimental results for the West Bay and the East Bay are presented in Sections 6.3.1a and 6.3.1b, respectively.

6.3.1a West Bay

A plot of gravity load versus midspan deflection is shown in Figure 6.15. The moment-rotation curves for the connections due to gravity load only are given in Figures 6.16 and 6.17. Note that all rotations are plotted relative to the start of the original monotonic frame test to emphasize the decreased stiffness at these large rotations. The experimental behavior of the connections was described in detail in Section 5.7.2a.

The load-carrying capacity of the system was limited by the formation of a plastic hinge approximately 52 inches from Interior Connection 1. As shear studs broke, the composite action between the steel beam and the concrete deck was removed locally. Thus the top flange of the W12x19 was no longer laterally supported and it buckled locally with a related crippling of the web.

The final failure mechanism for the West Bay gravity load test occurred at Interior Connection 1. The ATLSS Connector fractured through its net section just above the upper bolt hole closest to the column flange as shown in Figure 5.31. This implies that the composite neutral axis was below the top of the ATLSS Connector since it failed in tension.

6.3.1b East Bay

A plot of gravity load versus midspan deflection is shown in Figure 6.18. The moment-rotation curves for the connections due to gravity load only are

given in Figures 6.19 and 6.20. The experimental behavior of the connections was described in detail in Section 5.7.2b.

The load-carrying capacity of the system was limited by the formation of a plastic hinge approximately 52 inches from Interior Connection 2. As shear studs broke, the composite action between the steel beam and the concrete deck was removed locally. Thus the top flange of the W12x19 was no longer laterally supported and it buckled locally with a related crippling of the web.

The final failure mechanism for the East Bay gravity load test occurred at Interior Connection 2. The ATLSS Connector fractured through its net section just above the upper bolt hole closest to the column flange as shown in Figure 5.31. This implies that the composite neutral axis was below the top of the ATLSS Connector since it failed in tension.

6.3.2 Comparison with Analytical Predictions

6.3.2a West Bay

As discussed in Chapter 3, the ultimate rotation for the PRCCs was assumed to be 20 mrad. Both Exterior Connection 1 and Interior Connection 1 had surpassed this ultimate rotation before the gravity loading began. The connections behaved more like simply supported connections and thus were not able to resist the end moments as they did during the monotonic test. For these end conditions, the midspan moment increased much more quickly than the end moments. Figures 6.21 and 6.22 indicate the rapid moment increase at the

plastic hinge location as compared to the moment at each of the connections. The plastic moment strength of the bare steel beam, M_p of 1,260 inch-kips, was surpassed by the composite beam.

6.3.2b East Bay

As discussed in Chapter 3, the ultimate rotation for the PRCCs was assumed to be 20 mrad. Both Interior Connection 2 and Exterior Connection 2 had surpassed this ultimate rotation before the gravity loading began. The connections behaved more like simply supported connections and thus were not able to resist the end moments as they did during the monotonic test. For these end conditions, the midspan moment increased much more quickly than the end moments. Figures 6.23 and 6.24 indicate the rapid moment increase at the plastic hinge location as compared to the moment at each of the connections. The plastic moment strength of the bare steel beam, M_p of 1,260 inch-kips, was surpassed by the composite beam.

6.4 Cyclic Test

As discussed in Section 5.8, the objectives of testing the cyclic frame were to:

1. Evaluate the lateral load-lateral displacement behavior of the frame.

2. Assess the moment-rotation response of both the exterior and the interior partially restrained composite connections due to combined gravity and cyclic loads.

3. Determine the behavior of the ATLSS Connector when used as a component in partially restrained composite connections.

The experimental results for each objective are discussed in Section 6.4.1. Comparisons between these experimental results and the analytical predictions are provided in Section 6.4.2.

6.4.1 Results

A plot of lateral load versus story drift is shown in Figure 6.25. The maximum story drift attained by the frame before significant strength degradation was 2.0%. The allowable story drift for this frame is 0.5% (UBC, 1991). Thus, the frame was able to reach four times the allowable story drift safely.

The ATLSS Connectors satisfactorily provided resistance against both positive and negative shear forces at each of the connections. No noticeable deformations of the ATLSS Connectors occurred during the cyclic test.

6.4.2 Comparison with Analytical Predictions

The behavior of the cyclic frame was predicted using the results from the monotonic frame. Figure 6.26 compares the lateral load-lateral displacement behavior of the two frames. The monotonic test curve provides a boundary for the hysteresis loops from the cyclic test. The initial stiffnesses of the two frames are almost identical as shown by the elastic cycles of the cyclic test.

As predicted, the inelastic cycles began at 1.0% story drift and the frame began to dissipate energy. The amount of energy dissipated increased with

larger story drifts as expected. The frame behavior which caused the energy losses, (i.e., concrete cracking, concrete crushing, rebar yielding, etc.) was described in Section 5.8.2.

6.5 Comparison with University of Minnesota Test Results

As mentioned in Chapter 2, the test specimens described in this thesis are scaled down by approximately 58% from a similar cyclic specimen at the University of Minnesota. To facilitate comparisons between the cyclic tests, lateral displacements were nondimensionalized by the story height (story drift), lateral loads were nondimensionalized by the lateral load at the maximum allowable story drift (load ratio) and moments were nondimensionalized by the plastic moment strength of the bare steel beams (M/M_p).

Figures 6.27 and 6.28 compare the lateral load histories for the two tests. Similarly, Figures 6.29 and 6.30 contrast the lateral deflection histories for the two frames. The lateral load application scheme was identical for both frames. The lateral load-carrying capacity of the University of Minnesota test specimen decreased during the second cycle of load at 2.2% story drift due to a shear failure of the cantilevered portion of the slab beyond one of the exterior connections. The test was continued to find the ultimate failure mechanism for the frame, but no data was recorded past 2.2% story drift.

The maximum recorded load ratios were 2.5 and 2.2 for the Lehigh University and the University of Minnesota frames, respectively. Both peak loads

were reached at 2.0% story drift. Thus, the Lehigh University specimen was approximately 12.5% stiffer than the University of Minnesota specimen.

Chapter 7

Summary, Conclusions and Recommendations

7.1 Summary

This research project studied the behavior of frames with partially restrained composite connections using the ATLSS Connector which were designed to resist gravity and lateral loads. A previously designed interior partially restrained composite connection was applied to the planar frame and a new exterior partially restrained composite connection was tested. In addition, an analytical model was developed to predict the behavior of frames from the behavior of the individual connections when subjected to: (1) combined gravity loads plus monotonic lateral loads and (2) combined gravity loads plus cyclic lateral loads. Finally, the behavior of the ATLSS Connector when used as a component in partially restrained composite connections was analyzed.

7.2 Conclusions

The following conclusions may be drawn from this research project:

1. The results of tests on isolated connections in cruciform-shaped subassemblages tend to overestimate slightly the performance of the connections when used in frames.

2. With proper reinforcing bar anchorage, the same connection configuration may be used for exterior partially restrained composite connections as for interior partially restrained composite connections.

3. The behavior of frames with partially restrained composite connections can be predicted from the behavior of the individual connections.

4. The response of frames with partially restrained composite connections subjected to gravity loads plus cyclic lateral loads can be predicted accurately from the response of a similar frame subjected to gravity loads plus monotonic lateral loads.

5. At service and factored load levels, the ATLSS Connector satisfactorily provides resistance against both positive and negative shear forces when used as a component in partially restrained composite connections.

7.3 Recommendations

The results from this research project suggest several areas where future research is needed, including:

1. Design and experimentation of partially restrained composite connections which frame into the weak axis of wide-flange columns.

2. Design and experimentation of partially restrained composite connections between floor beams and girders.

3. Use of the ATLSS Connector in the tests described in (1) and (2).

4. Modifications to the ATLSS Connector to make it amenable to use with a larger number of beams.

Table 1.1 Construction Savings Using the ATLSS Connector

Economic Aspect	Using the ATLSS Connector	Using Standard Methods	Savings/ Improvement (%)
Duration	7.5 days	8.5 days	12
Cost	$42,800	$48,300	11
Danger Index	1651	2290	28
Resources	1 crane, 10 workers	1 crane, 10 workers	0

Table 2.1 Prototype Building P-Delta Analysis Comparison

	Interstory Drift @ Service Load (in)		
Level	First Order	Iterative	Direct
4	0.11	0.11	0.12
3	0.23	0.24	0.25
2	0.30	0.30	0.29
1	0.27	0.27	0.26

Table 2.2 Basic Scale Factors

Quantity	Scale Factor, S_l
Linear dimension	S_l
Angular dimension	1
Area	$(S_l)^2$
Moment of inertia	$(S_l)^4$
Concentrated load and shear	$(S_l)^2$
Moment and connection stiffness	$(S_l)^3$

Table 3.1 4000 PSI Concrete Mix Design

Component	Quantity/yd^3
Cement (Lonestar Type 1)	621 lb
Coarse Aggregate (3/8" Max Crushed Stone)	1269 lb
Fine Aggregate (Natural Sand)	1716 lb
Water	354 lb
Air	1%
Water Reducing Admixture (Grace Industries)	18.6 oz
Air Entraining Admixture (Grace Industries)	--

--: Not Available

Table 4.1 Frame Scale Comparison With University of Minnesota Test Specimen

Frame Component	Lehigh University	University of Minnesota
Floor Beams	15'-0" W12x19	25'-8" W14x38
Concrete Deck	3"	5 1/4"
Reinforcing Bars	#3	#4
Exterior Columns	7'-7" W8x35	13'-0" W14x120
Interior Column	7'-7" W8x48	13'-0" W14x120

Table 4.2 Monotonic Test Predictions

	Lateral Load (kips)	Lateral Displacement (in)
Service Wind Load	7.25	0.15
East Peak	41.5	2.73

Table 4.3 Cyclic Test Predictions

Story Drift (%)	Lateral Displacement (in)	Lateral Load (kips)	Cycles
0.25	± 0.228	± 11.7	1-3
0.50	± 0.455	± 13.6	4-6
0.75	± 0.683	± 17.3	7-9
1.0	± 0.910	± 19.2	10, 11
1.5	± 1.365	± 22.5	12, 13
2.0	± 1.820	± 30.0	14, 15
2.5	± 2.275	± 37.4	16, 17

Table 5.1 ATLSS Connector Chemical Composition

	Batch I.D.	
Element	C-10, C-12	C-11
Carbon (C)	0.04	0.04
Manganese (Mn)	0.67	1.54
Phosphorus (P)	0.014	0.017
Sulfur (S)	0.004	0.006
Silicon (Si)	0.34	0.30
Nickel (Ni)	1.00	0.91
Chromium (Cr)	0.75	0.71
Molybdenum (Mo)	0.19	0.20
Copper (Cu)	1.00	1.01
Vanadium (V)	0.004	0.004
Aluminum (Al)	0.028	0.012
Columbium	0.08	0.08

Table 5.2 ATLSS Connector Weldability

Batch I.D.	C_{eq} Eq. 5.1	C_{eq} Eq. 5.2	C_{eq} Eq. 5.3	Preheat Required (°F)
C-10, C-12	0.15	0.53	0.32	≥65
C-11	0.30	0.66	0.46	≥175

Table 5.3 ATLSS Connector Material Properties

Batch I.D.	Yield Strength (ksi)	Tensile Strength (ksi)	Elongation Over 2" (%)	Reduction of Area (%)
C-10, C-12	74.5	87.9	22.8	--
C-11	87.5	99.2	21.9	61.9

--: Not Available

Table 5.4 ATLSS Connector Charpy V Notch Results

Batch I.D.	-50° (ft-lb)	0° (ft-lb)	70° (ft-lb)
C-10, C-12	50.5	98.0	--
C-11	25.3	38.7	71.0

--: Not Available

Table 5.5 Frame Material Properties

Section	ASTM Designation	F_{yf} (ksi)	F_{yw} (ksi)	F_u (ksi)
W12x19	A36	51	51	72.5
W8x35	A572 Gr. 50	56	64.3	80.8
W8x48	A588 Gr. 50	50.6	56.2	74.1
3/8x2 1/2 Shear Studs	--	50.1	50.1	60.1
L7x4x3/8	A36	41.3	41.3	61.7
Tube 4x4x1/4	A500 Gr. B	67.9	67.9	75.1

--: Not Available

Table 5.6 Concrete Cylinder Strengths-Monotonic Frame

	7 Days (6/28/95)	14 Days (7/5/95)	28 Days (Test Day) (7/19/95)
Cylinder Strengths (psi)	3574 3737 3833	4018 4066 4695	4198 4439 4463
Average Strength (psi)	3715	4260	4367

Table 5.7 Concrete Cylinder Strengths-Cyclic Frame

	7 Days (9/26/95)	14 Days (10/3/95)	Test Day (10/10/95)	28 Days (10/17/95)
Cylinder Strengths (psi)	4110 4131 4164	4788 4841 4834	4934 5029 5242	5217 5295 5312
Average Strength (psi)	4135	4821	5068	5275

Table 5.8 Rebar Material Properties

Frame Test	ASTM Designation	F_y (ksi)	F_u (ksi)
Monotonic	Gr. 60	69.3	108
Cyclic	Gr. 60	68.0	105

Table 5.9 Instrumentation for Frame Tests

Type of Transducer	Monotonic Frame	Cyclic Frame
Clip Gage	12	12
LVDT	7	3
Load Cell	5	5
Strain Gage	91	78
Tiltmeter	7	7
Trim Pot	5	5
Total	127	110

Table 5.10 Behavior Summary-Monotonic Test

Point in Test	Lat Load (kips)	Displ (in)	Ext 1		Ext 2		Int 1		Int 2	
			Mom (k-in)	Rot (mrad)	Mom (k-in)	Rot (mrad)	Mom (k-in)	Rot (mrad)	Mom (k-in)	Rot (mrad)
Gravity only	0	0	-258	-1.02	-40.9	-1.34	-203	-1.23	-170	-2.49
First cracking	9.7	0.24	N/A	N/A	-100	-3.50	-293	-2.71	N/A	N/A
Service rotation	N/A	N/A	163	3.06	-134	-4.05	-404	-5.15	87.6	1.44
First crushing	41.0	2.22	556	15.7	N/A	N/A	N/A	N/A	--	--
East peak	36.1	2.73	354	24.6	--	--	-806	-24.0	433	13.0
First cracking	-35.3	-1.01	-776	-11.2	N/A	N/A	N/A	N/A	-592	-15.2
West peak	-25.6	-2.73	-677	-35.4	--	--	458	29.0	-451	-41.0
End of test	0	-1.47	-12.5	-24.0	--	--	6.2	17.1	-4.4	-23.7

N/A : Not Applicable
-- : Not Available

Table 5.11 Behavior Summary-West Bay Gravity Load Test

Point in Test	Gravity Load (kips)	Midspan Defl (in)	Ext 1		Int 1	
			Approx Moment (k-in)	Rotation (mrad)	Approx Moment (k-in)	Rotation (mrad)
First cracking	39.4	0.99	-273	-29.8	182	13.6
Peak load	45.3	1.5	-362	-35.0	--	--
Break stud (#1)	36.3	4.3	-313	-39.5	--	--
Break stud (#2)	36.6	3.8	-291	-37.7	--	--
Break stud (#3), local failure	35.3	6.3	-314	-41.0	--	--
Peak defl	32.5	6.7	-270	-44.7	--	--

--: Not Available

Table 5.12 Behavior Summary-East Bay Gravity Load Test

Point in Test	Gravity Load (kips)	Midspan Defl (in)	Ext 2		Int 2	
			Approx Moment (k-in)	Rotation (mrad)	Approx Moment (k-in)	Rotation (mrad)
Peak load	44.8	1.6	--	--	-760	-49.7
Break stud (#1)	39.2	3.0	--	--	-625	-70.6
Break stud (#2)	40.0	4.4	--	--	-625	-112.3
Peak defl	40.4	4.6	--	--	-550	-145.7

--: Not Available

Table 5.13 Lateral Loading Procedure-Cyclic Test

Story Drift (%)	Lateral Displacement (in)	Number of Cycles	Cycles
0.25	± 0.228	3	1-3
0.50	± 0.455	3	4-6
0.75	± 0.683	3	7-9
1.0	± 0.910	2	10, 11
1.5	± 1.365	2	12, 13
2.0	± 1.820	2	14, 15
2.5	± 2.275	2	16, 17

Table 5.14 Behavior Summary-Cyclic Test

Excursion	Starting Displacement (in)	Peak Displacement (in)	Load at Peak Displacement (kips)
1^+	0	0.228	8.47
1^-	0.032	-0.238	-7.23
2^+	0.007	0.228	8.96
2^-	-0.004	-0.232	-5.84
3^+	-0.020	0.236	9.02
3^-	-0.012	-0.223	-6.21
4^+	-0.037	0.454	16.60
4^-	0.032	-0.468	-13.50
5^+	-0.055	0.459	16.00
5^-	-0.004	-0.449	-12.41
6^+	-0.057	0.466	16.37
6^-	-0.007	-0.455	-12.71
7^+	-0.055	0.683	21.34
7^-	0.005	-0.683	-19.83
8^+	-0.067	0.682	20.96
8^-	-0.024	-0.683	-19.09
9^+	-0.061	0.683	20.98
9^-	0.047	-0.685	-17.95
10^+	-0.016	0.908	26.29
10^-	0.049	-0.909	-19.82
11^+	-0.234	0.888	23.45
11^-	0.032	-0.905	-20.33
12^+	-0.230	1.358	28.97
12^-	0.402	-1.349	-26.28
13^+	-0.461	1.345	29.41
13^-	0.374	-1.383	-27.14
14^+	-0.469	1.81	34.42
14^-	0.53	-1.796	-33.80
15^+	-0.744	1.824	27.45
15^-	0.496	-1.853	-24.48
16^+	-0.799	2.289	24.50
16^-	1.028	-2.311	-15.48
17^+	-1.085	2.289	19.42
17^-	1.013	-2.281	-4.19

Table 6.1 Monotonic Test Results

Test Parameter	Ext 1		Ext 2		Int 1		Int 2	
	Pred	Exp	Pred	Exp	Pred	Exp	Pred	Exp
R	0.59	0.48	1.18	0.63	0.83	0.64	0.57	0.47
K_i (k-in/mrad)	258	253	328	--	203	165	170	68
K_{sec} (k-in/mrad)	145	103	187	33	98	91	117	66
μ_θ	2.9	2.1	--	--	2.5	3.0	2.9	1.7

--: Not Available

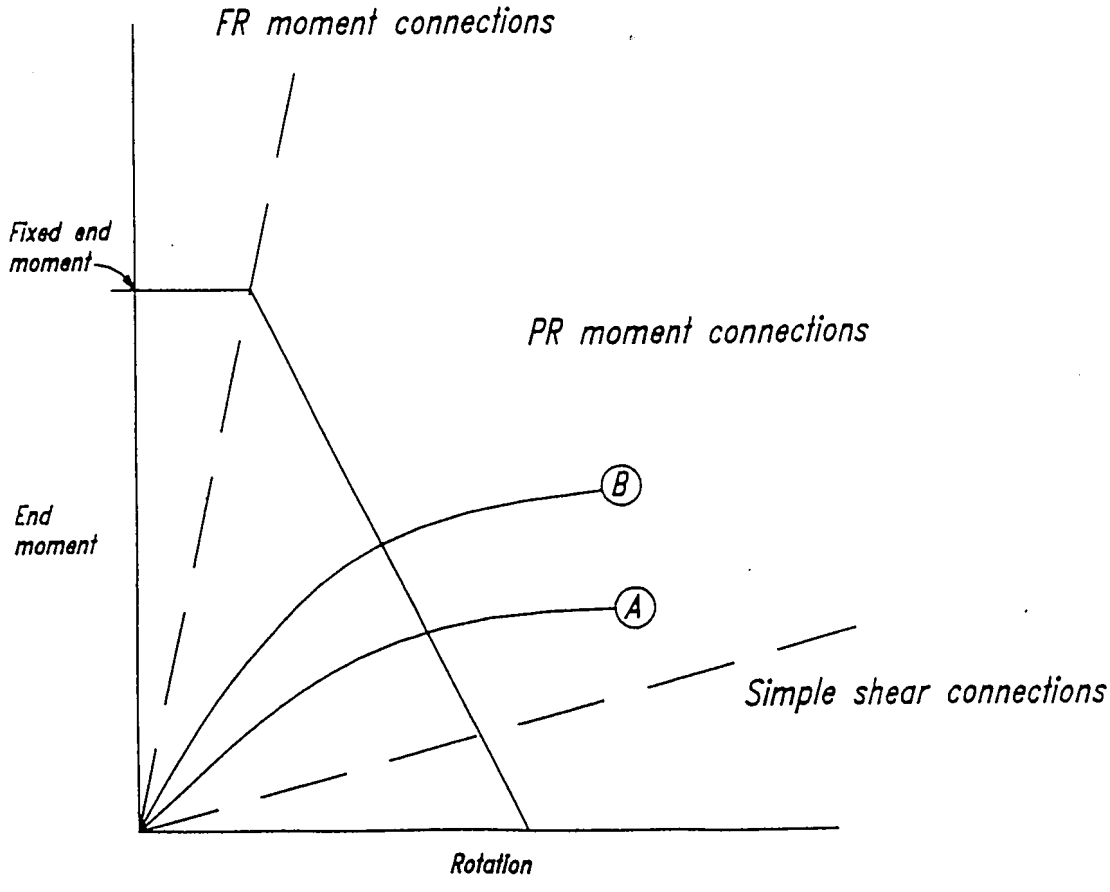

Figure 1.1 Connection Classification (AISC, 1993)

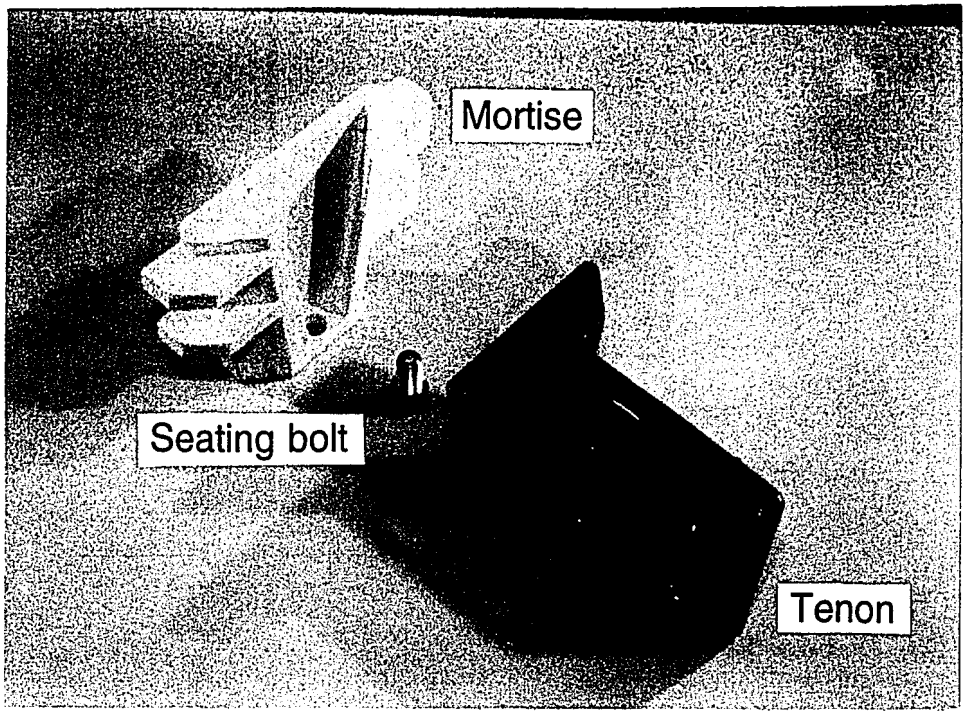

Figure 1.2 ATLSS Connector Components

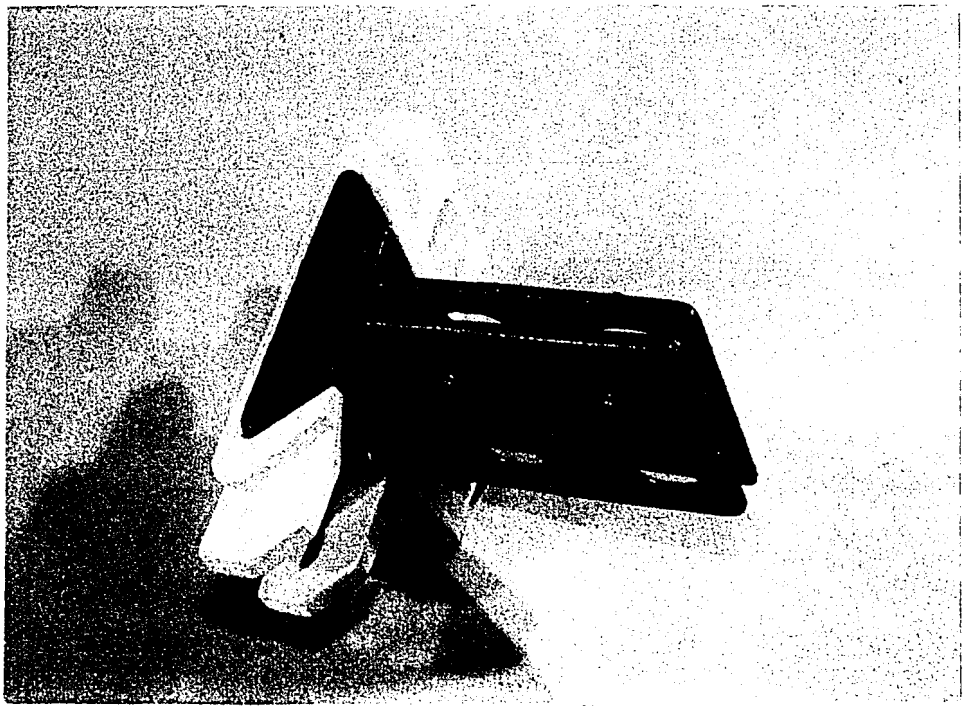

Figure 1.3 ATLSS Connector

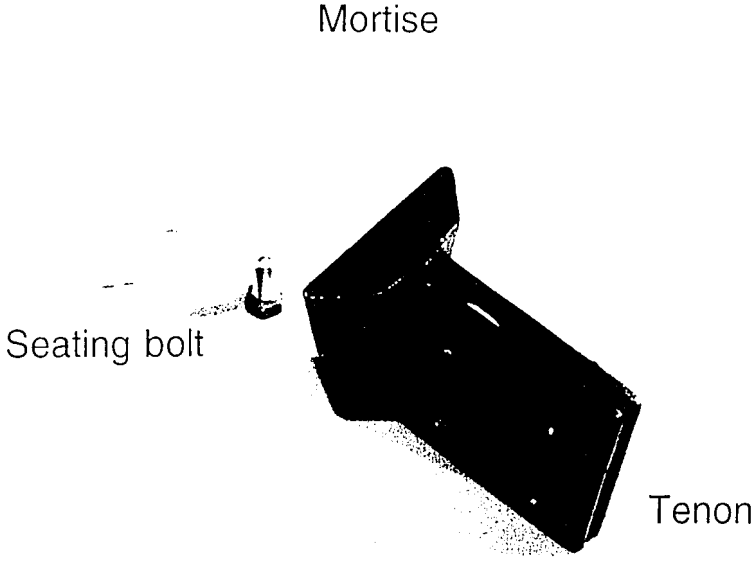

Figure 1.2 ATLSS Connector Components

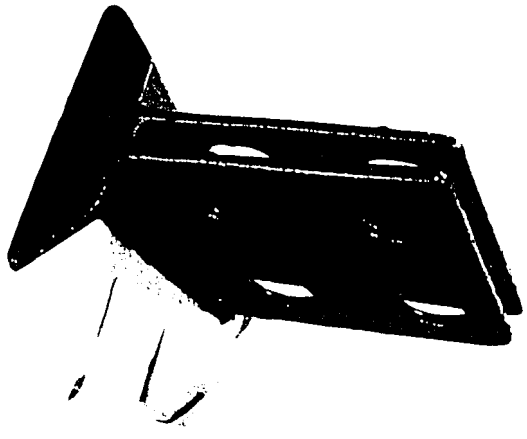

Figure 1.3 ATLSS Connector

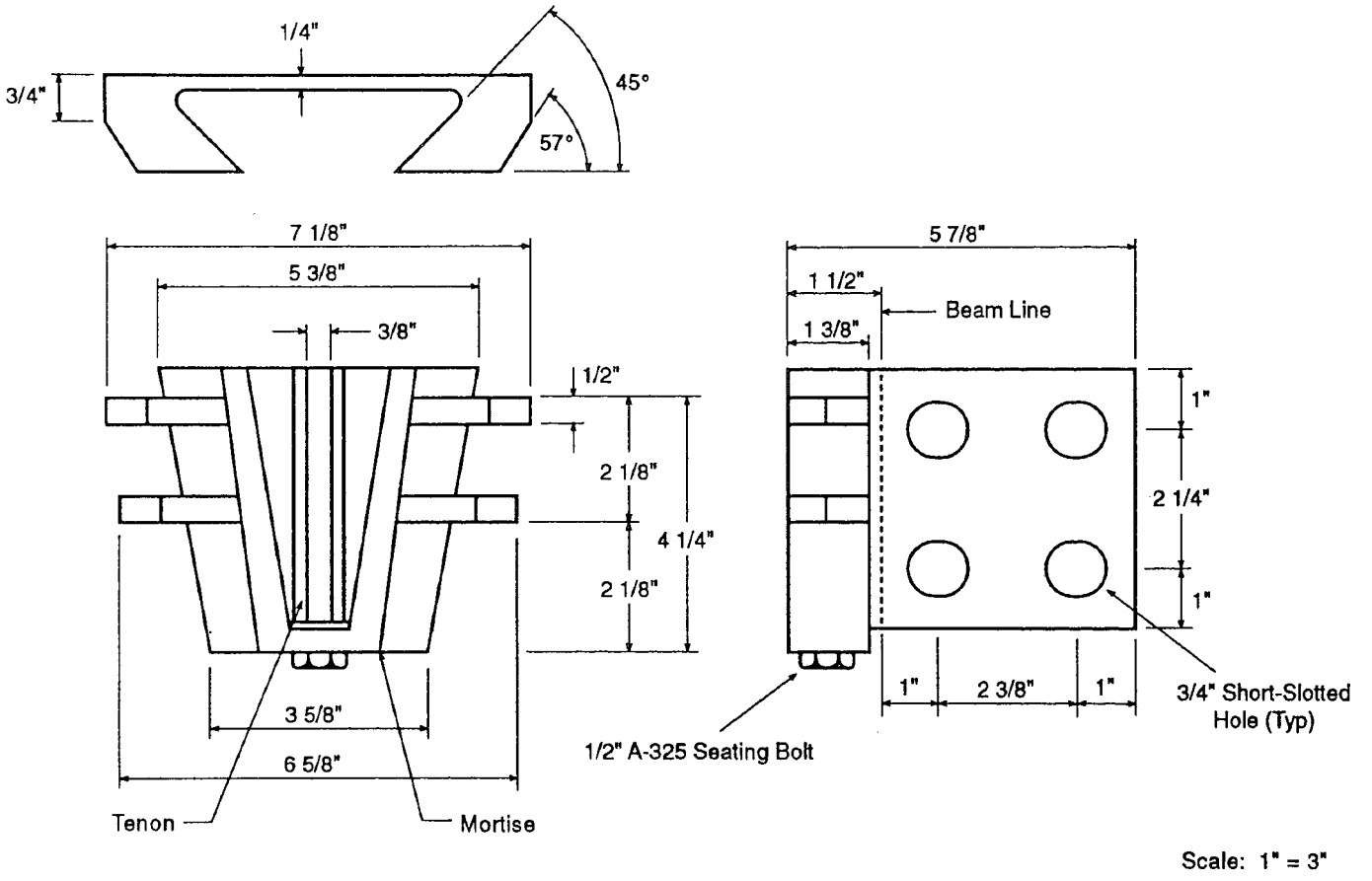

Figure 1.4 ATLSS Connector Dimensions

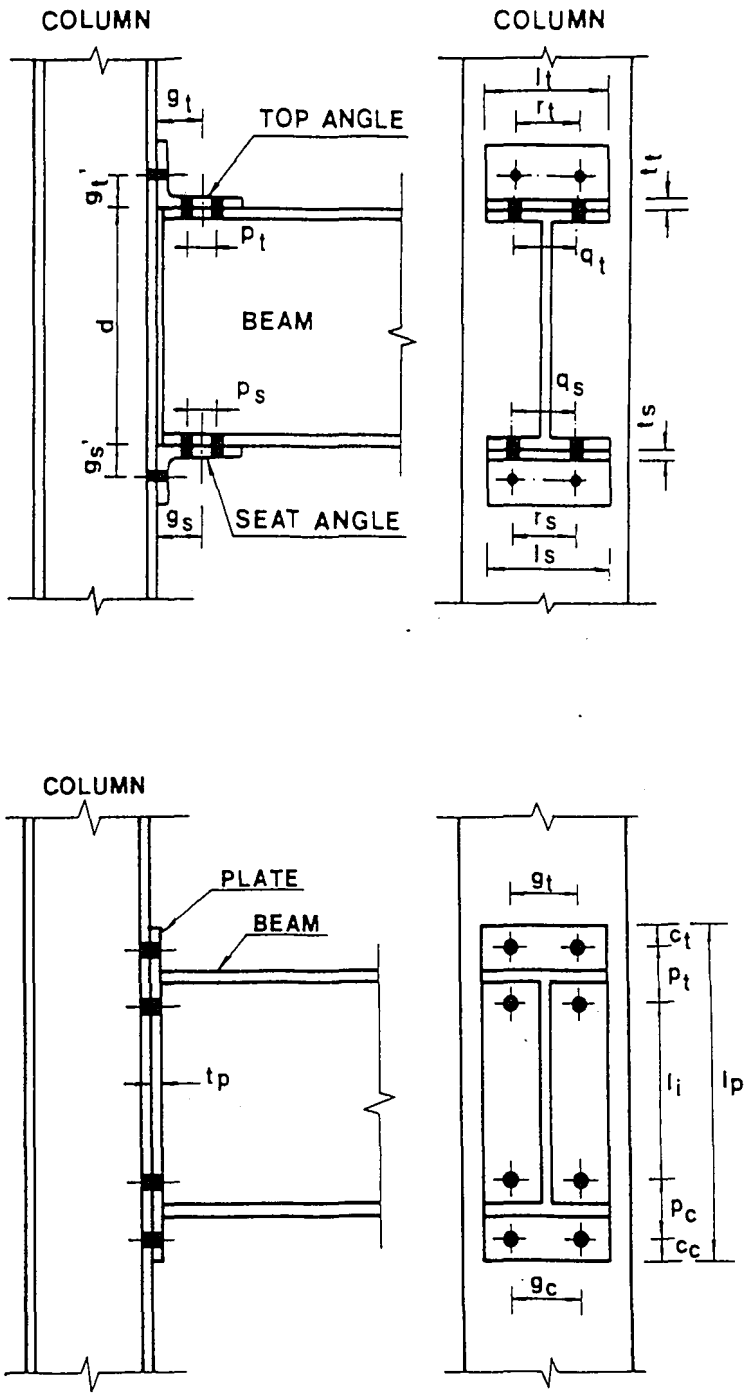

Figure 1.5 Typical Partially Restrained Connections (Chen, 1993)

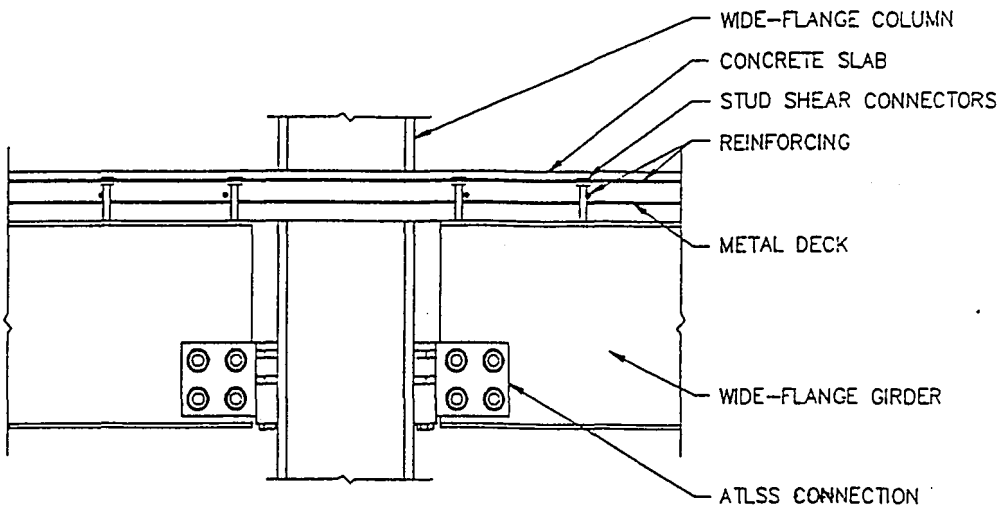

Figure 1.6 Flexible Partially Restrained Composite Connection (Rosa, 1993)

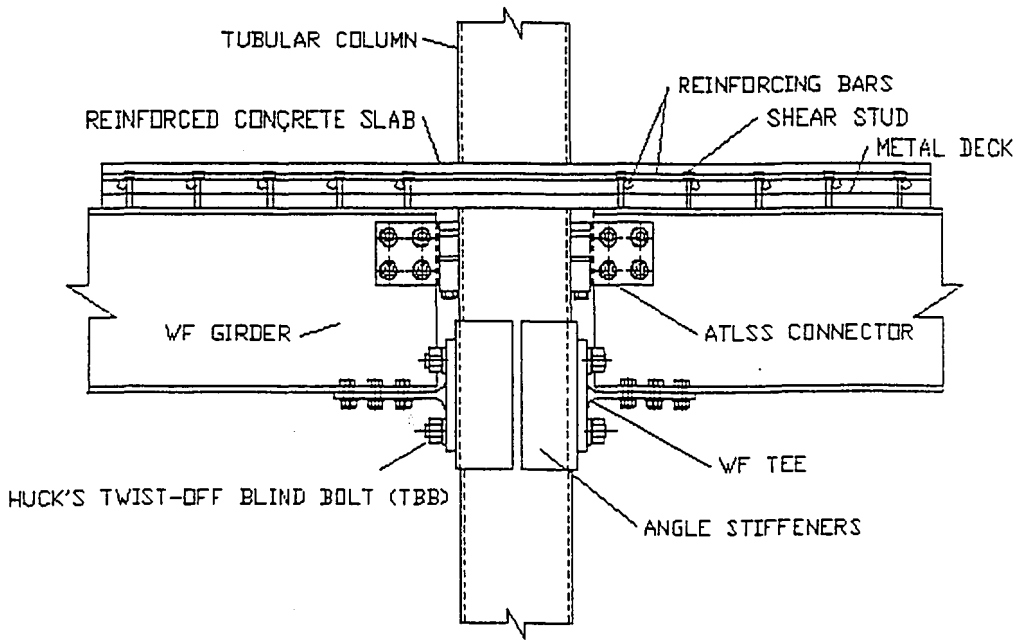

Figure 1.7 Stiff Partially Restrained Composite Connection (Lawrence, 1994)

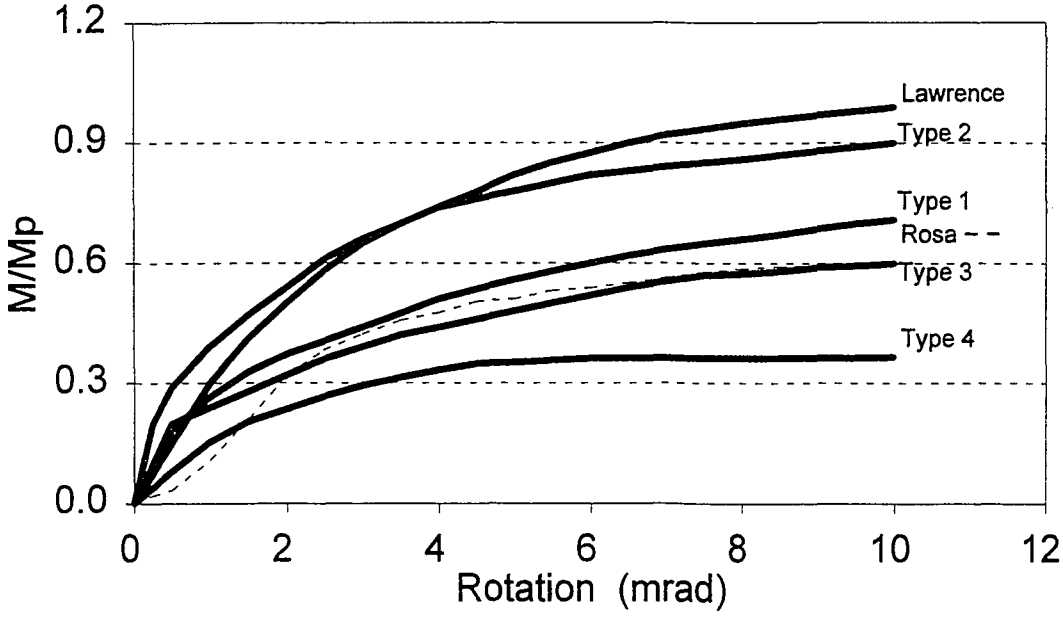

Figure 1.8 Moment-Rotation Comparison

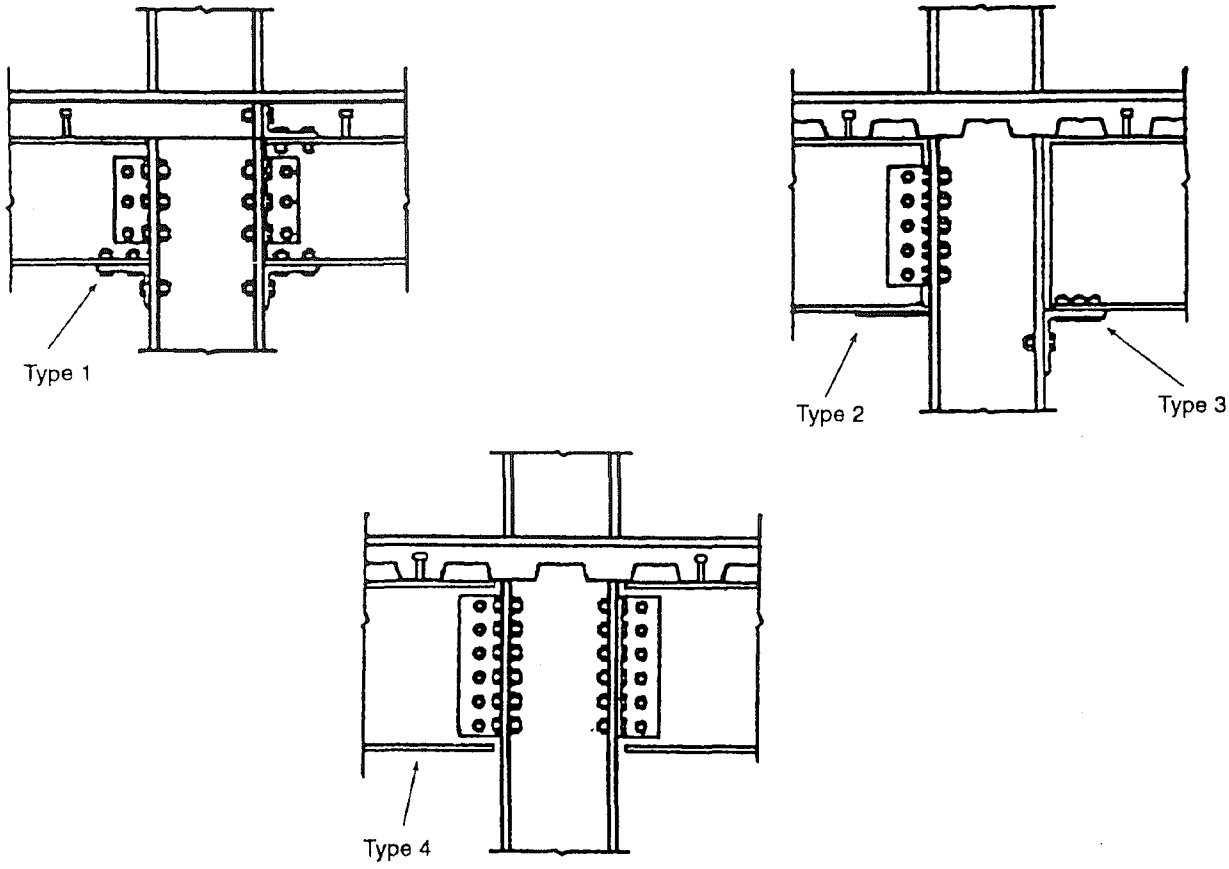

Figure 1.9 University of Minnesota Typical Connections (Leon, 1992)

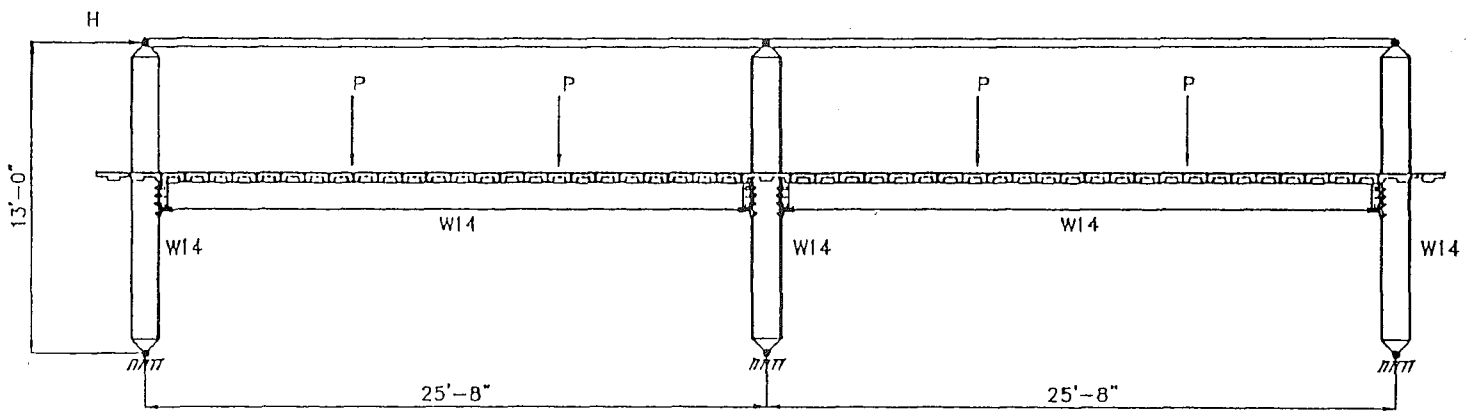

Figure 1.10 University of Minnesota Frame Test (Ammerman, 1988)

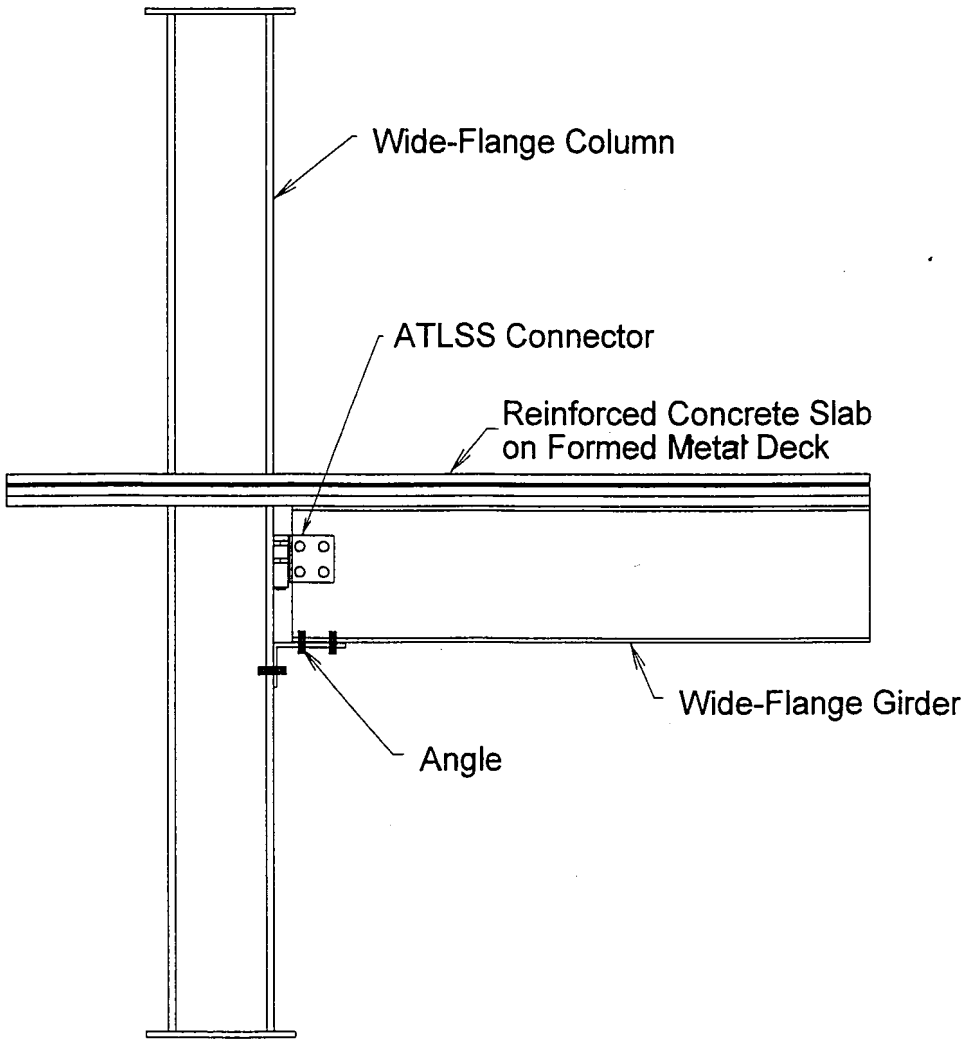

Figure 1.11 Exterior Partially Restrained Composite Connection
-Monotonic Frame

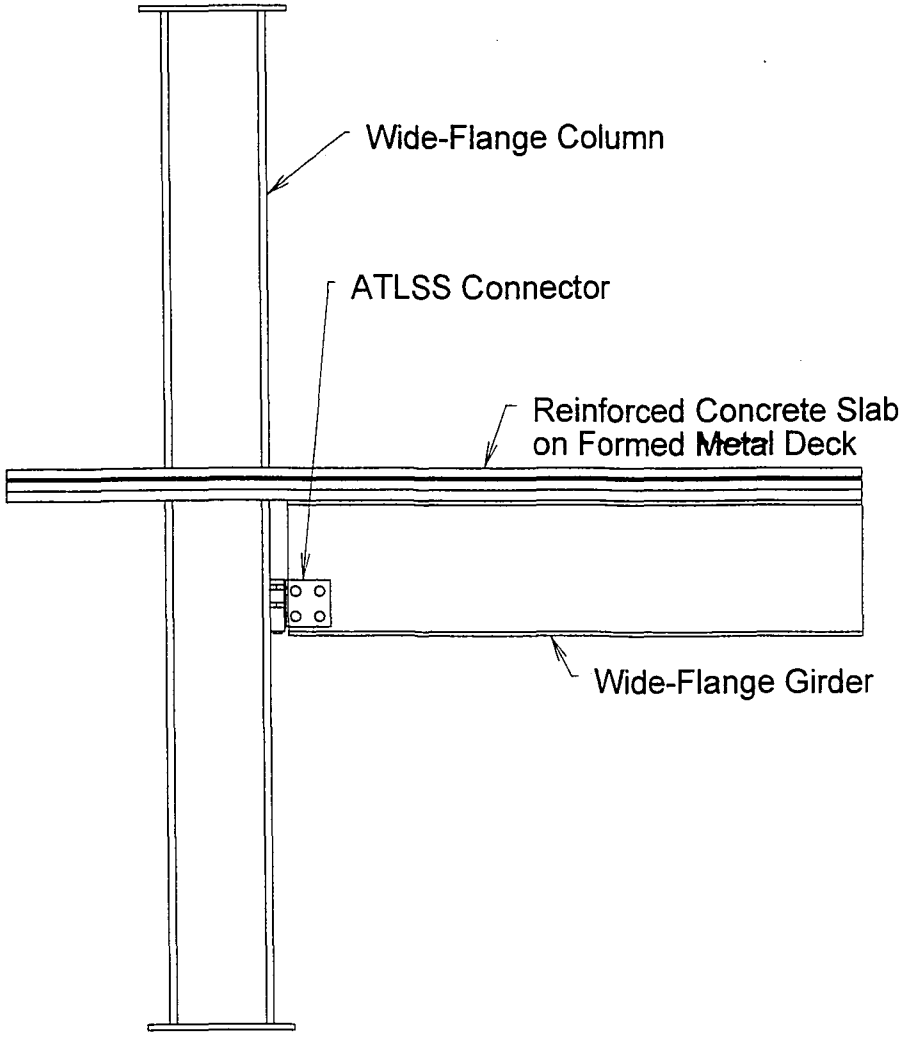

Scale: 1" = 1.5'

Figure 1.12 Exterior Partially Restrained Composite Connection
-Cyclic Frame

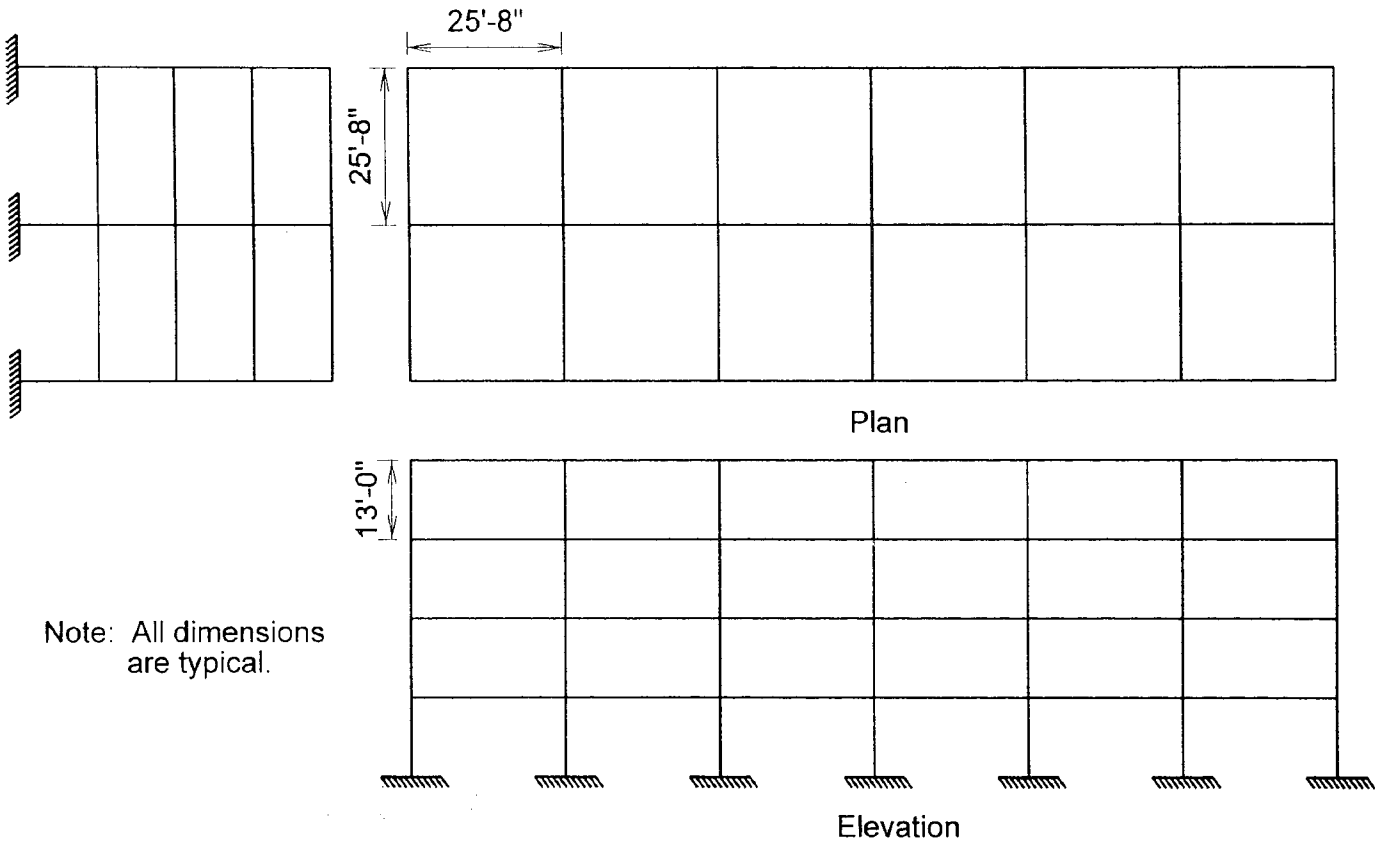

Figure 2.1 Prototype Building Plan and Elevation

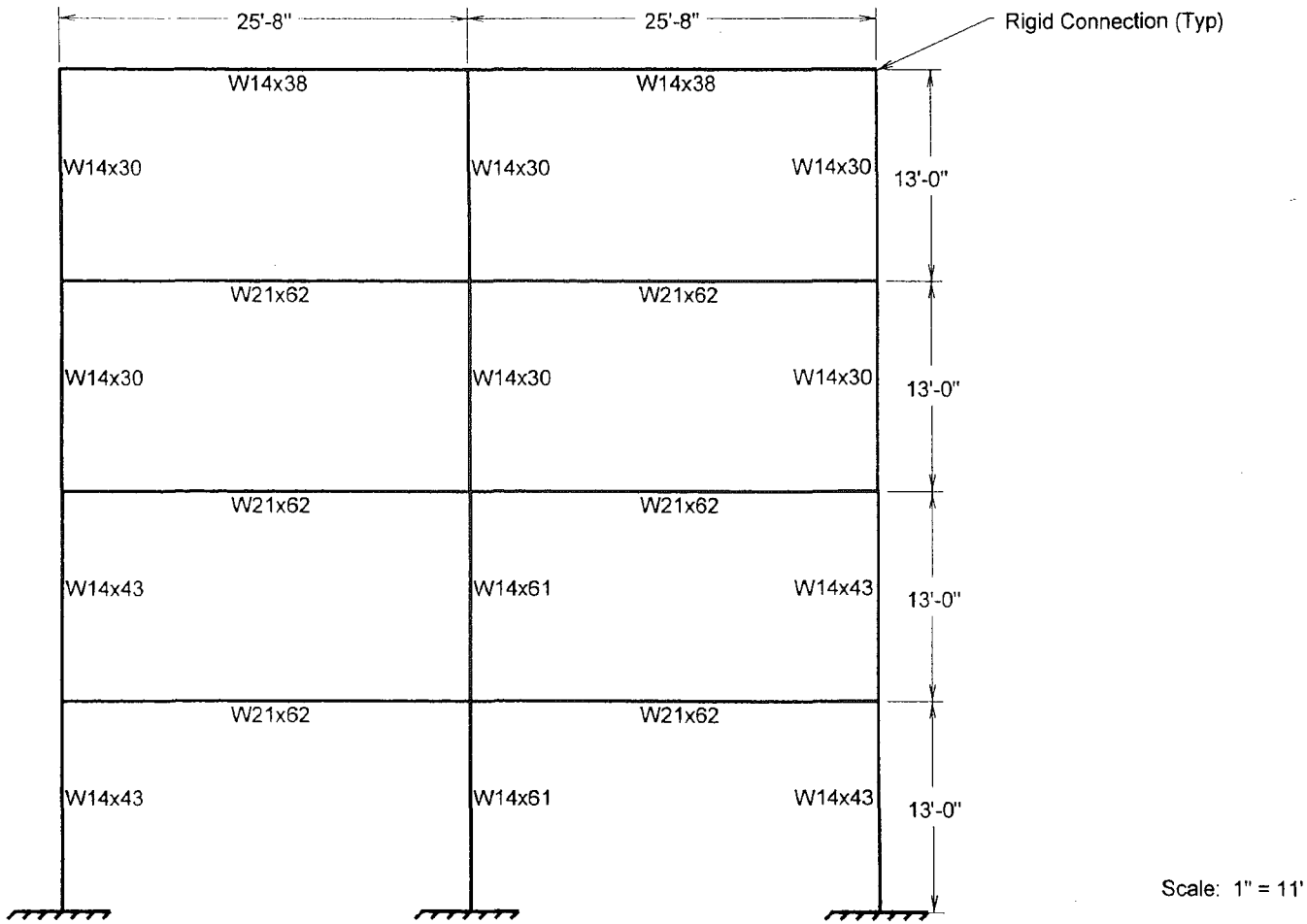

Figure 2.2 Prototype Building with Rigid Connections

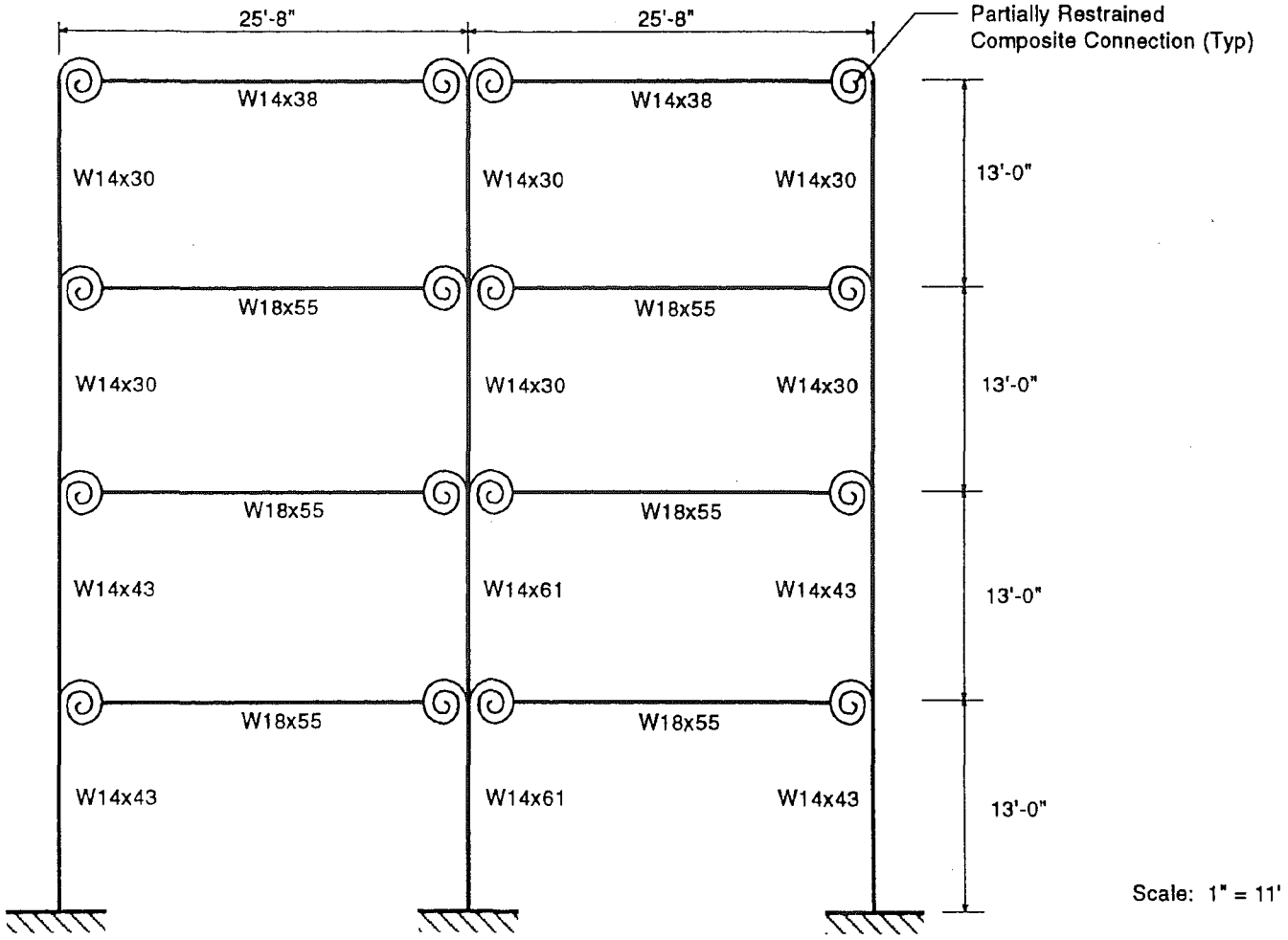

Figure 2.3 Prototype Building with Partially Restrained Composite Connections

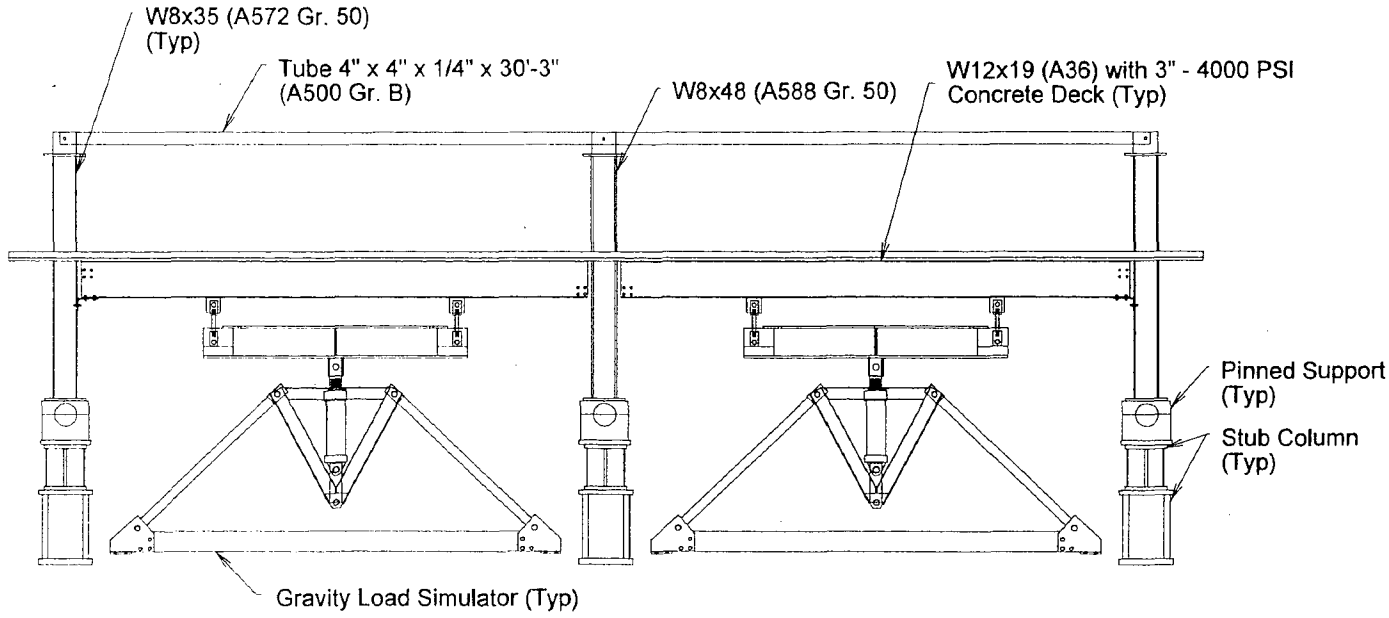

Figure 3.1 Overall View of Monotonic Frame

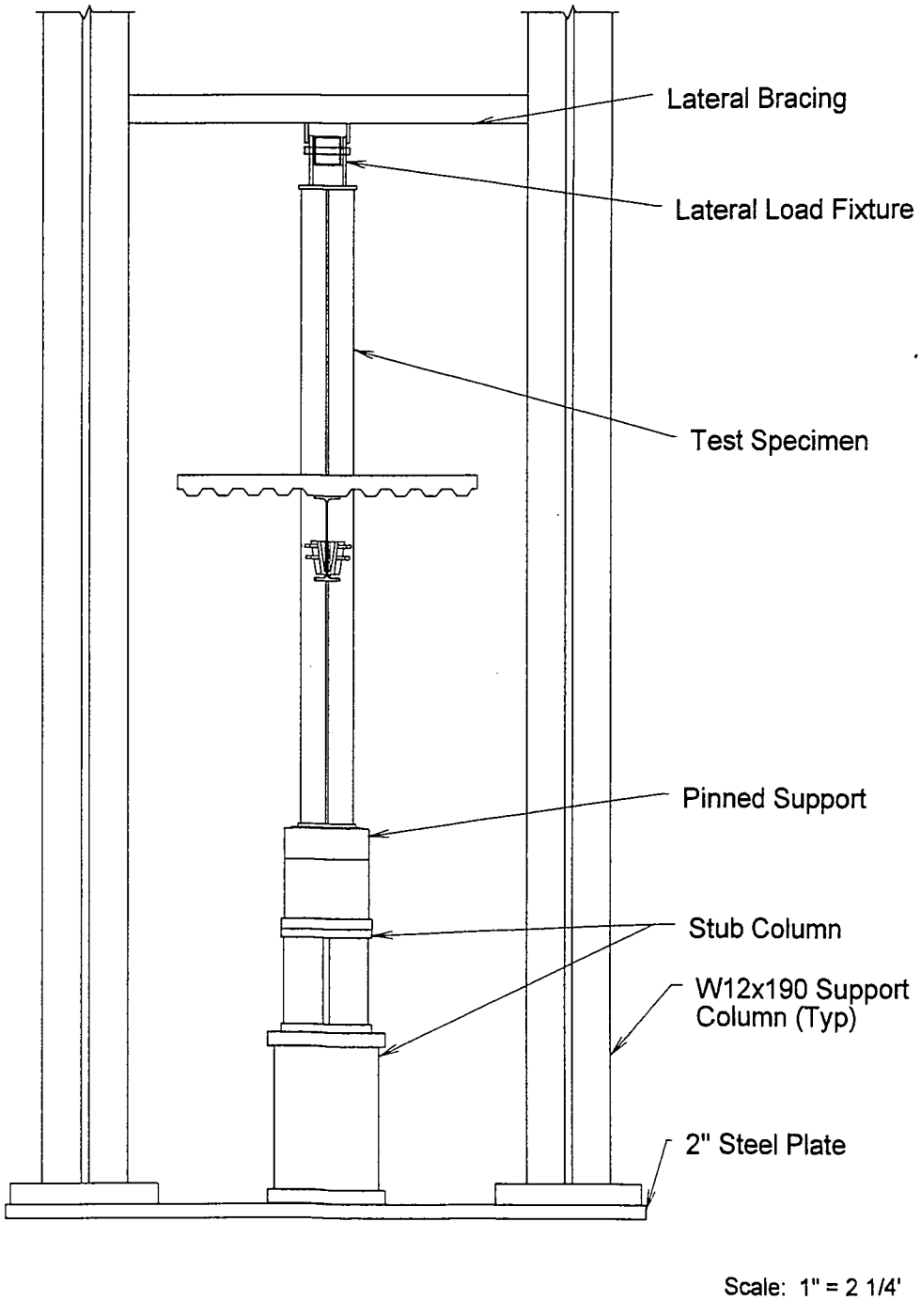

Figure 3.2 End View of Monotonic Frame

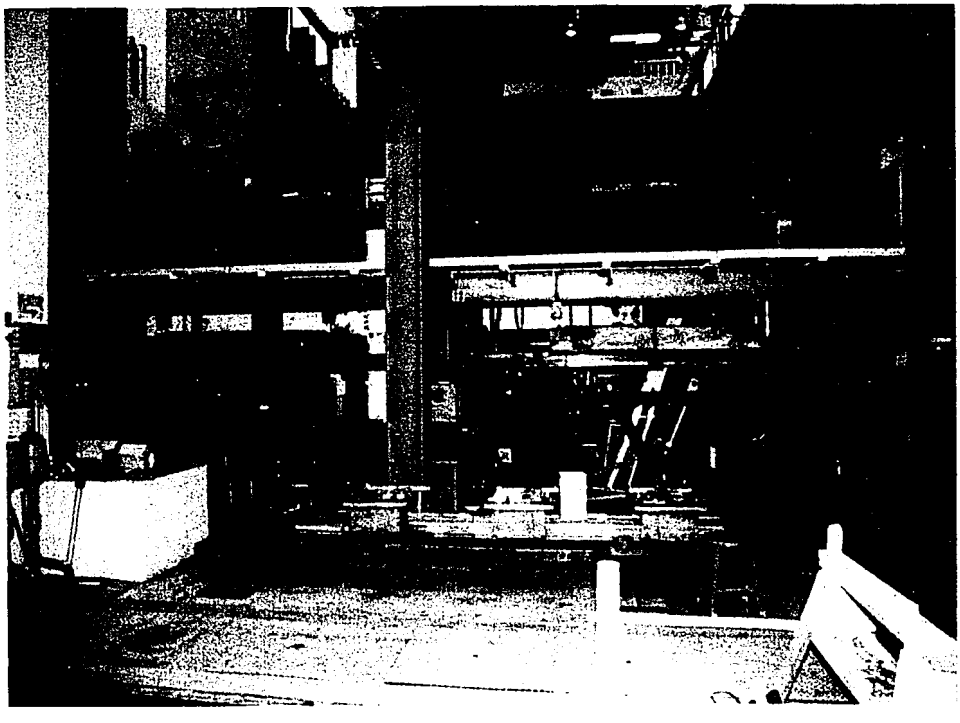

Figure 3.3 Photograph of Monotonic Frame

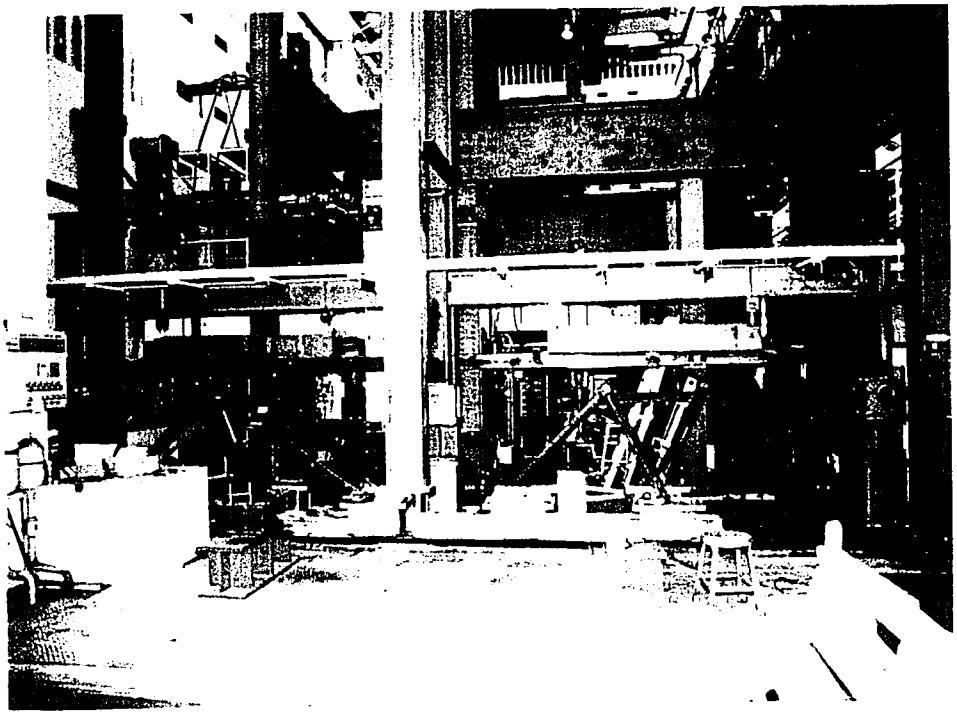

Figure 3.3 Photograph of Monotonic Frame

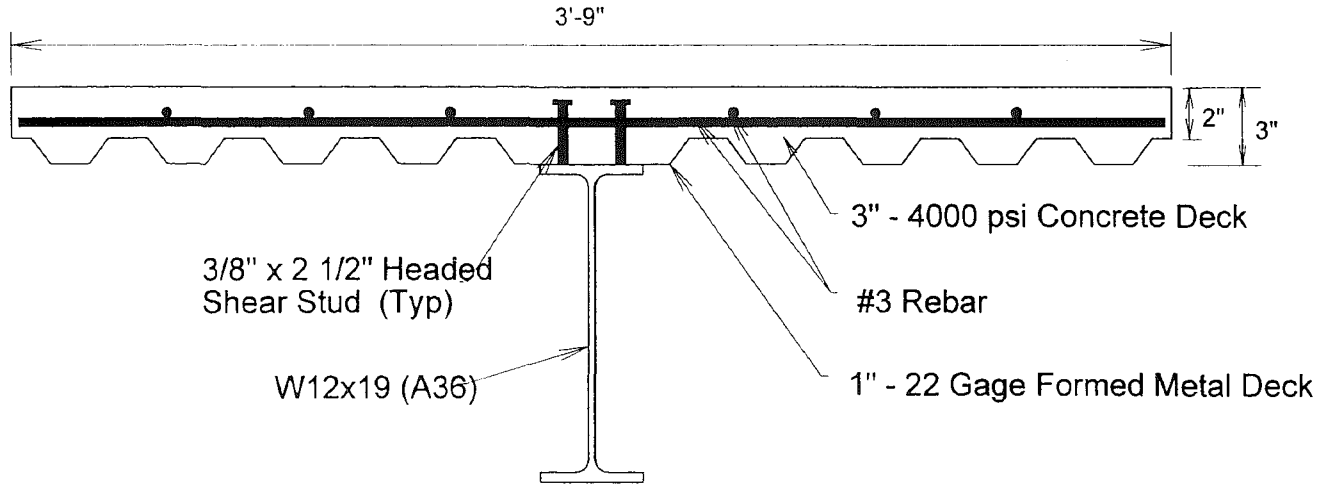

Scale: 1" = 7"

Figure 3.4 Composite Deck

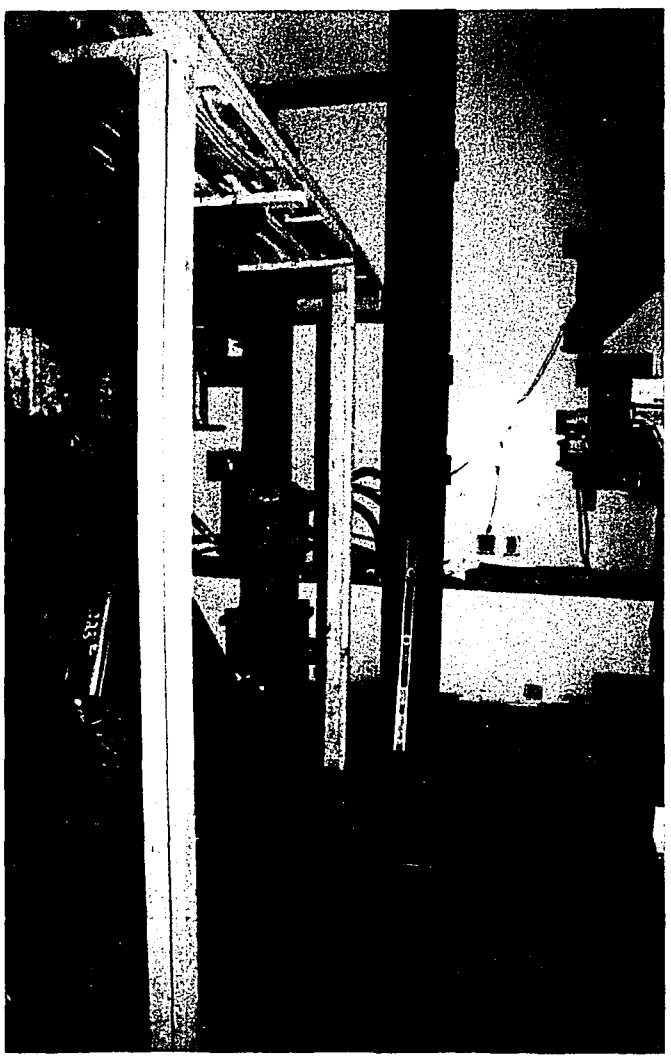

Figure 3.5 Concrete Deck Shoring

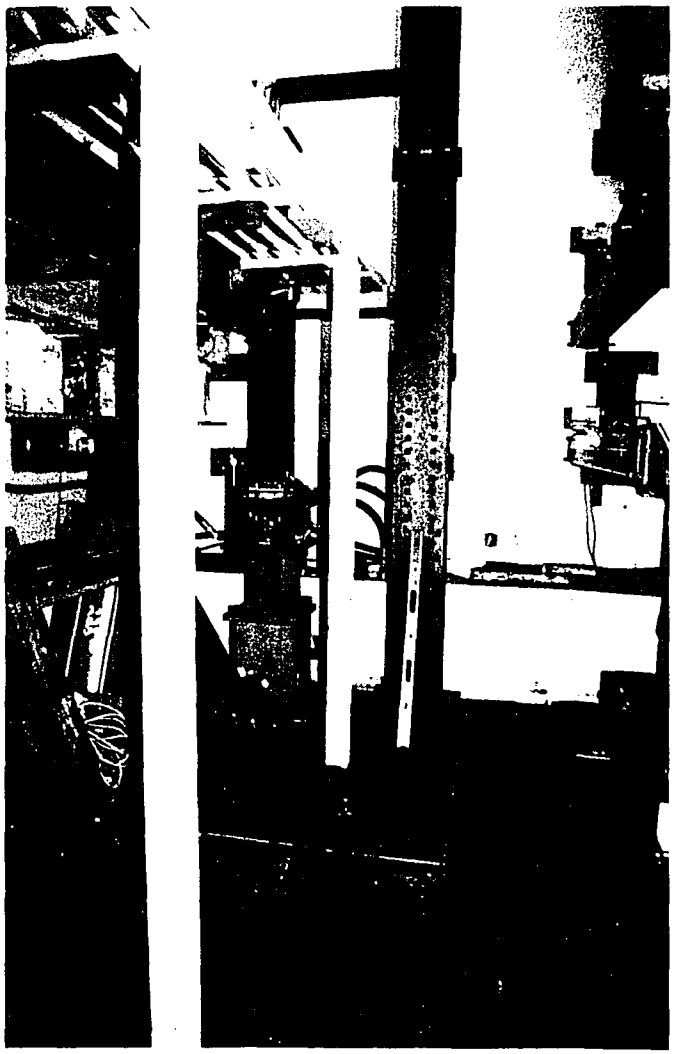

Figure 3.5 Concrete Deck Shoring

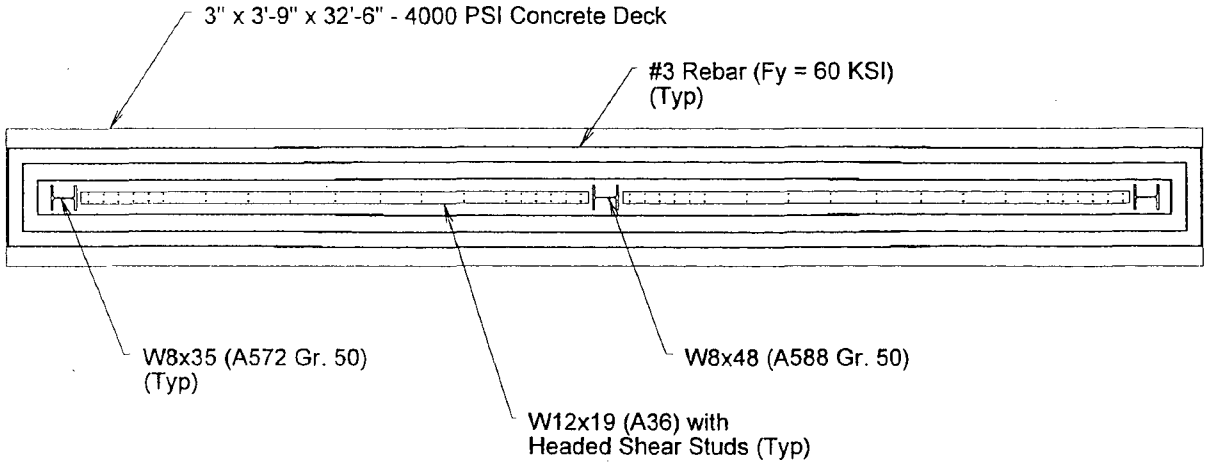

Note: A more detailed view of the reinforcement layout is provided in Figure 3.7.

Scale: 1" = 5'

Figure 3.6 General Reinforcement Layout

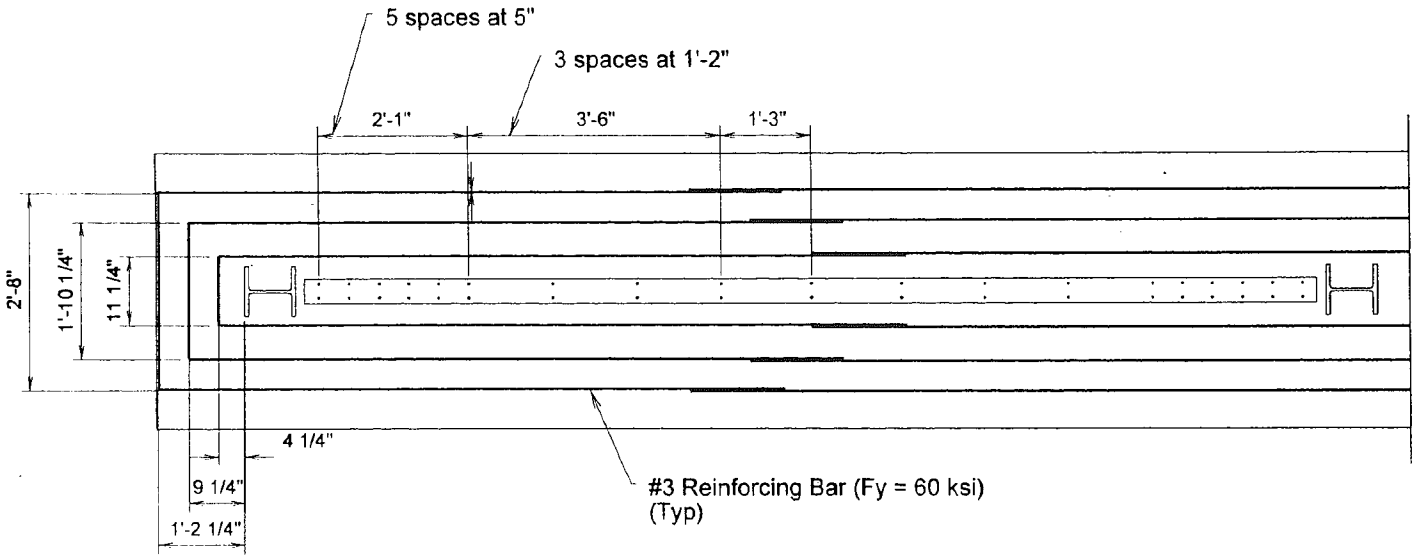

Note: All dimensions are typical about the beam centerline.

Scale: 1" = 2.5'

Figure 3.7 Detailed Reinforcement Layout

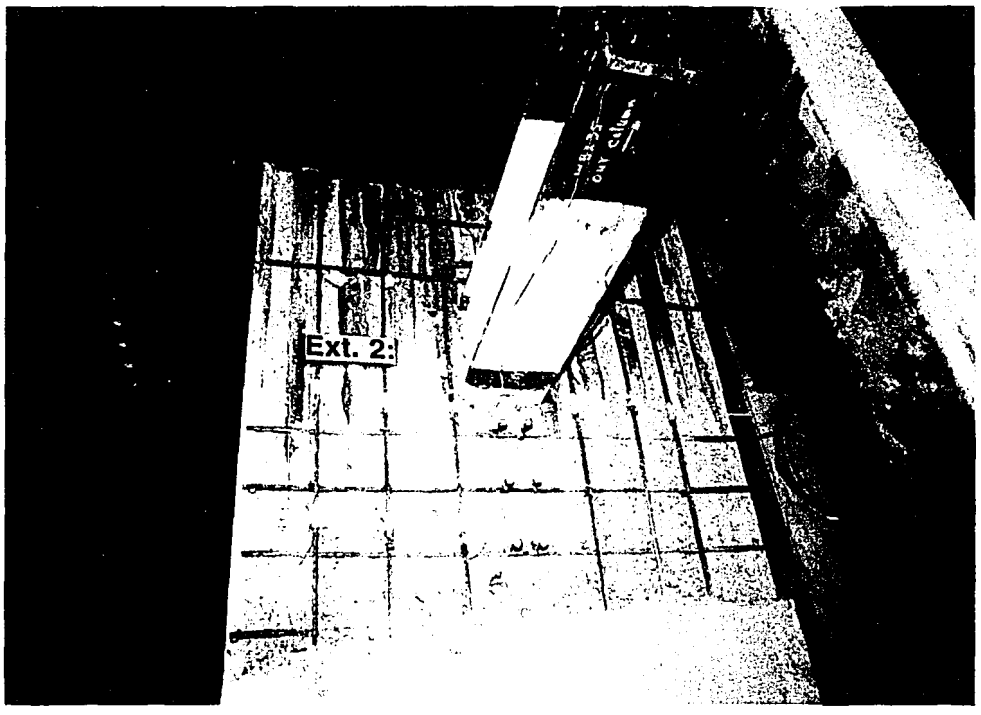

Figure 3.8 Exterior Connection Rebar Pattern

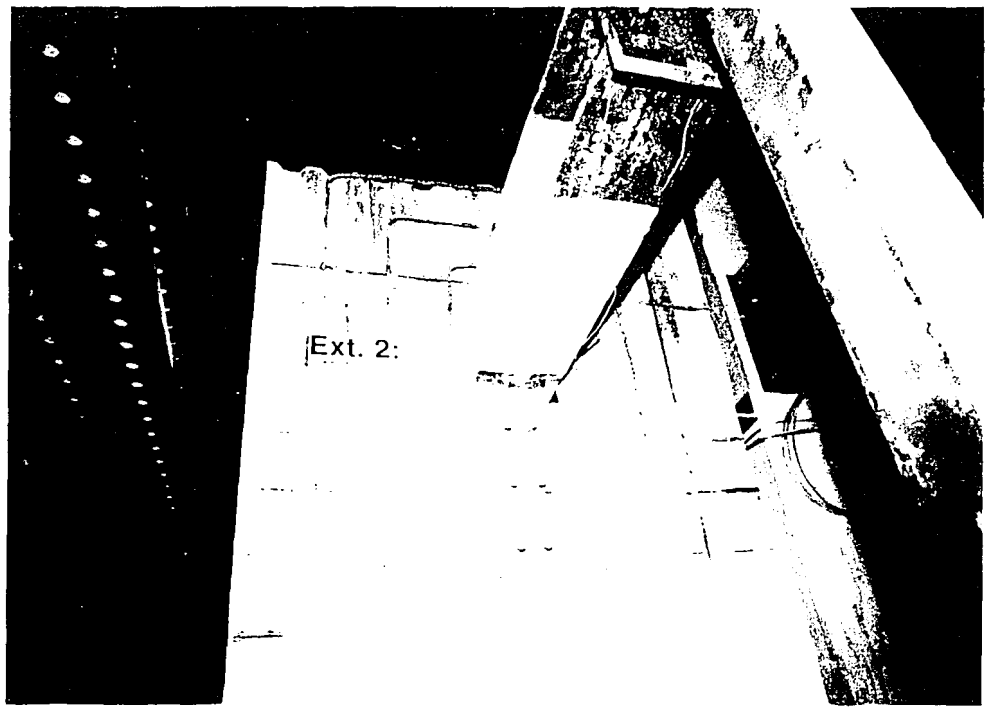

Figure 3.8 Exterior Connection Rebar Pattern

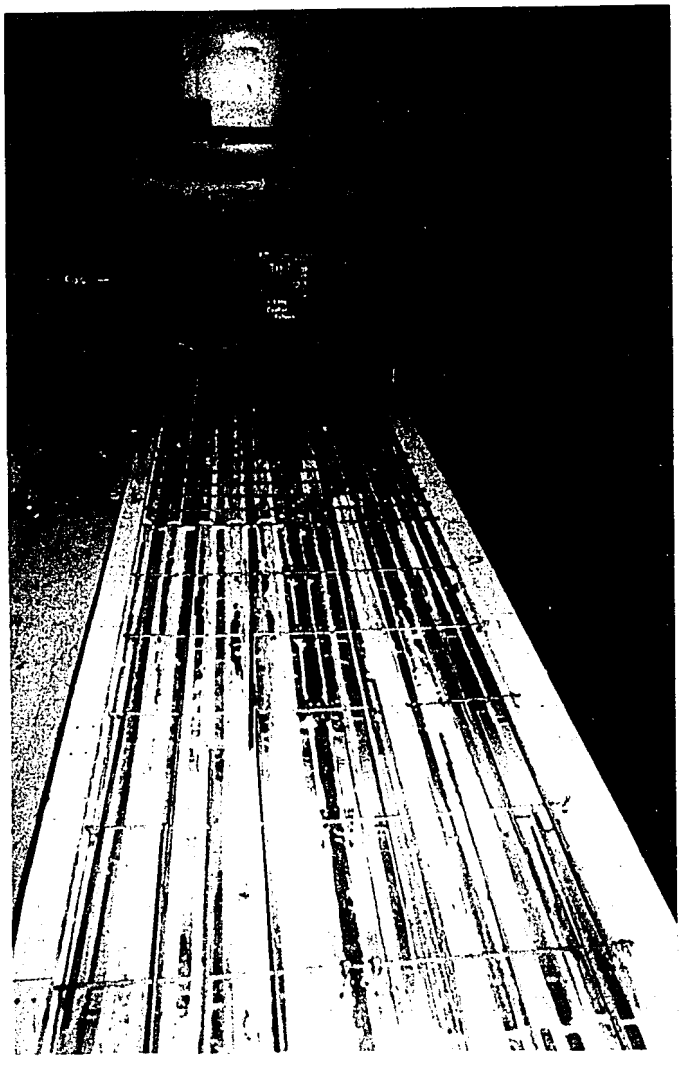

Figure 3.9 Frame Prior to Concrete Pour

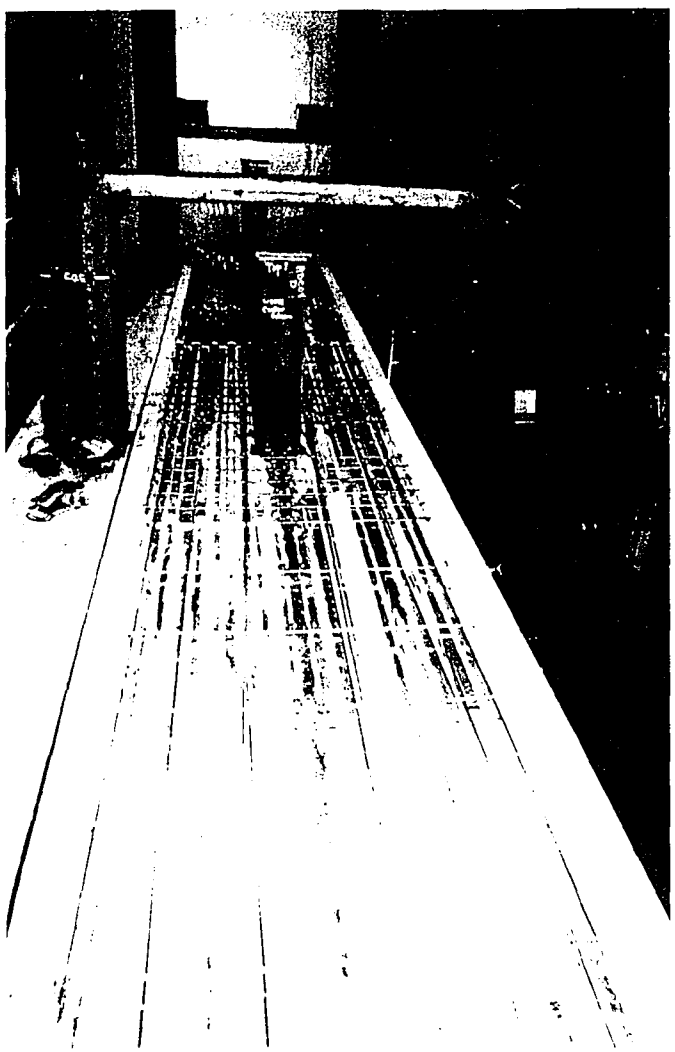

Figure 3.9 Frame Prior to Concrete Pour

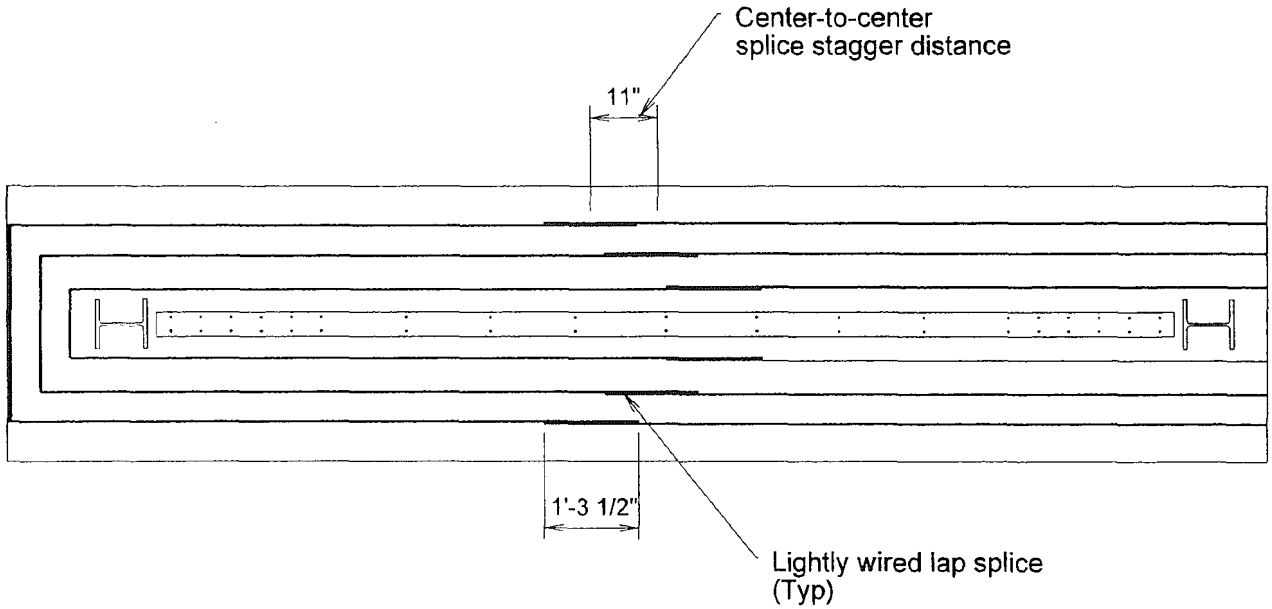

Scale: 1" = 2.5'

Figure 3.10 Reinforcement Lap Splices

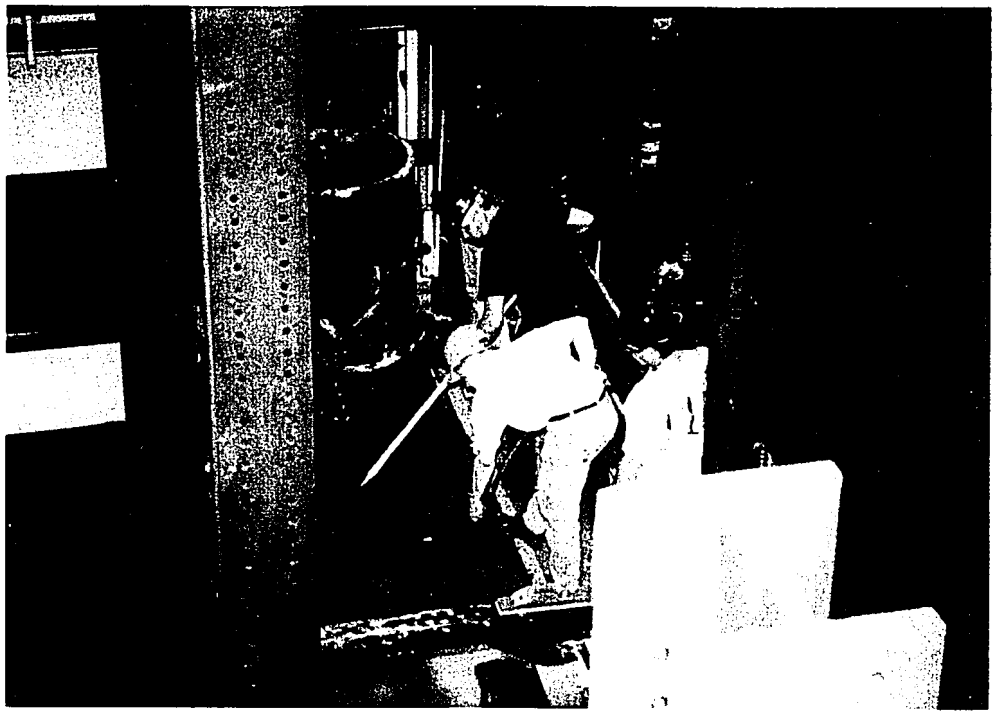

Figure 3.11 Placing Concrete Deck

Figure 3.12 Leveling Concrete Deck

Figure 3.11 Placing Concrete Deck

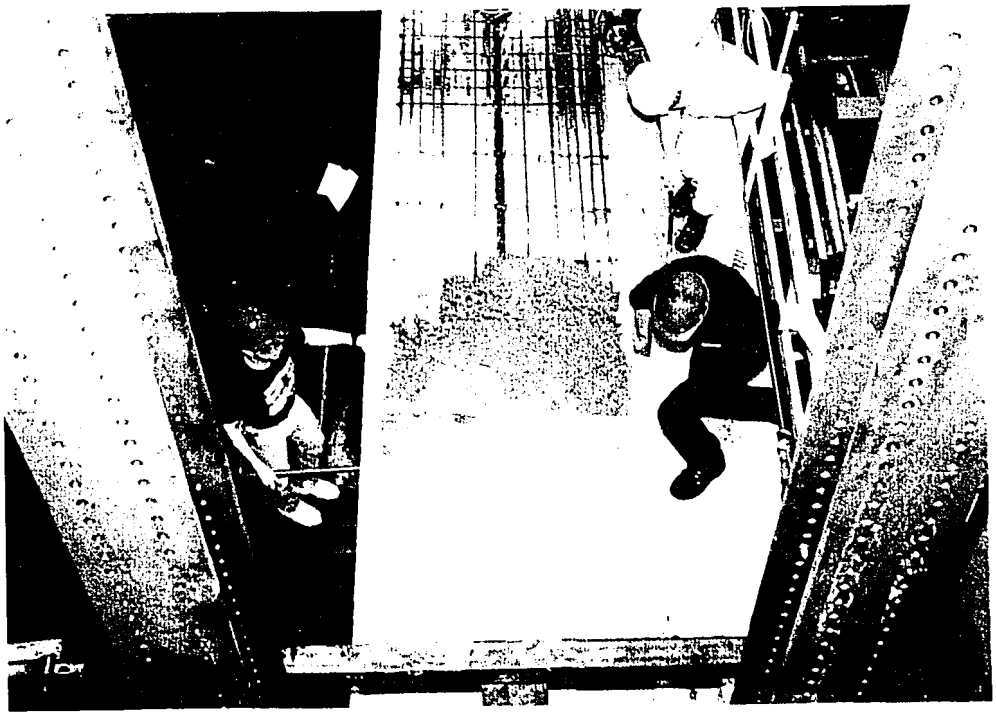

Figure 3.12 Leveling Concrete Deck

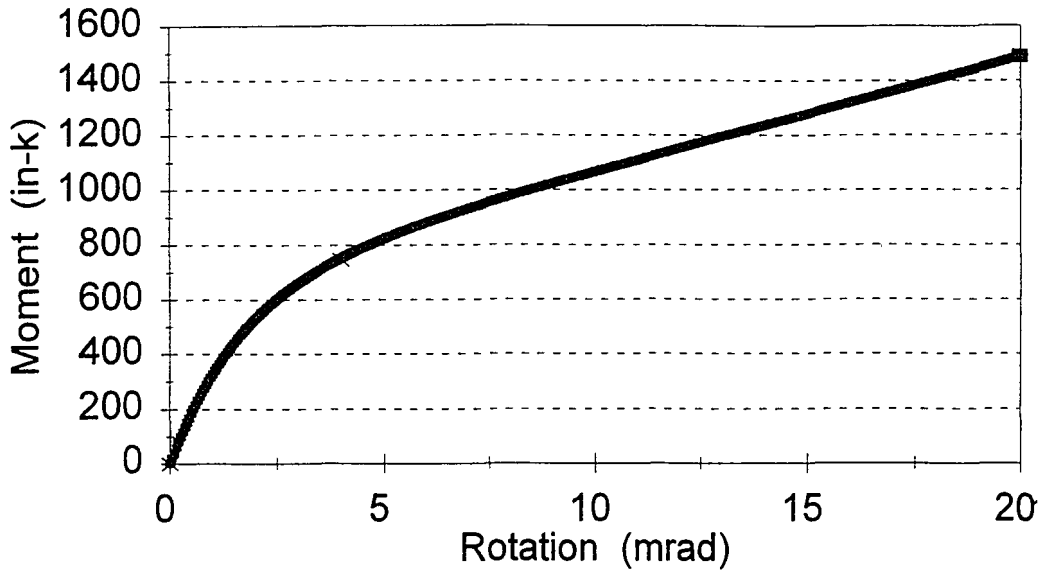

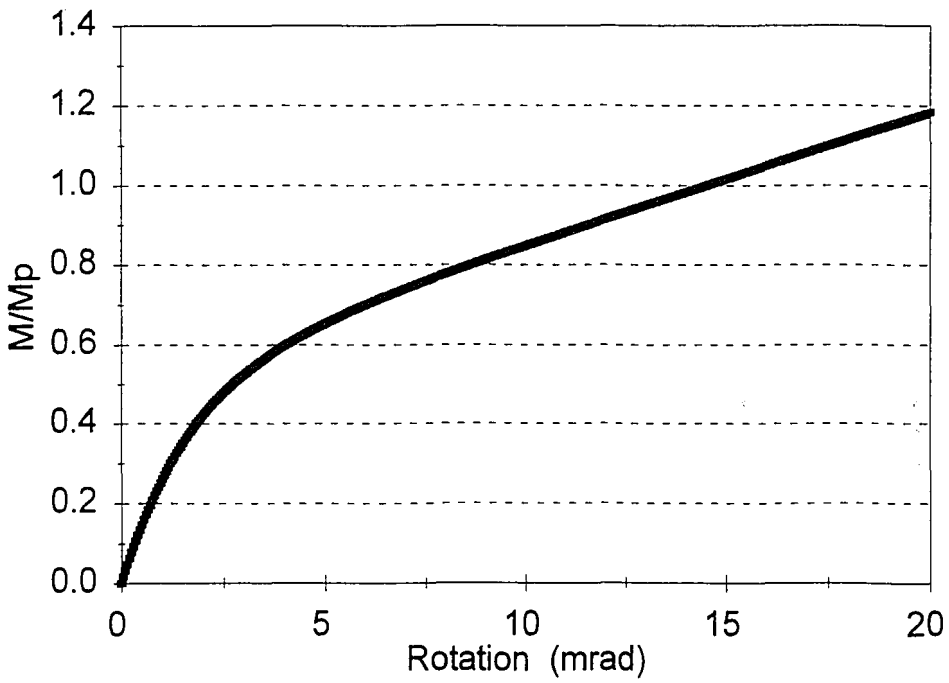

Figure 3.13 Exterior PRCC Moment-Rotation Prediction
-Monotonic Frame

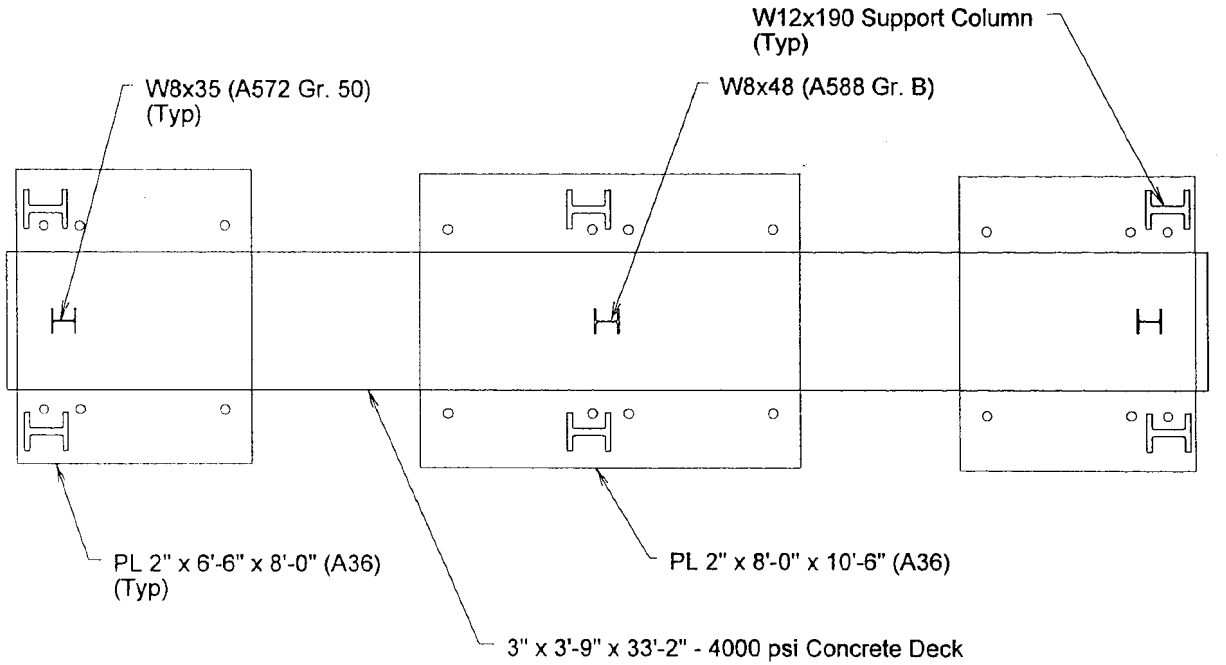

Scale: 1" = 5'

Figure 4.1 Support Frame

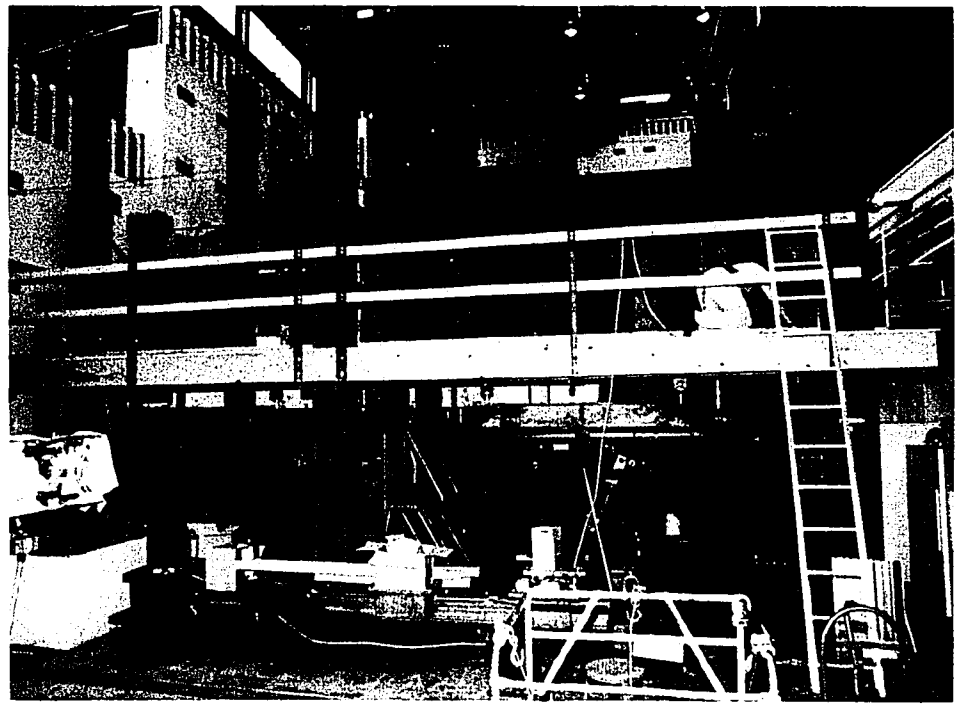

Figure 4.2 Frame with Wooden Work Platform

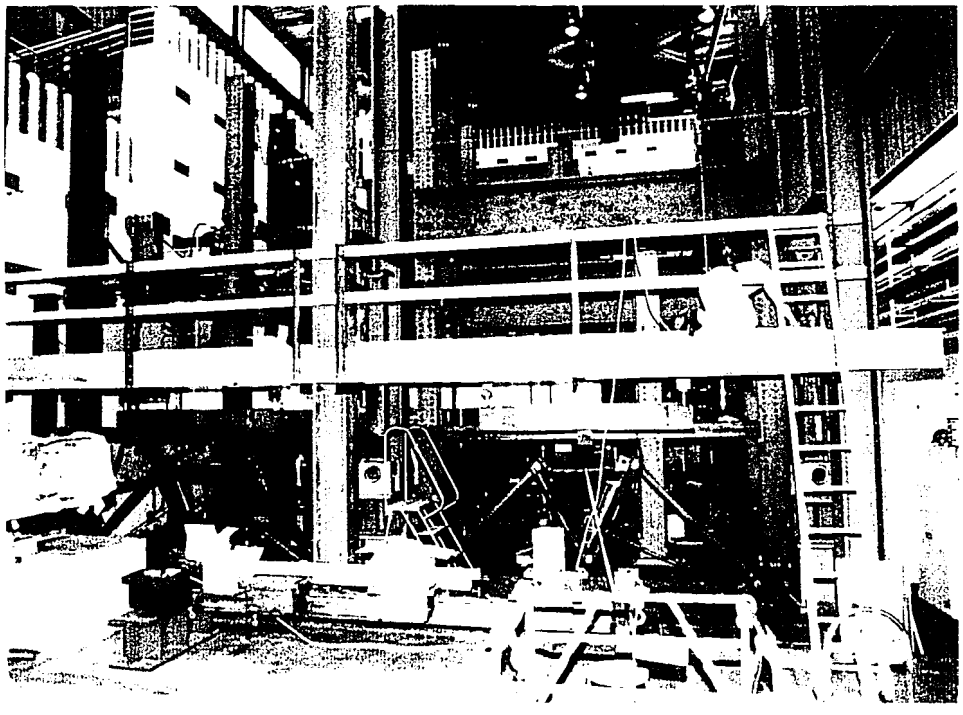

Figure 4 2 Frame with Wooden Work Platform

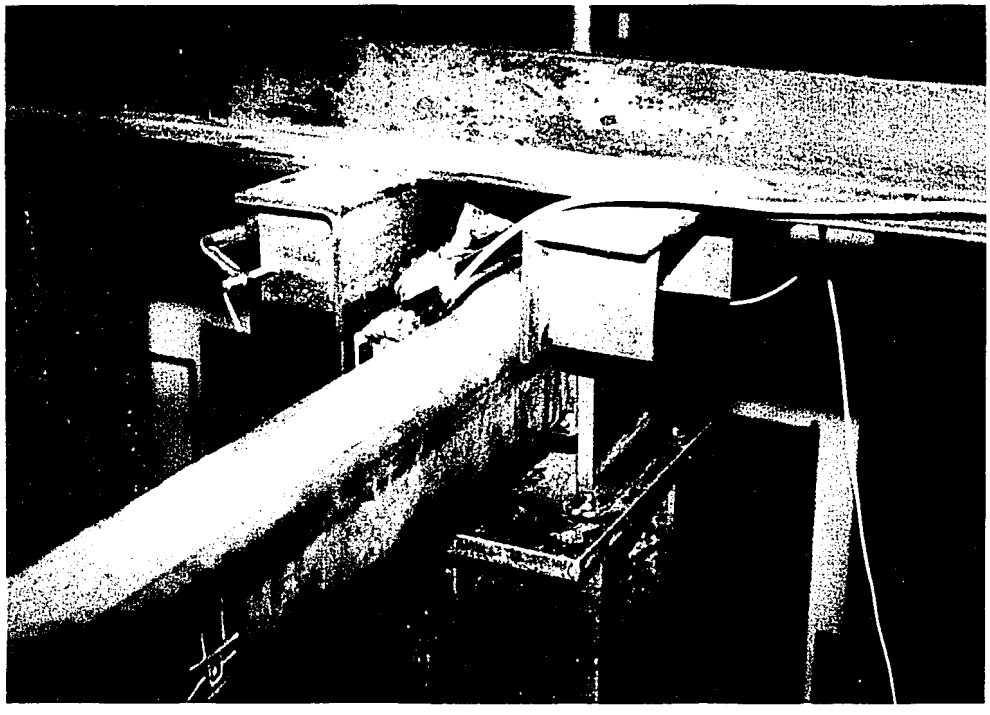

Figure 4.3 Lateral Bracing System

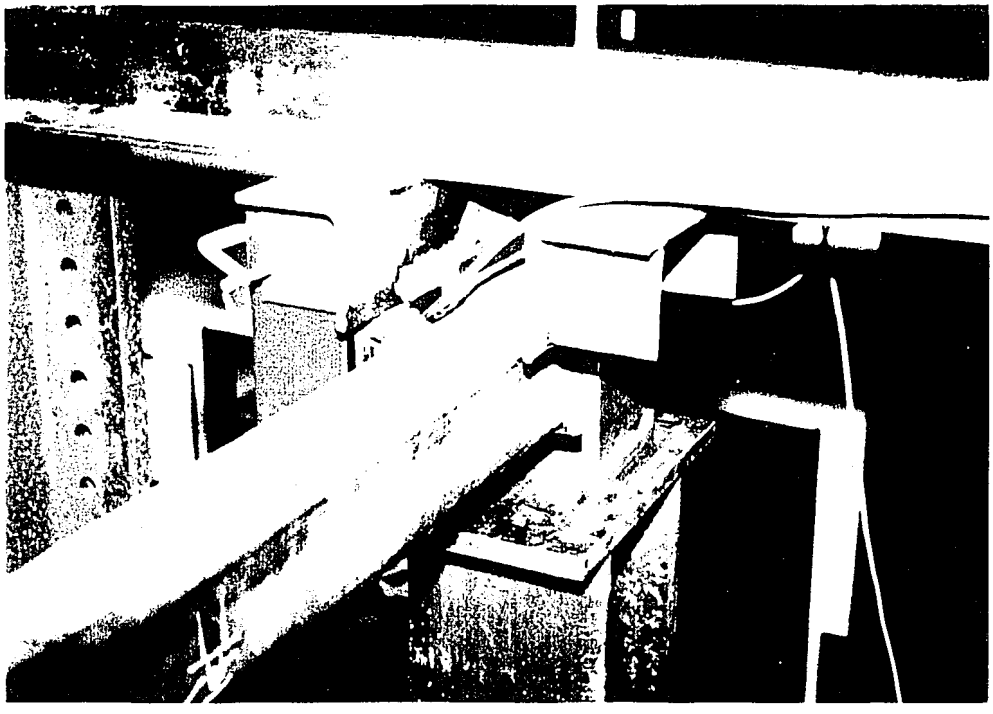

Figure 4.3 Lateral Bracing System

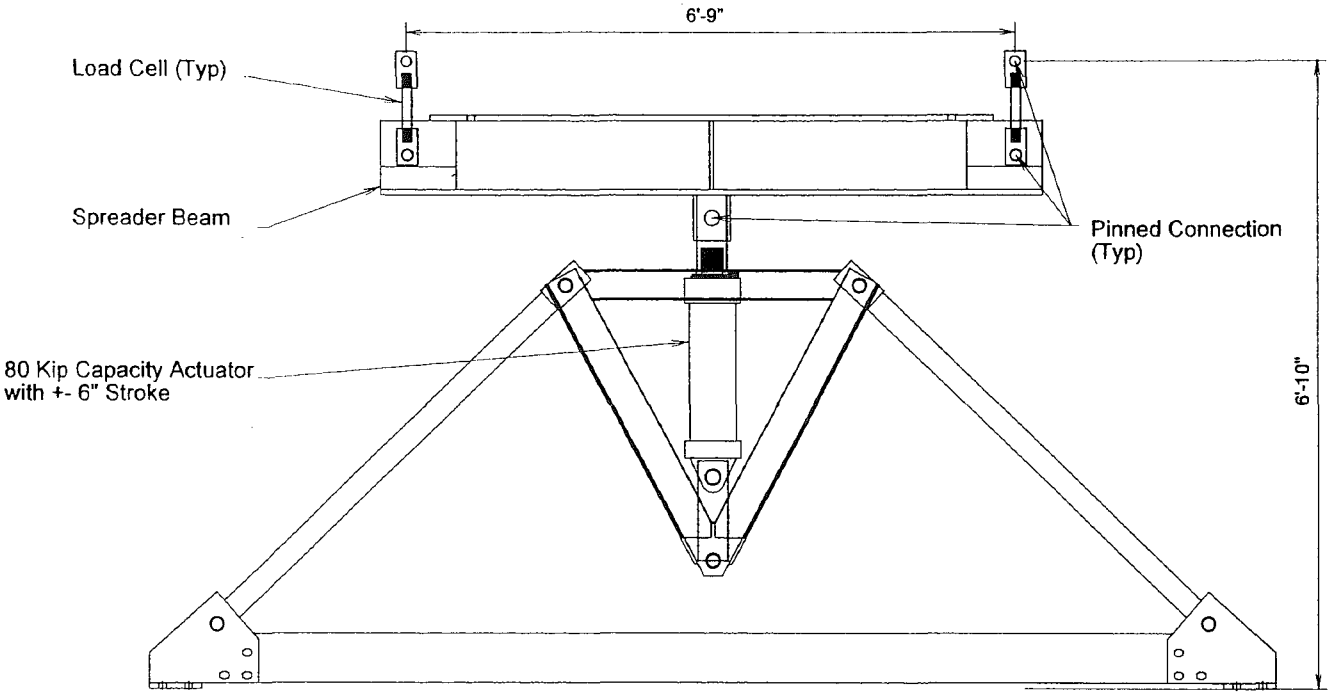

Scale: 1" = 2'

Figure 4.4 Gravity Loading System

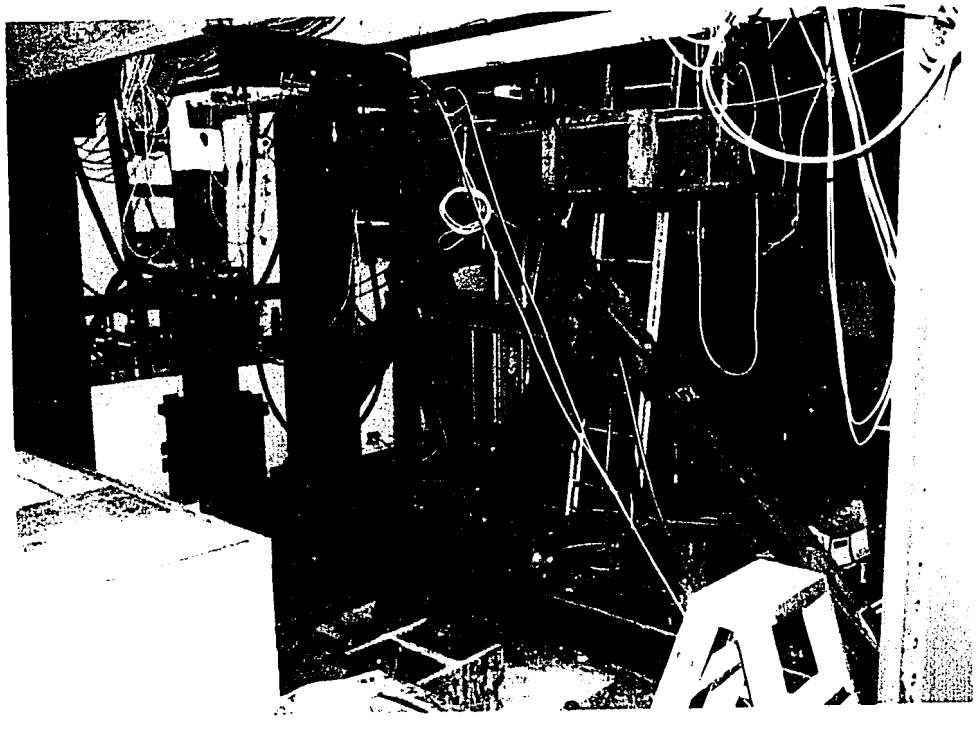

Figure 4.5 East Bay with Gravity Load Simulator

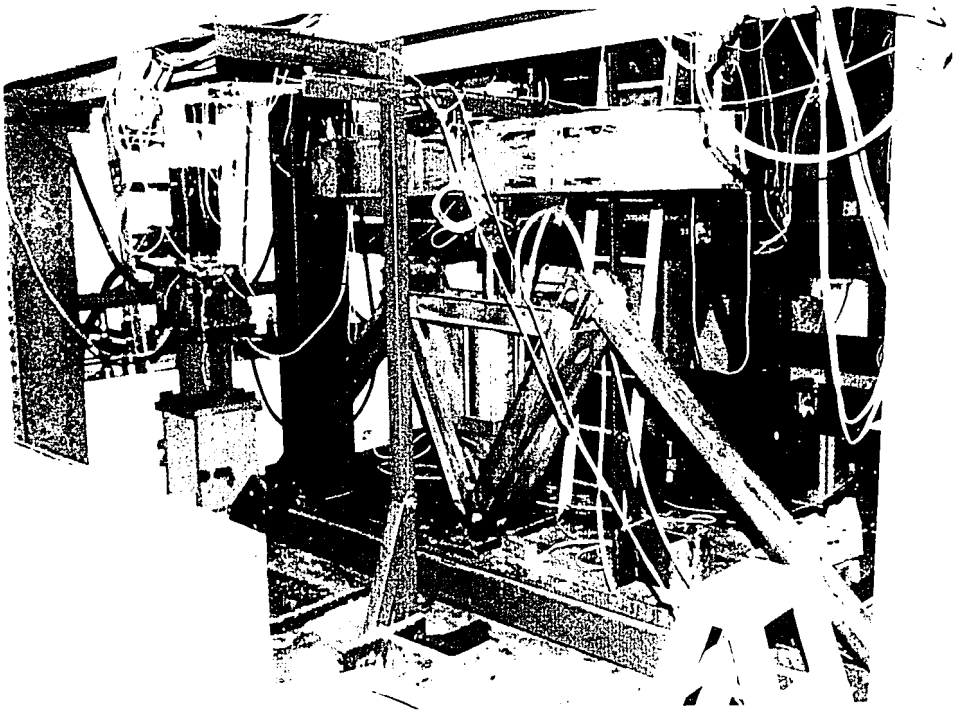

Figure 4.5 East Bay with Gravity Load Simulator

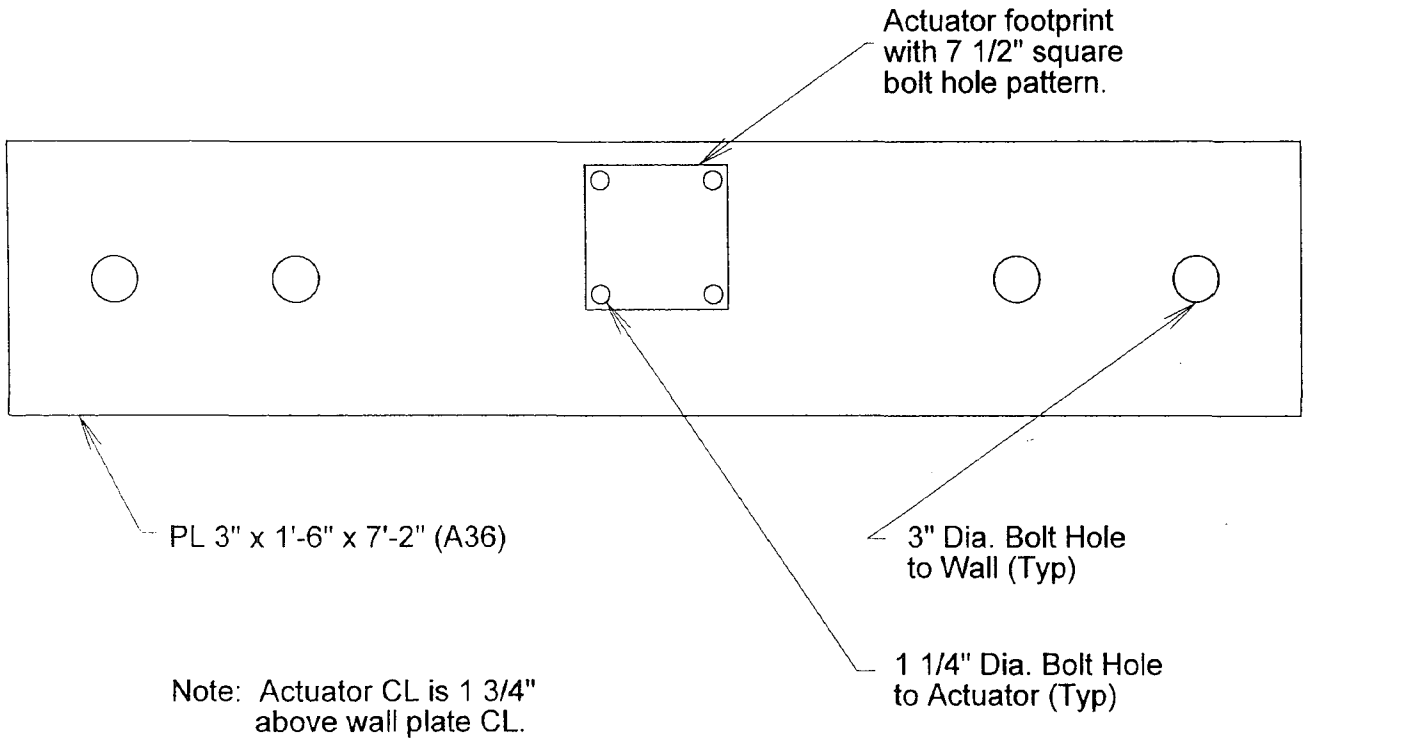

Figure 4.6 Actuator Wall Plate

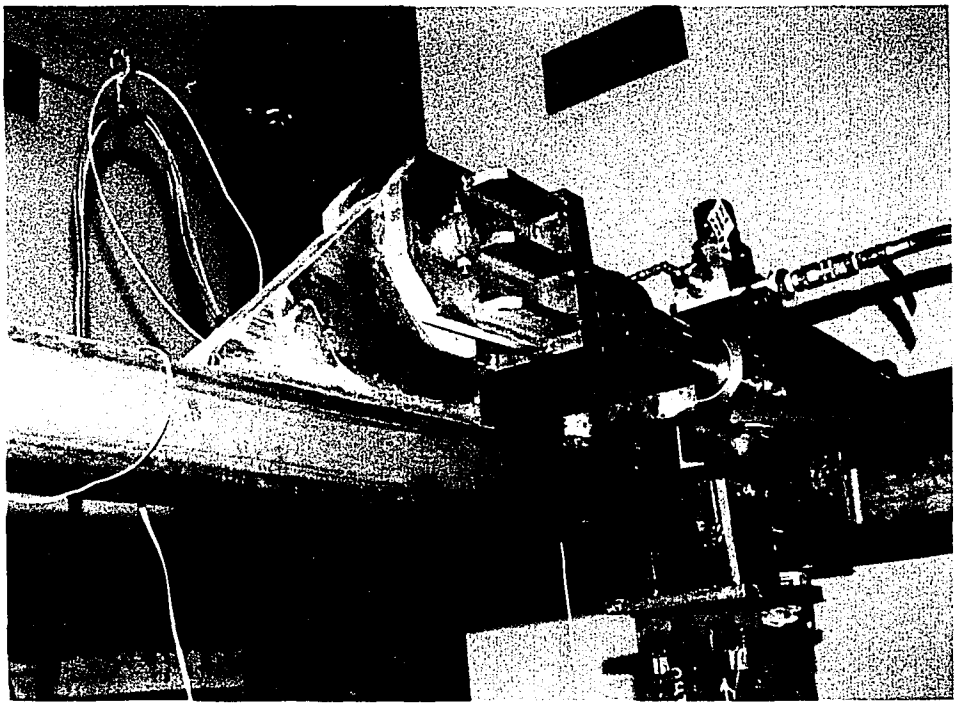

Figure 4.7 Lateral Loading System

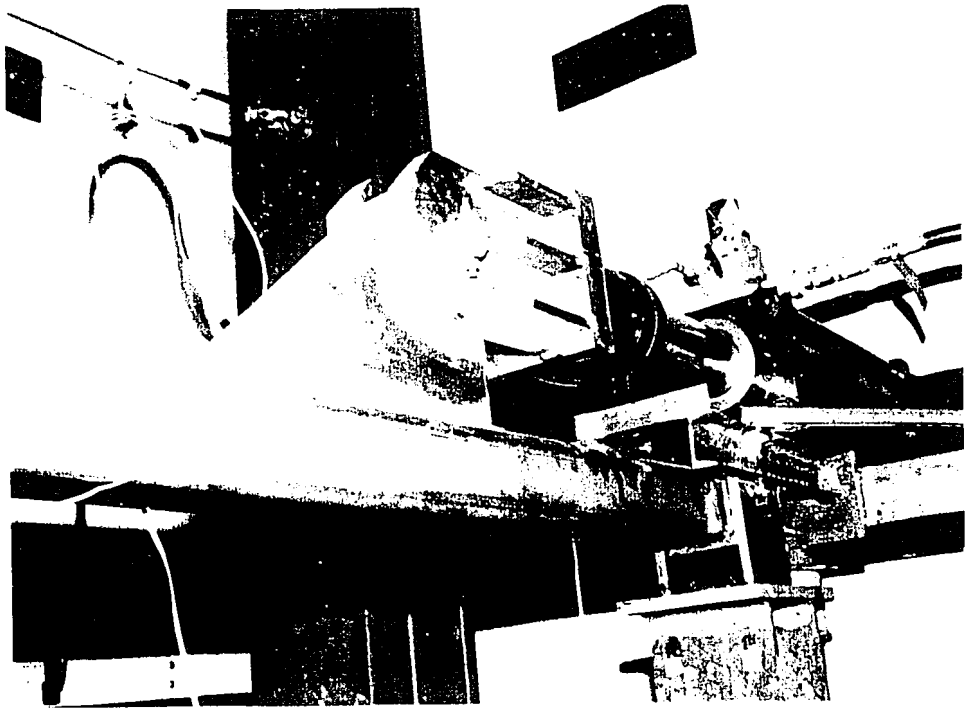

Figure 4.7 Lateral Loading System

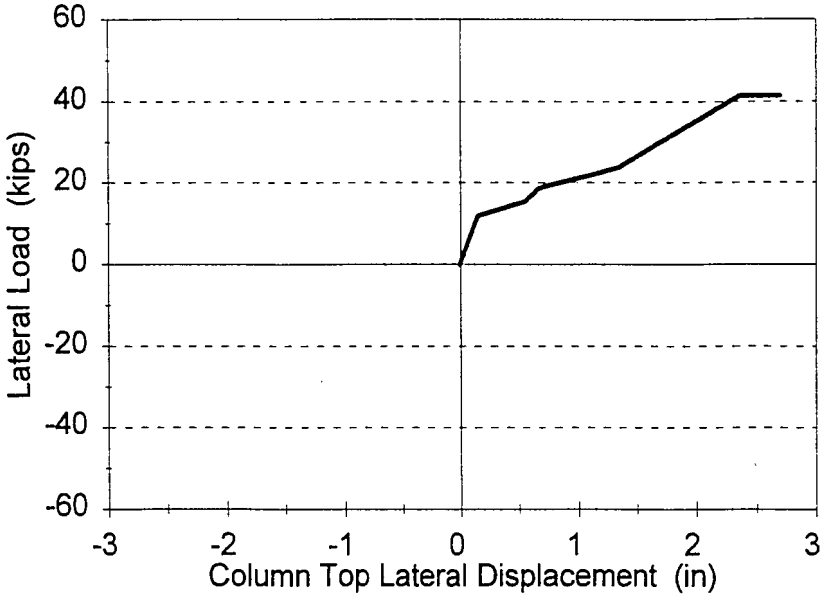

Figure 4.8 Monotonic Frame Lateral Load-Lateral Displacement Prediction

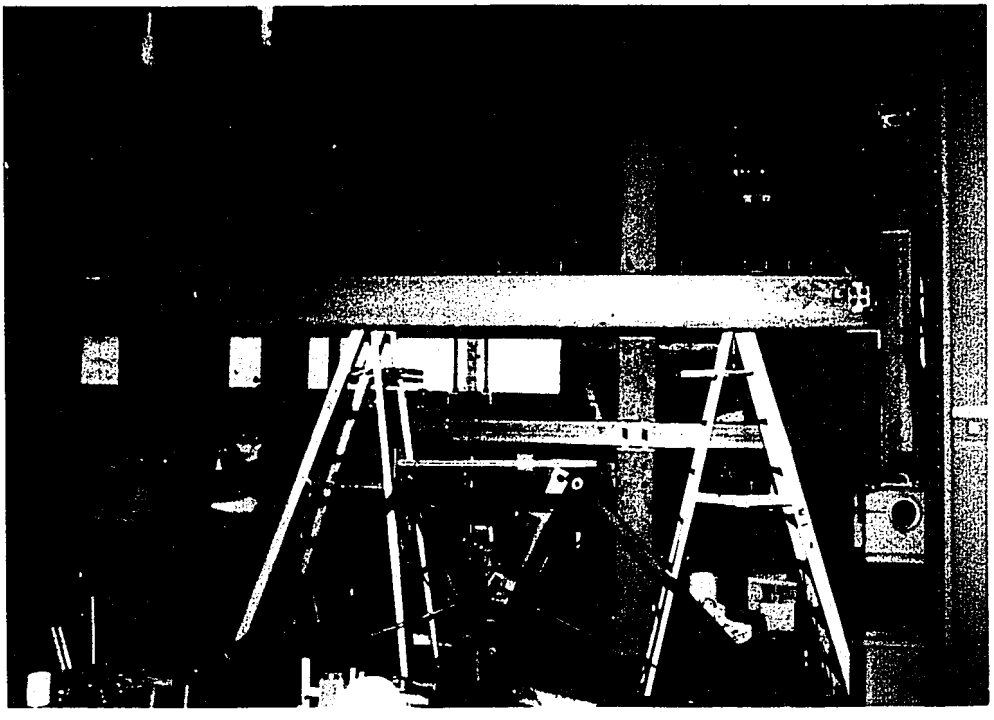

Figure 5.1 East Bay Steel Frame

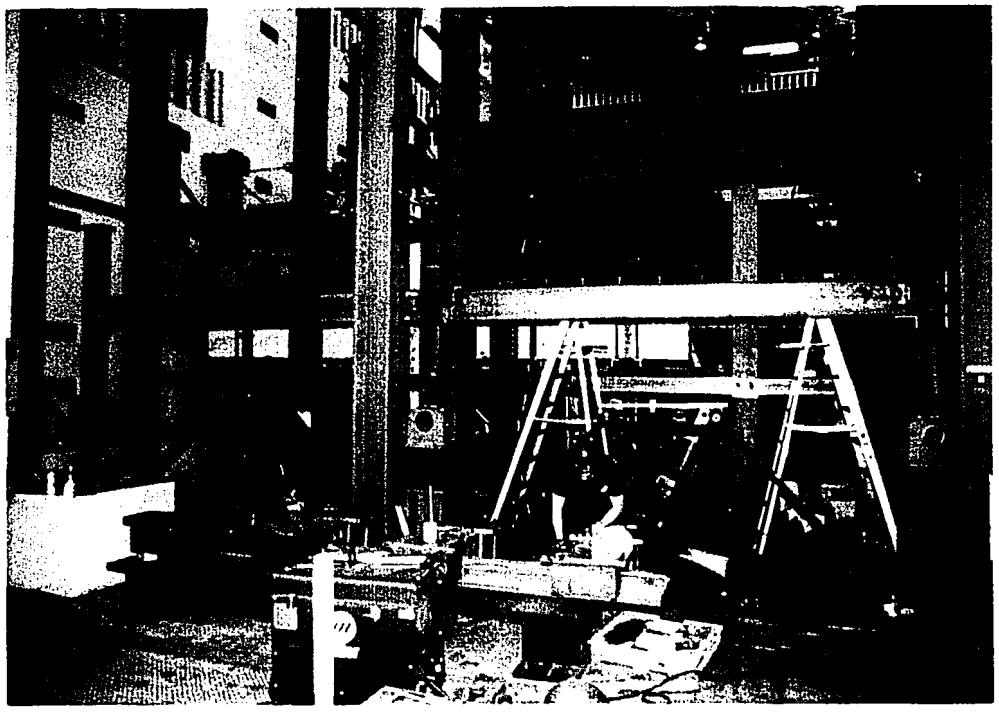

Figure 5.2 Steel Frame

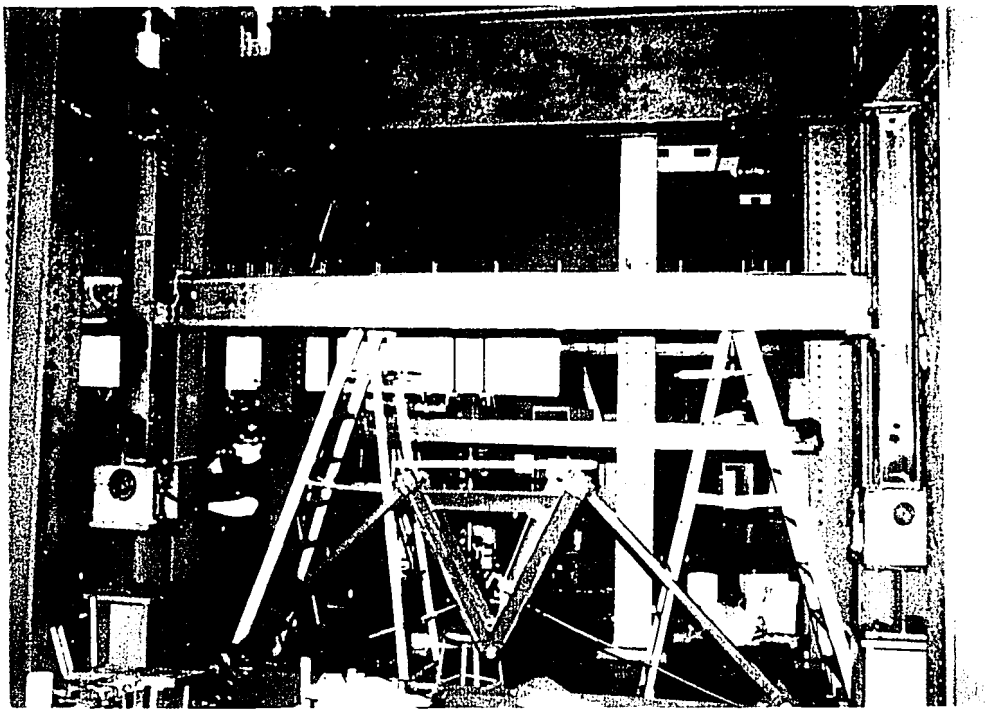

Figure 5.1 East Bay Steel Frame

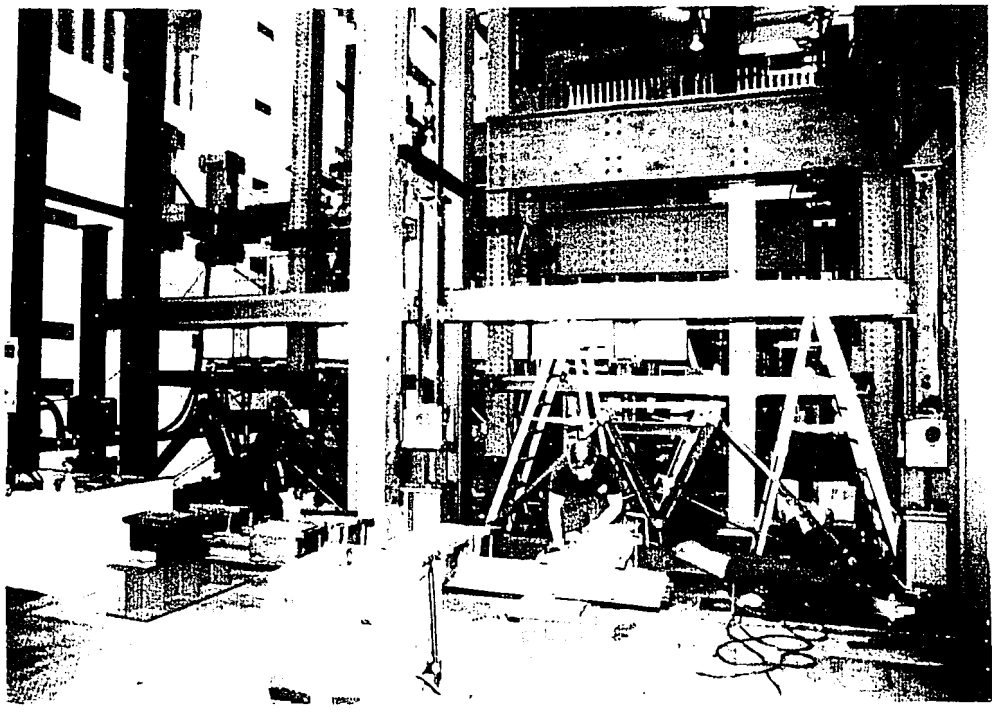

Figure 5.2 Steel Frame

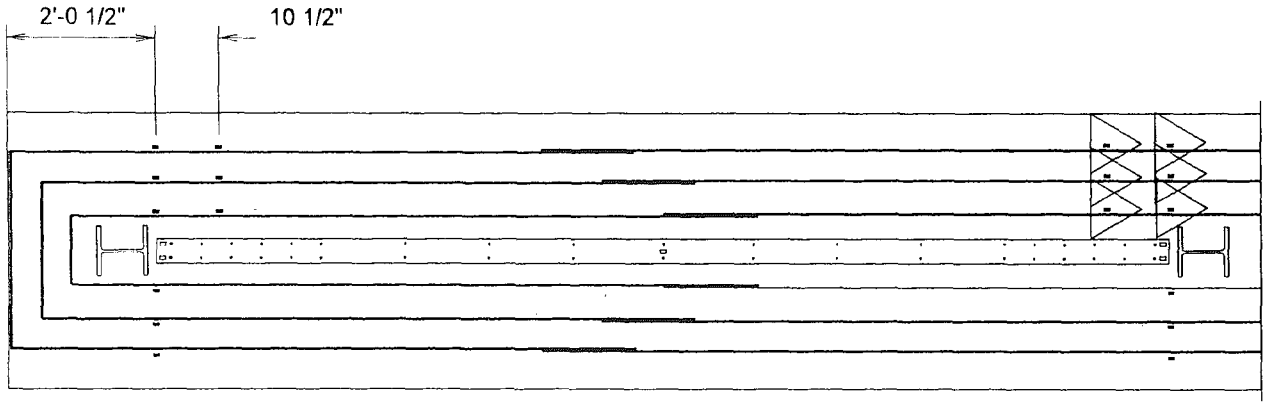

Note: All dimensions are typical for both bays.

- Strain Gage

Clip Gage

Figure 5.3 Monotonic Frame Instrumentation-Plan

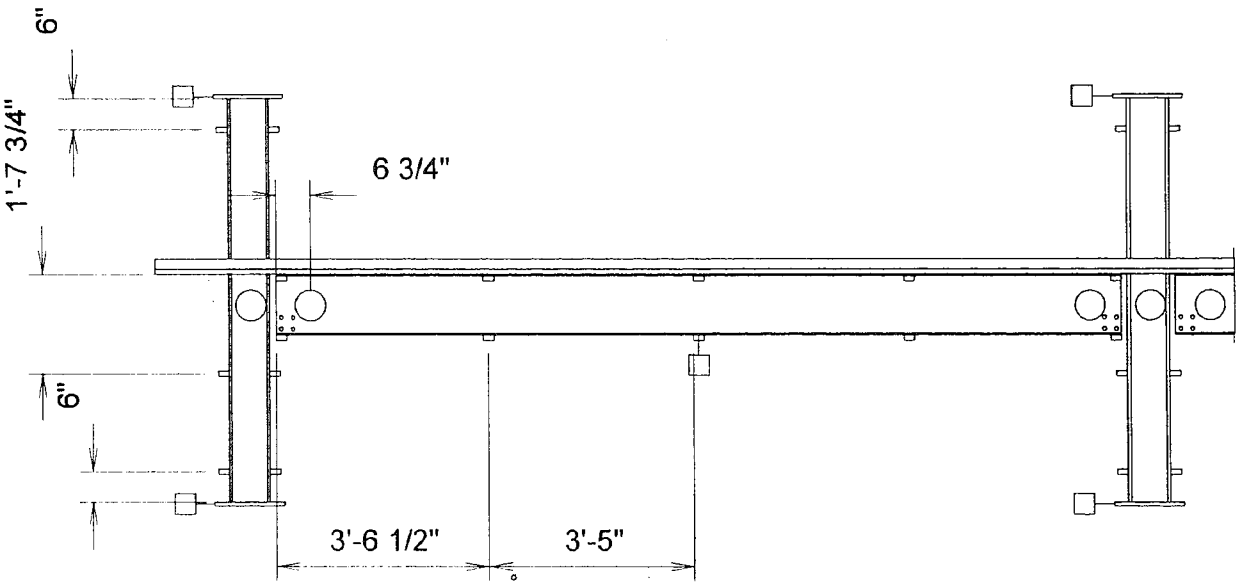

Note: All dimensions are typical for both bays.

LVDT or Trimpot
Strain Gage
Tiltmeter

Figure 5.4 Monotonic Frame Instrumentation-Elevation

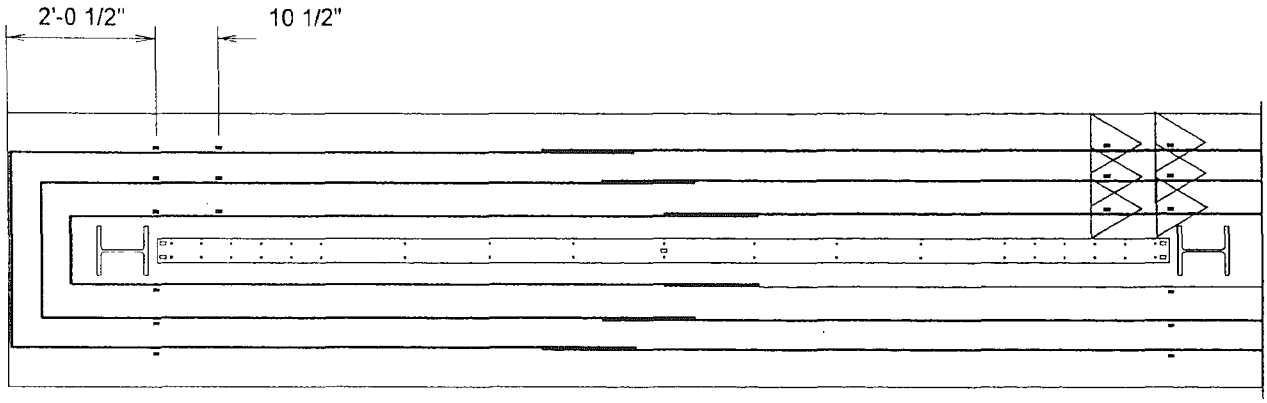

Note: All dimensions are typical for both bays.

- Strain Gage

Clip Gage

Figure 5.5 Cyclic Frame Instrumentation-Plan

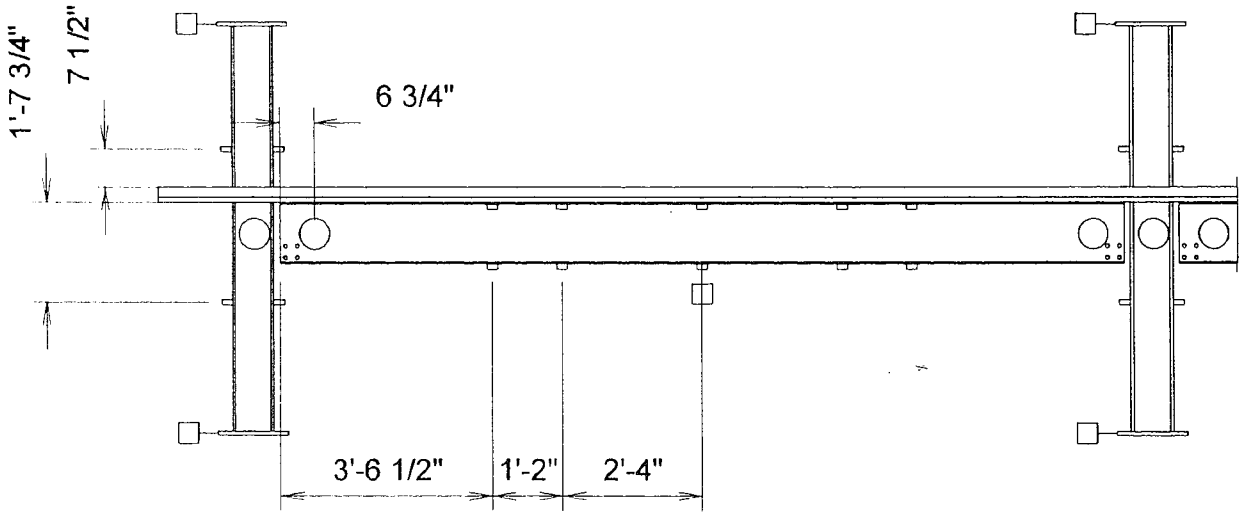

Note: All dimensions are typical for both bays.

LVDT or Trimpot
Strain Gage
Tiltmeter

Figure 5.6 Cyclic Frame Instrumentation-Elevation

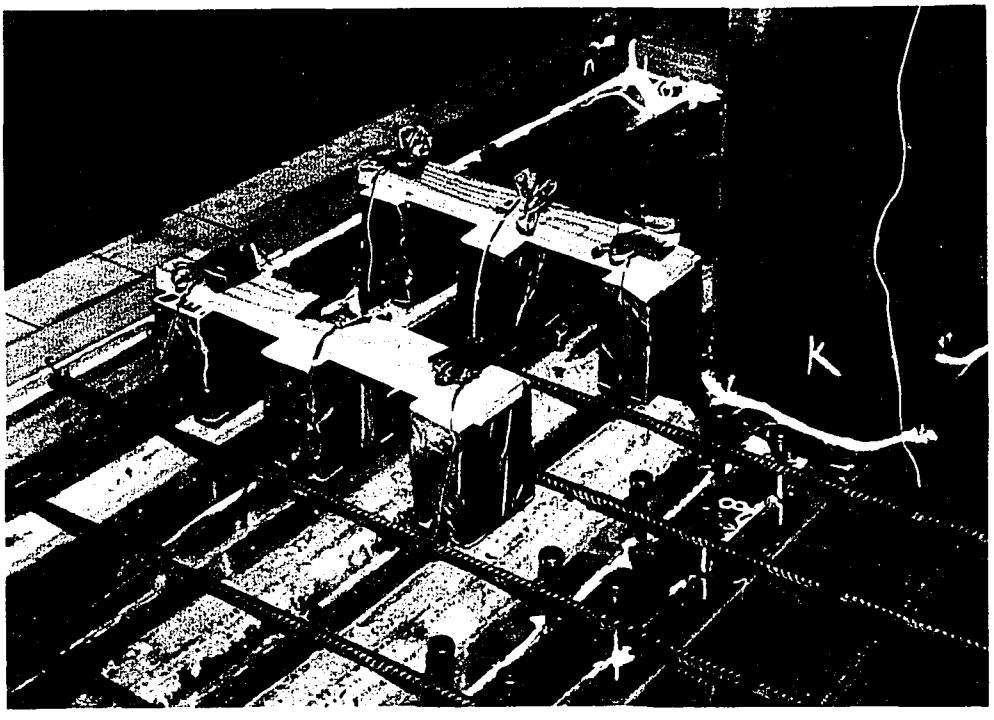

Figure 5.7 Concrete Blockouts for Clip Gages

Figure 5.8 Clip Gages

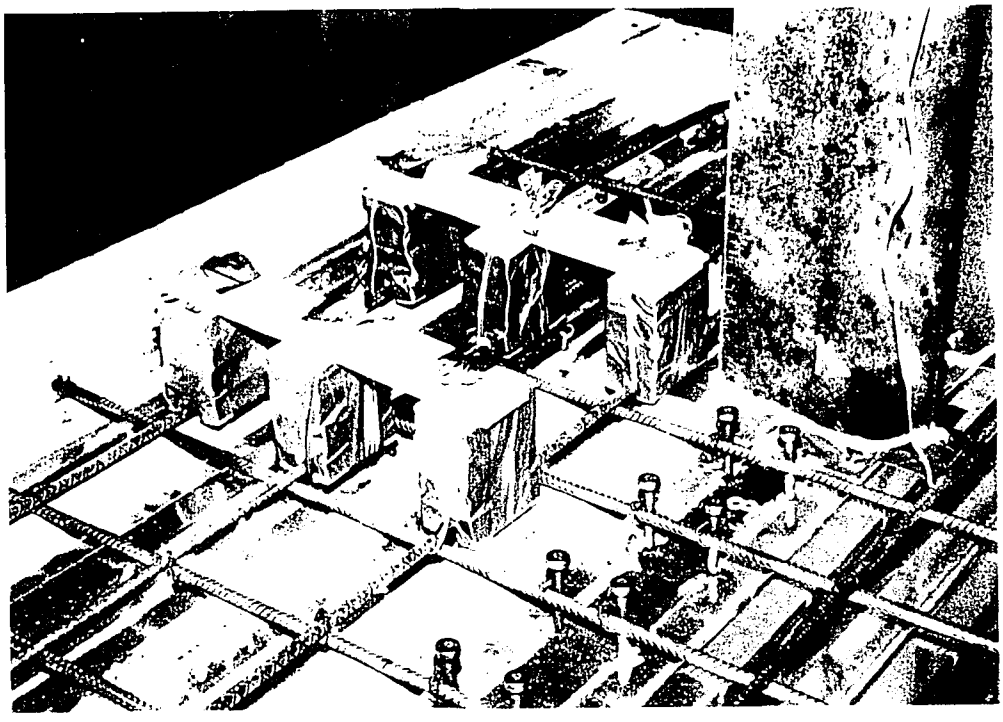

Figure 5.7 Concrete Blockouts for Clip Gages

Figure 5.8 Clip Gages

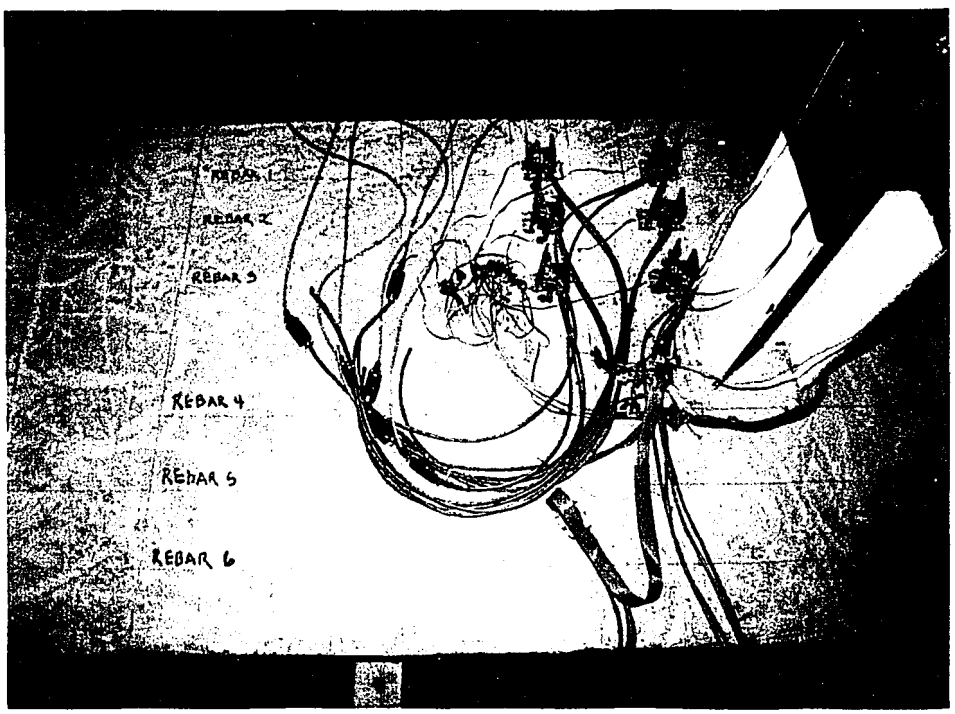

Figure 5.9 Exterior Connection

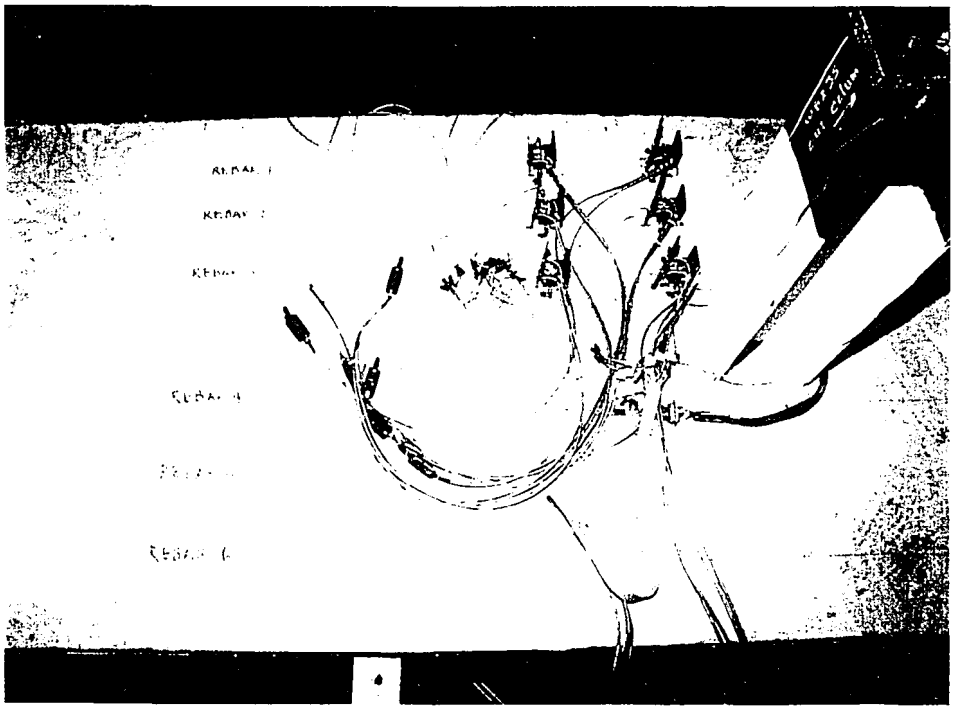

Figure 5.9 Exterior Connection

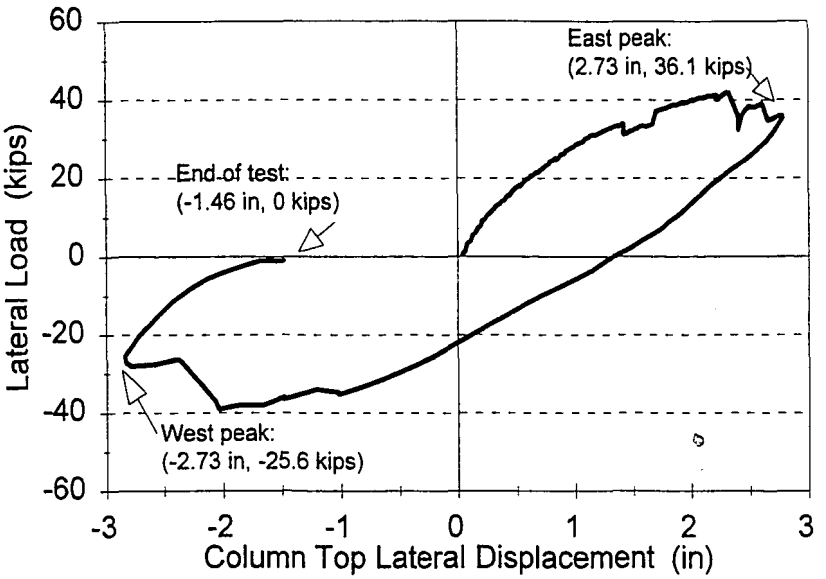

Figure 5.10 Monotonic Frame Lateral Load-Lateral Displacement Curve

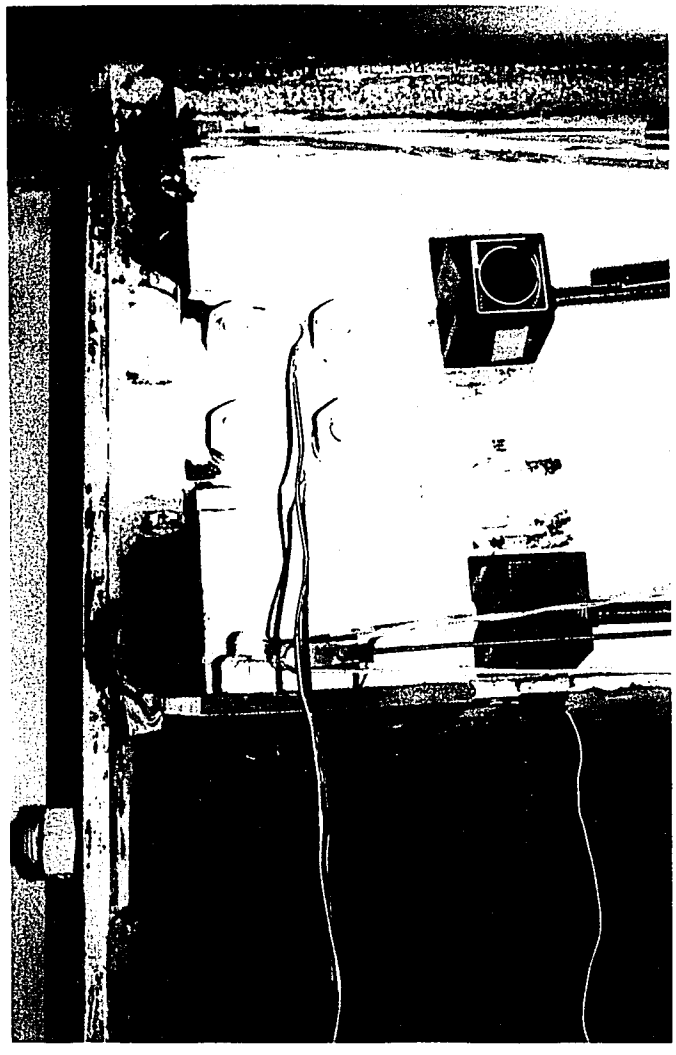

Figure 5.11 Seat Angle Separation at Exterior Connection 1 at East Peak

Figure 5.11 Seat Angle Separation at Exterior Connection 1 at East Peak

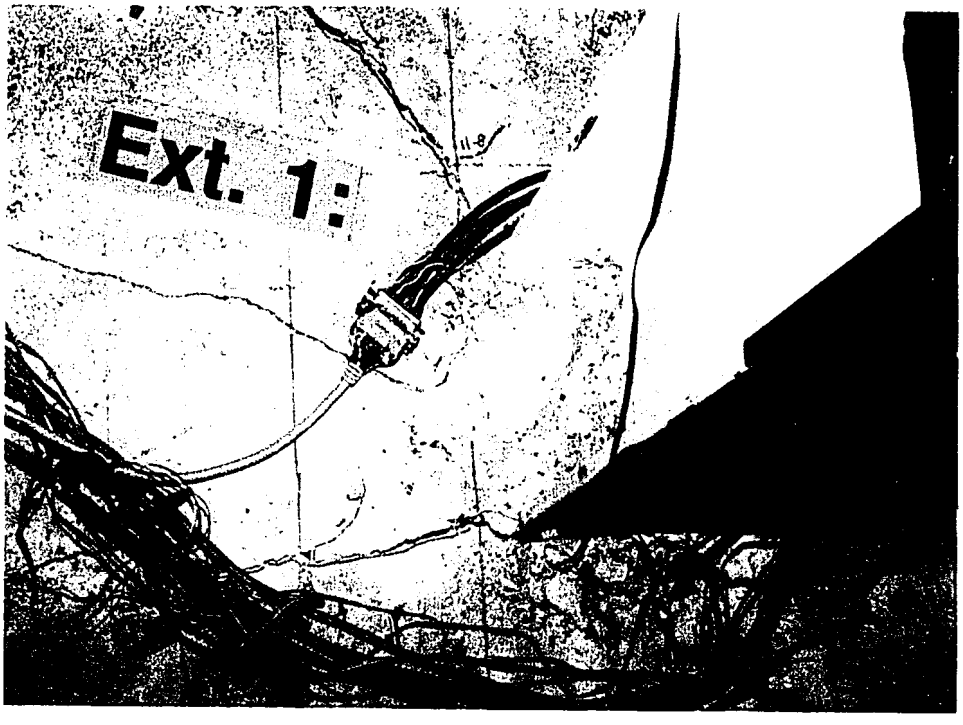

Figure 5.12 Concrete Crushing at Exterior Connection 1

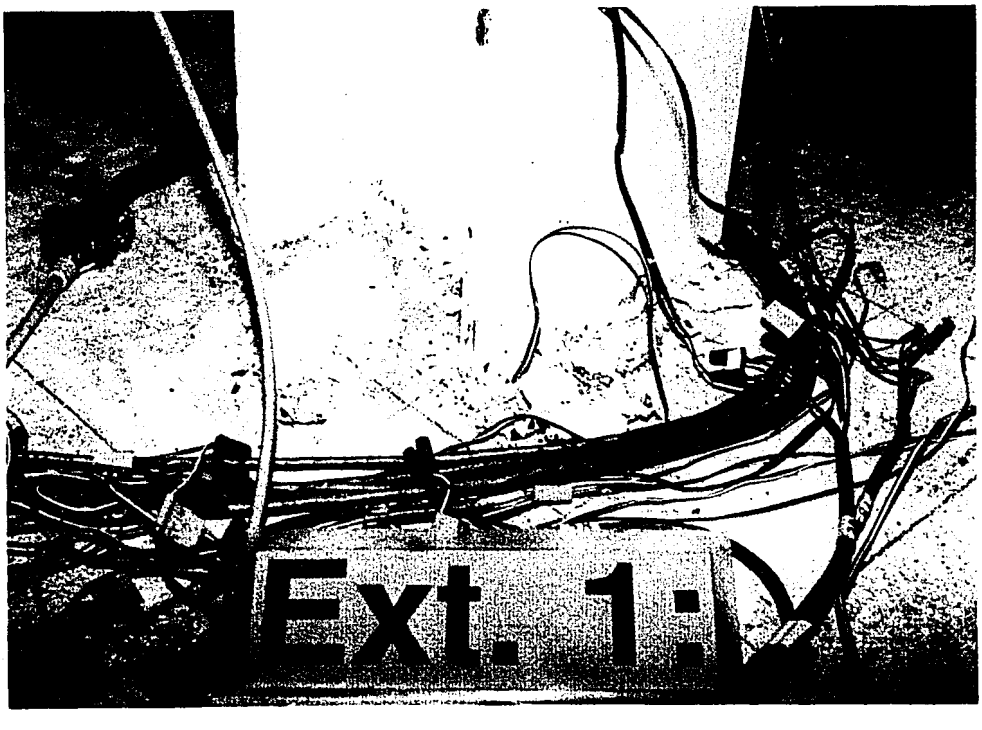

Figure 5.13 Exterior Connection 1 at East Peak

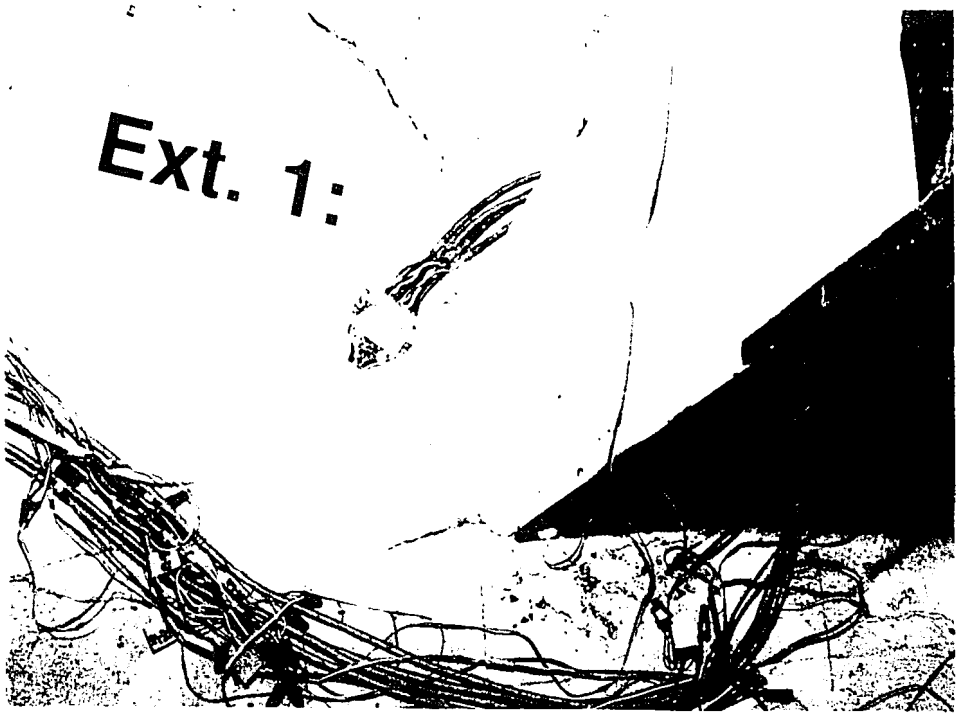

Figure 5.12 Concrete Crushing at Exterior Connection 1

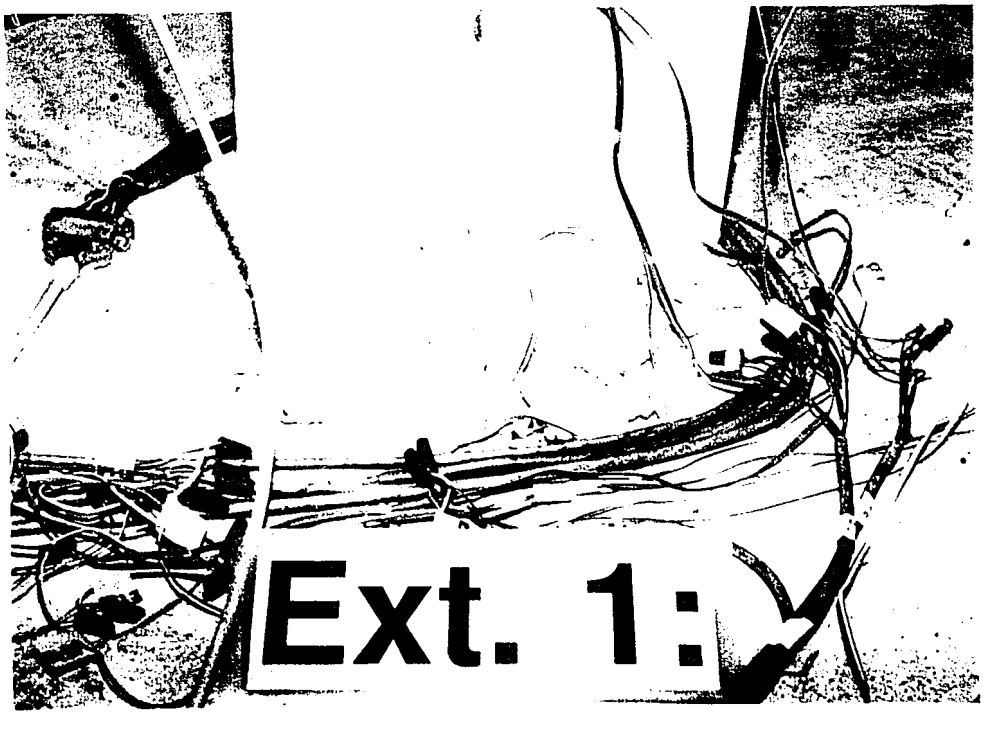

Figure 5.13 Exterior Connection 1 at East Peak

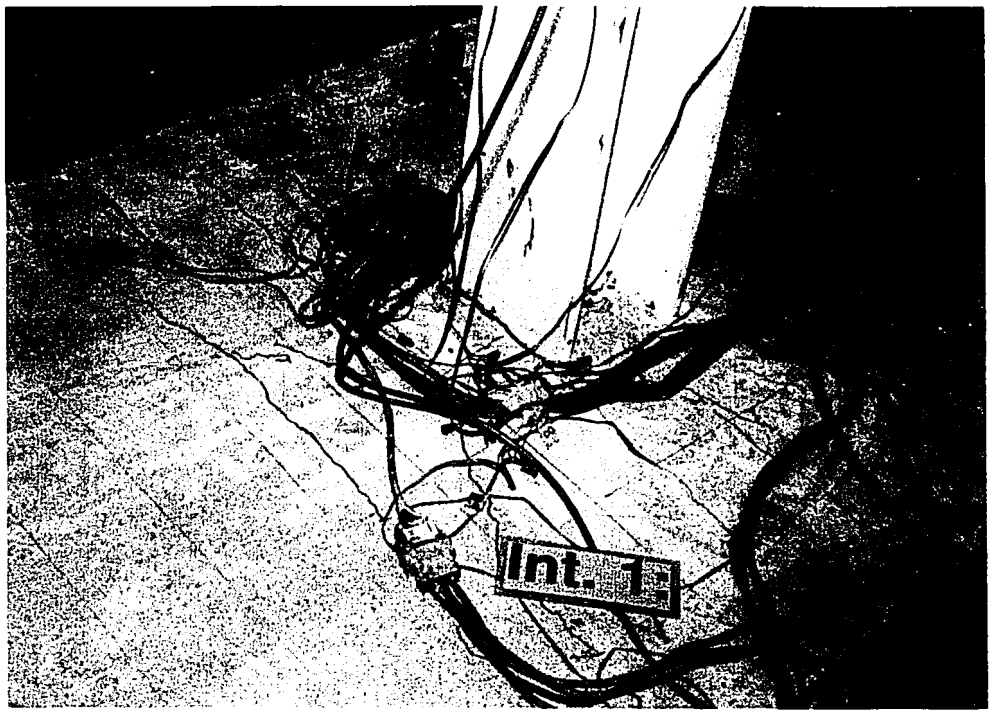

Figure 5.14 Concrete Cracking at Interior Connection 1 at East Peak

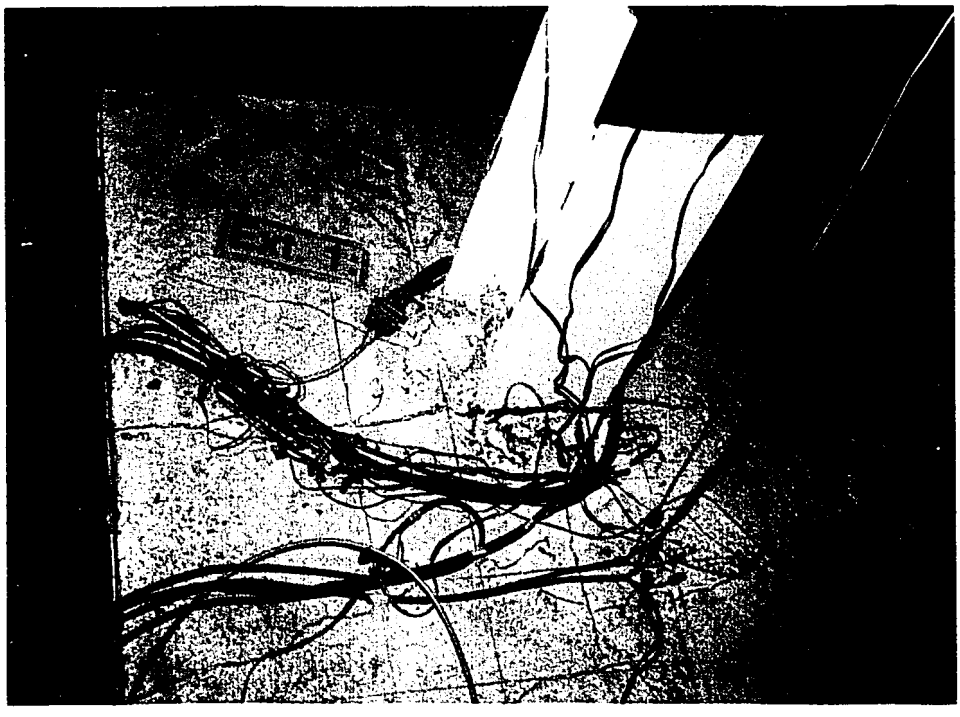

Figure 5.15 Concrete Cracking at Exterior Connection 1 at West Peak

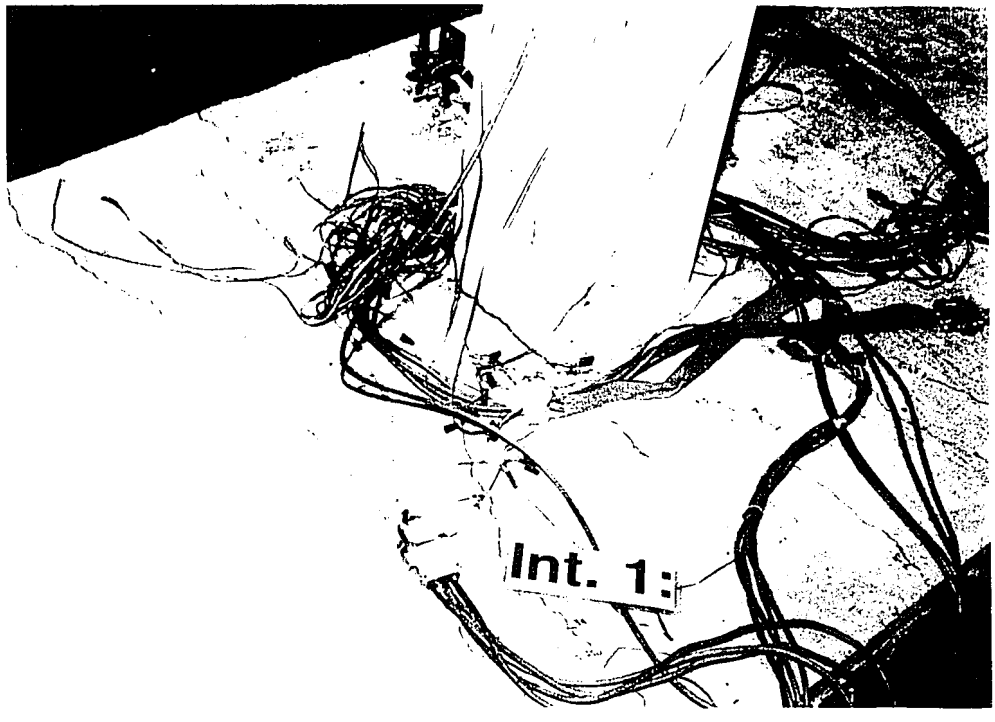

Figure 5.14 Concrete Cracking at Interior Connection 1 at East Peak

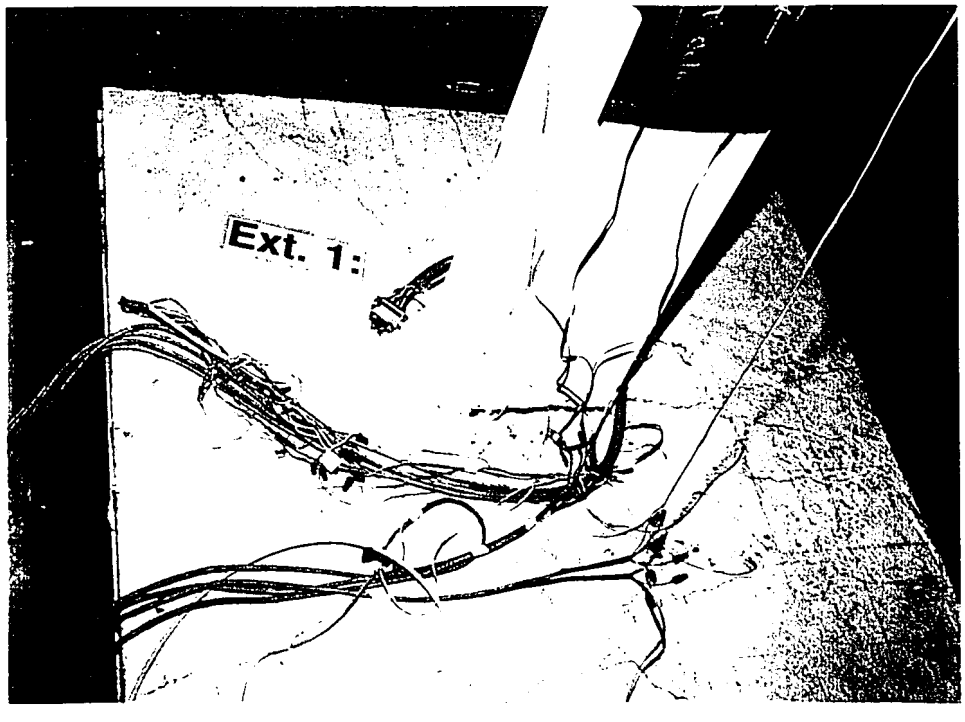

Figure 5.15 Concrete Cracking at Exterior Connection 1 at West Peak

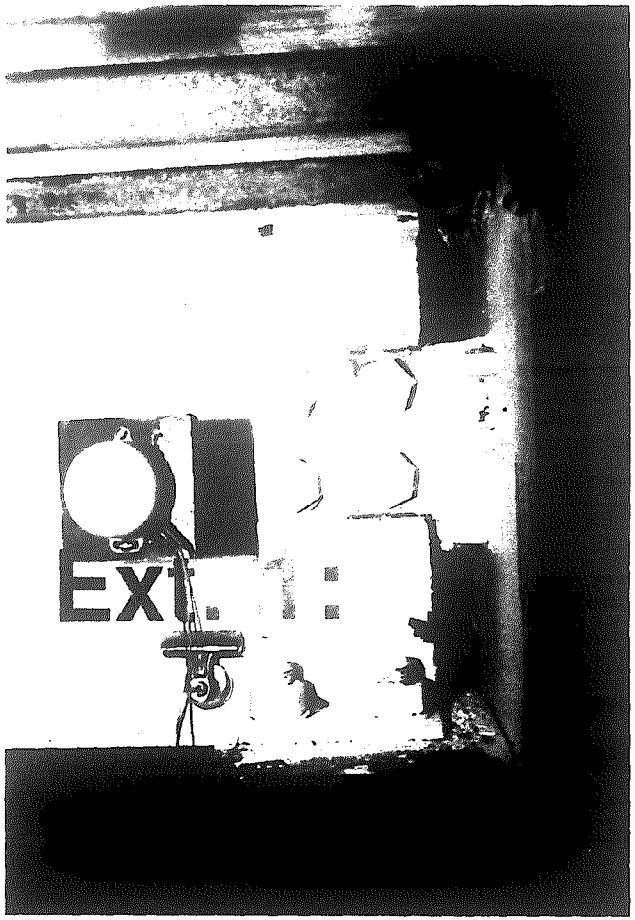

Figure 5.16 Exterior Connection 1 at West Peak

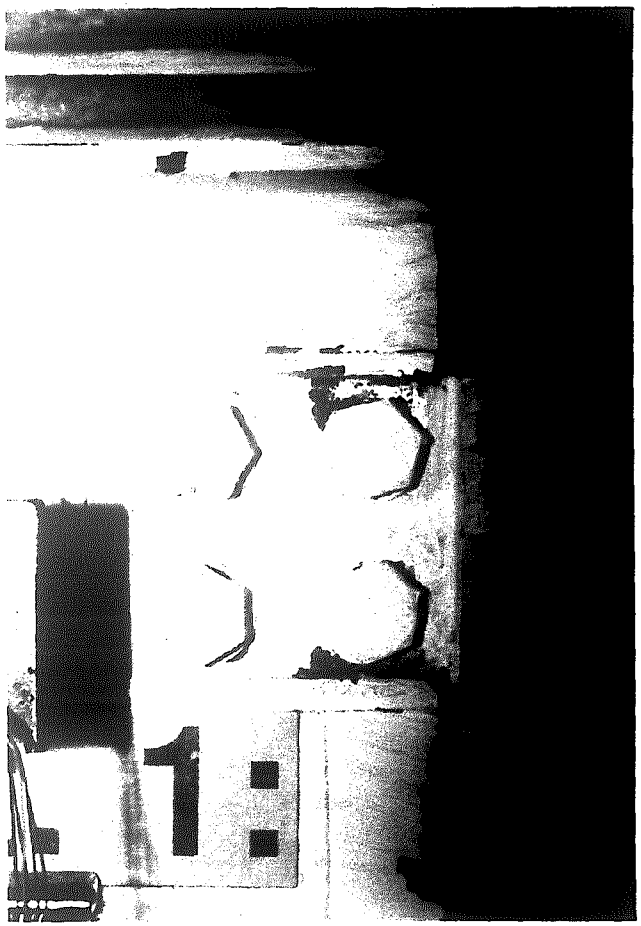

Figure 5.17 Exterior Connection 1

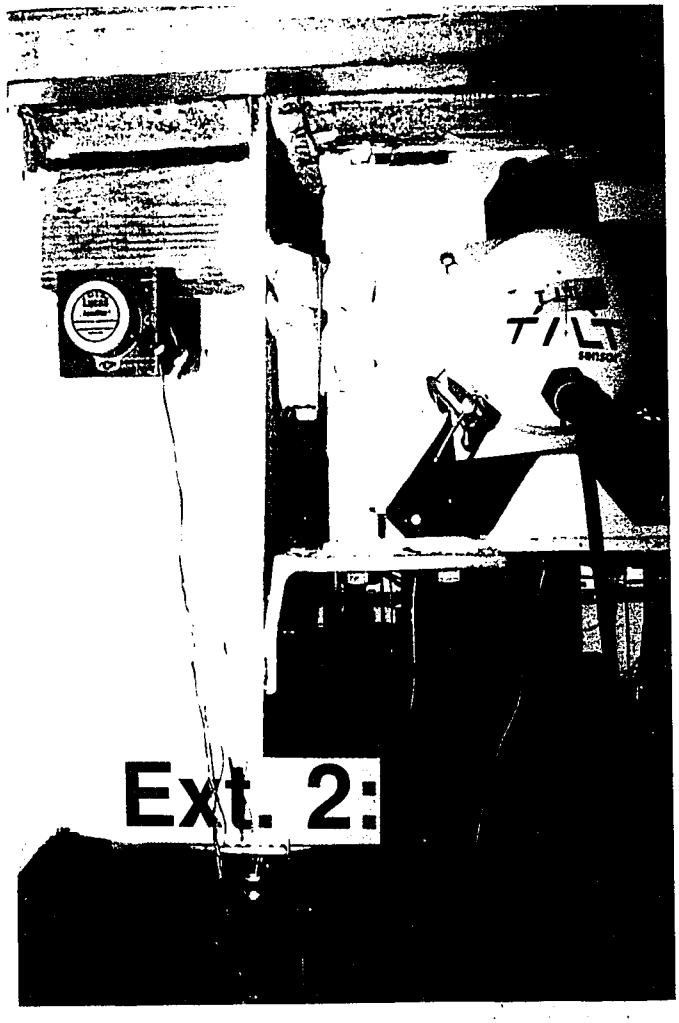

Figure 5.18 Rotation at Exterior Connection 1

Figure 5.18 Rotation at Exterior Connection 1

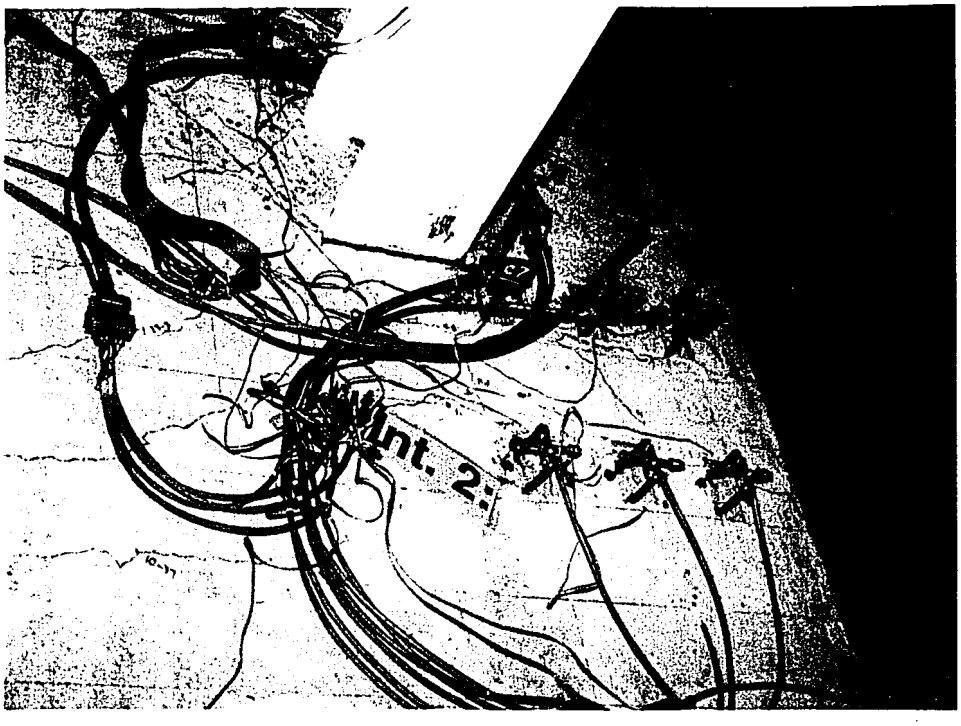

Figure 5.19 Interior Connection 2 at West Peak

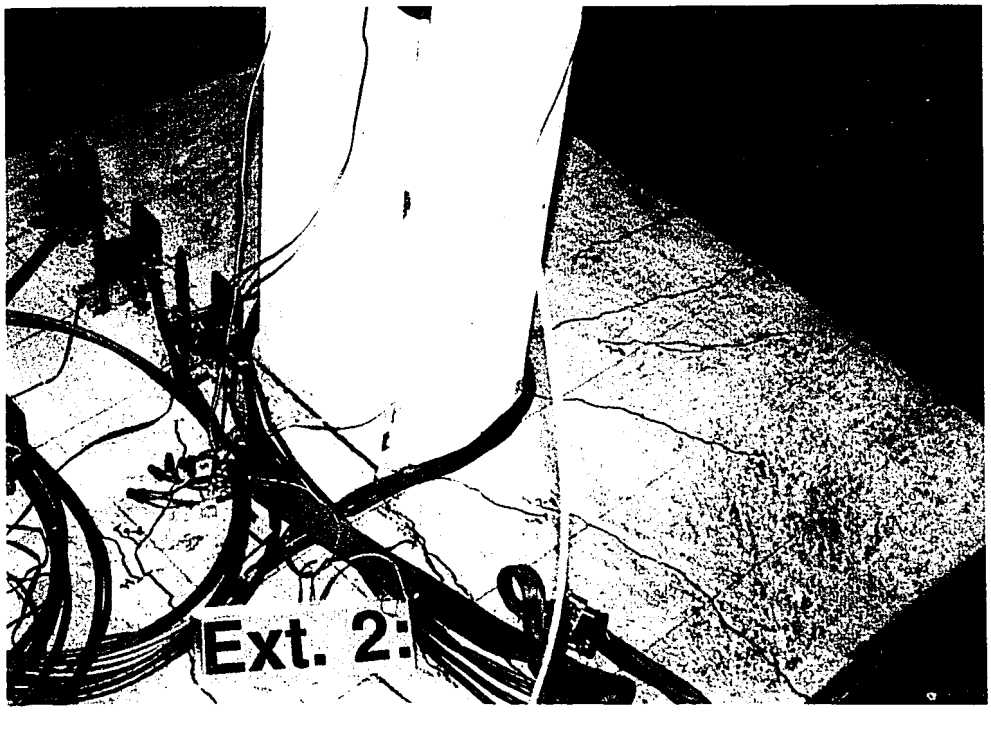

Figure 5.20 Exterior Connection 2 at West Peak

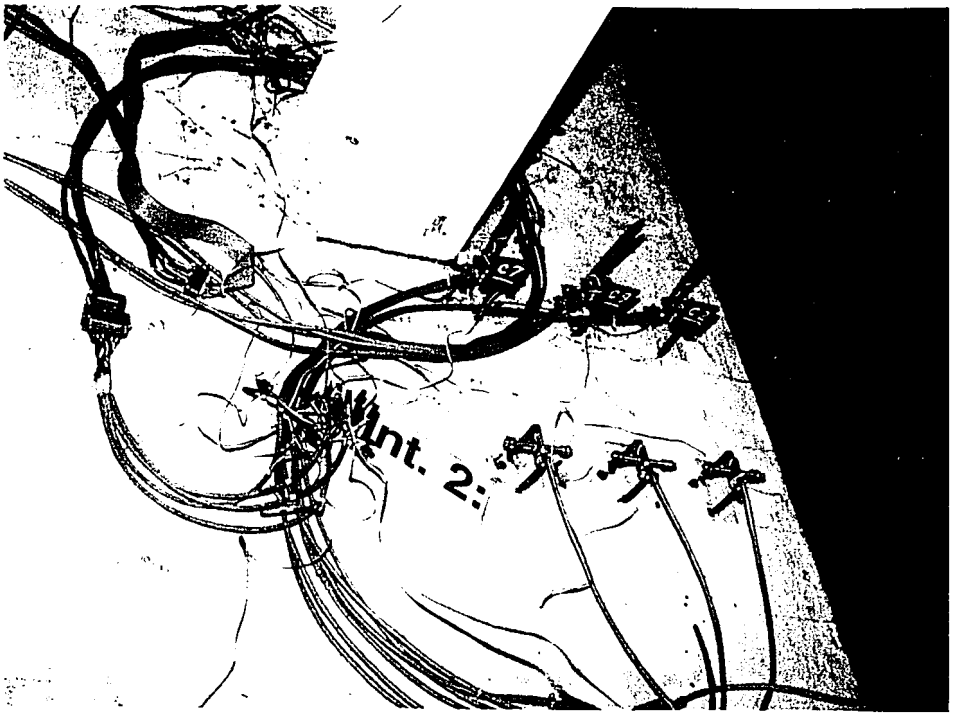

Figure 5.19 Interior Connection 2 at West Peak

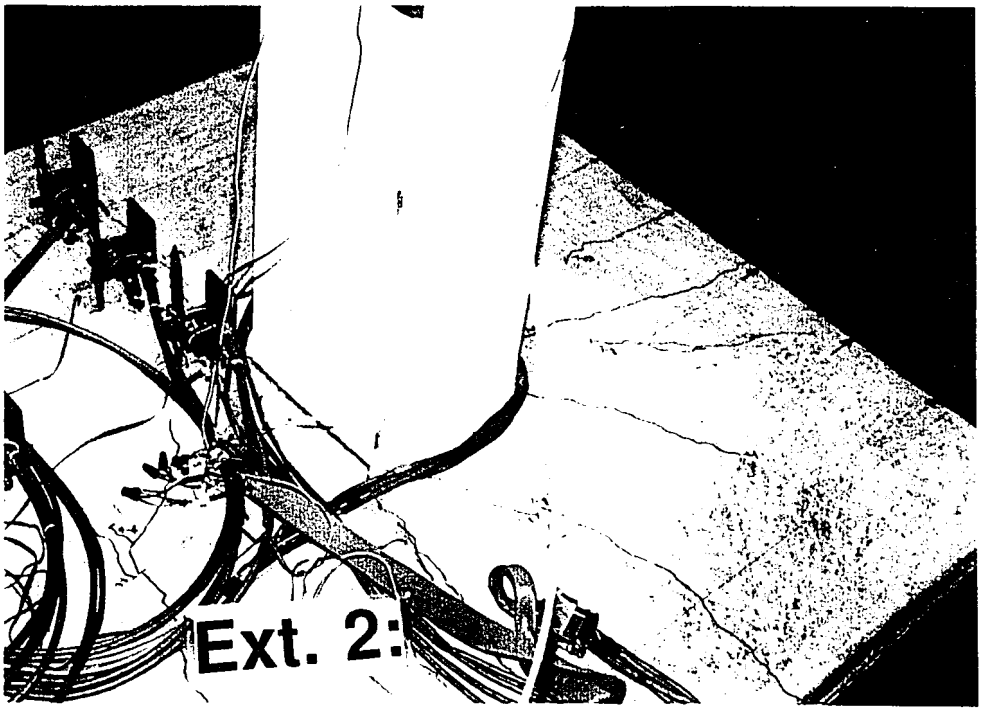

Figure 5.20 Exterior Connection 2 at West Peak

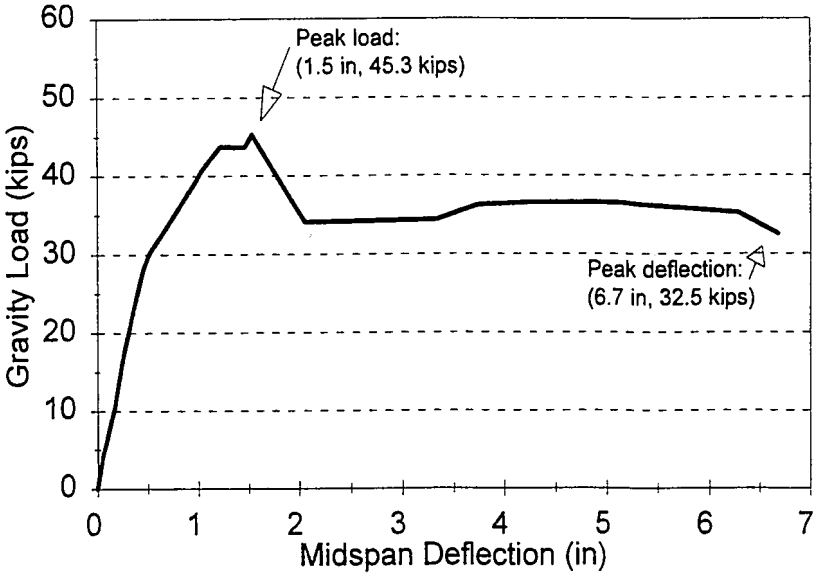

Figure 5.21 West Bay Gravity Load Test Load-Deflection Curve

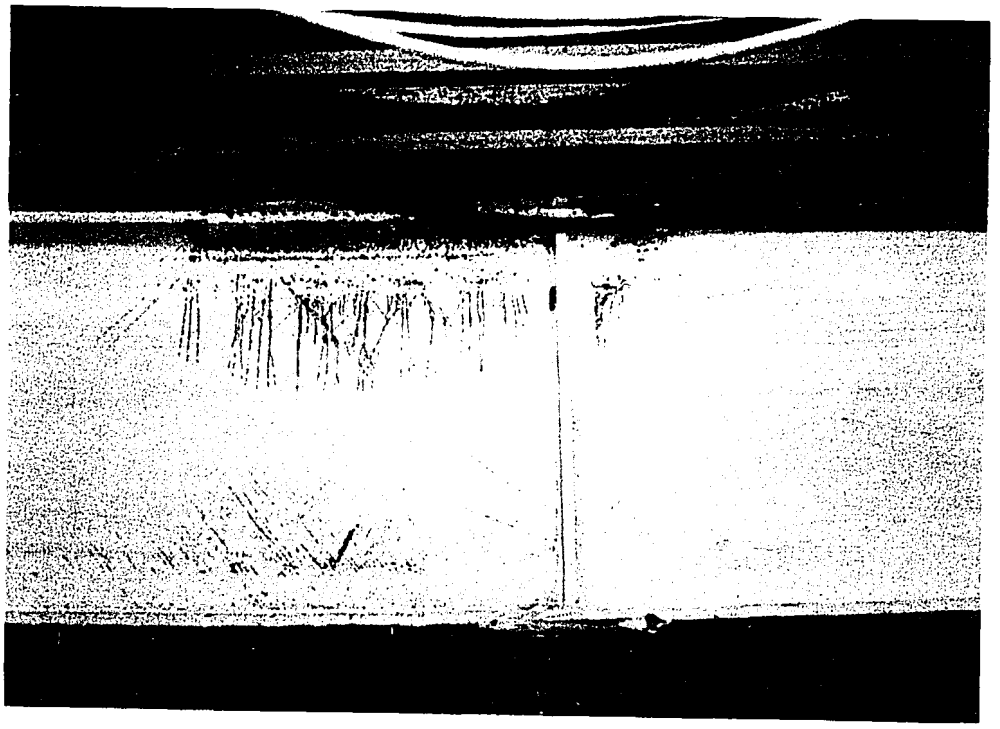

Figure 5.22 West Bay--Start of Plastic Hinge

Figure 5.23 West Bay--Plastic Hinge Formation

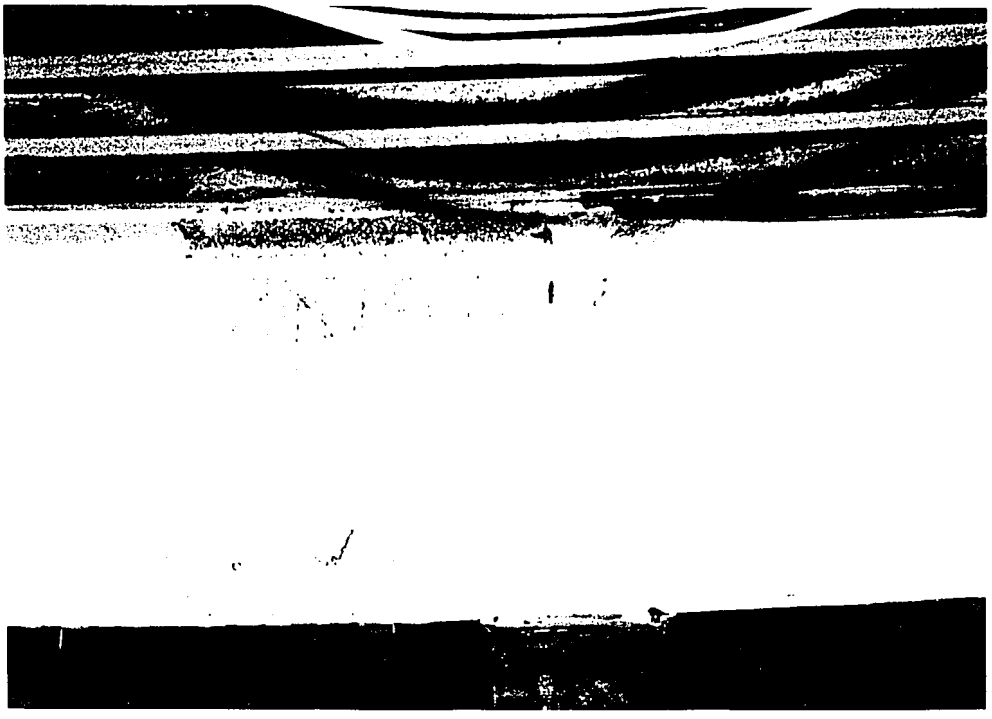

Figure 5.22 West Bay--Start of Plastic Hinge

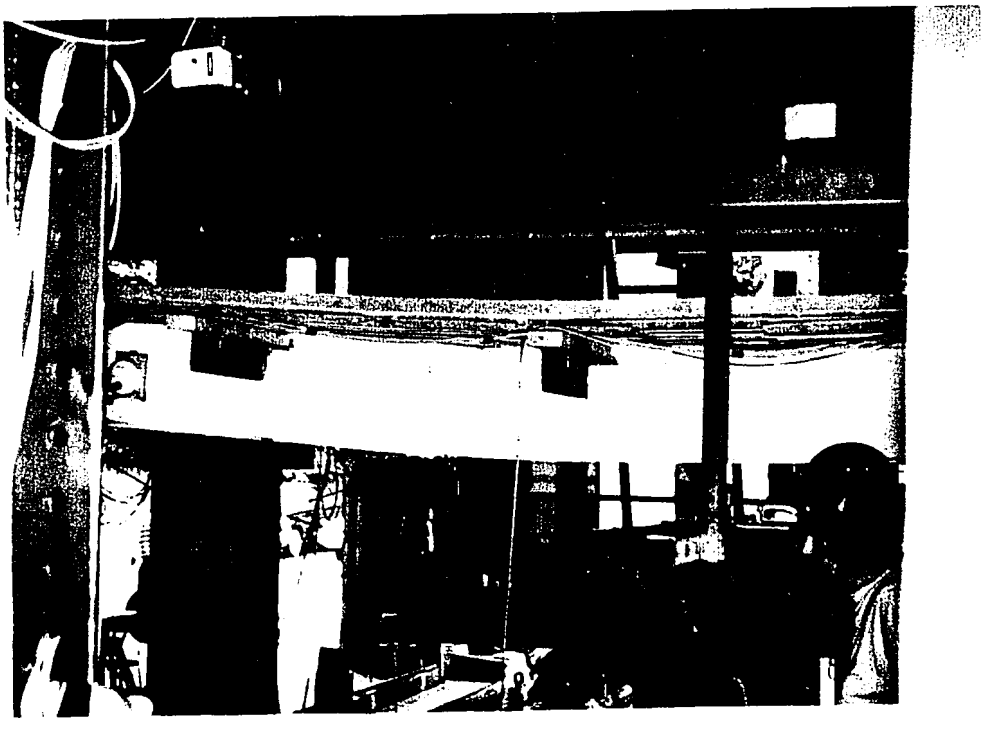

Figure 5.23 West Bay--Plastic Hinge Formation

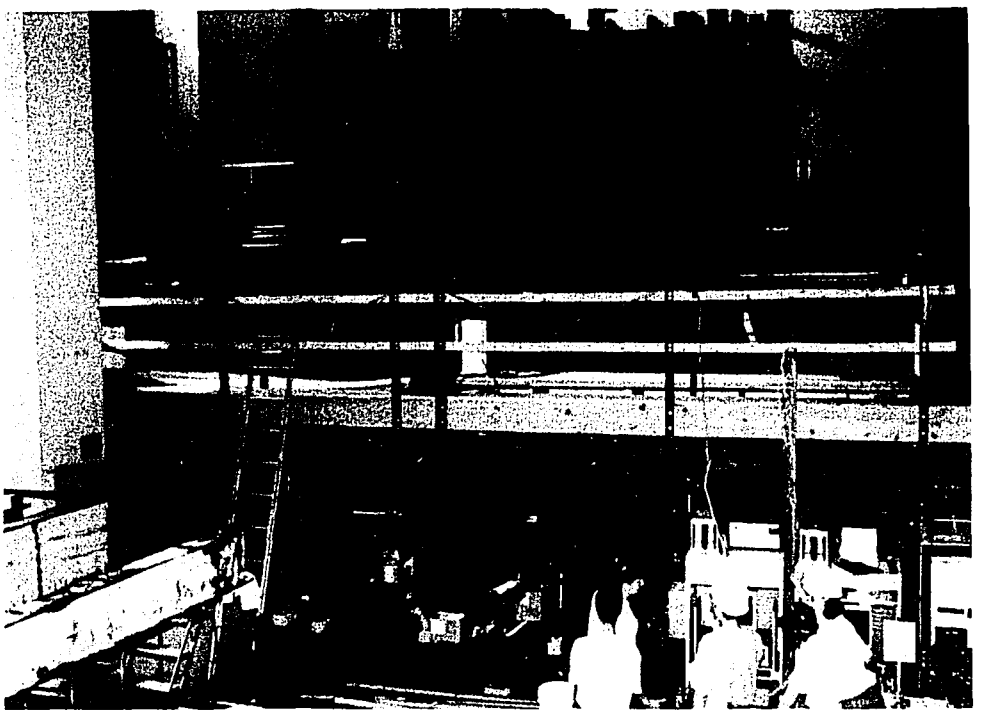

Figure 5.24 During West Bay Test

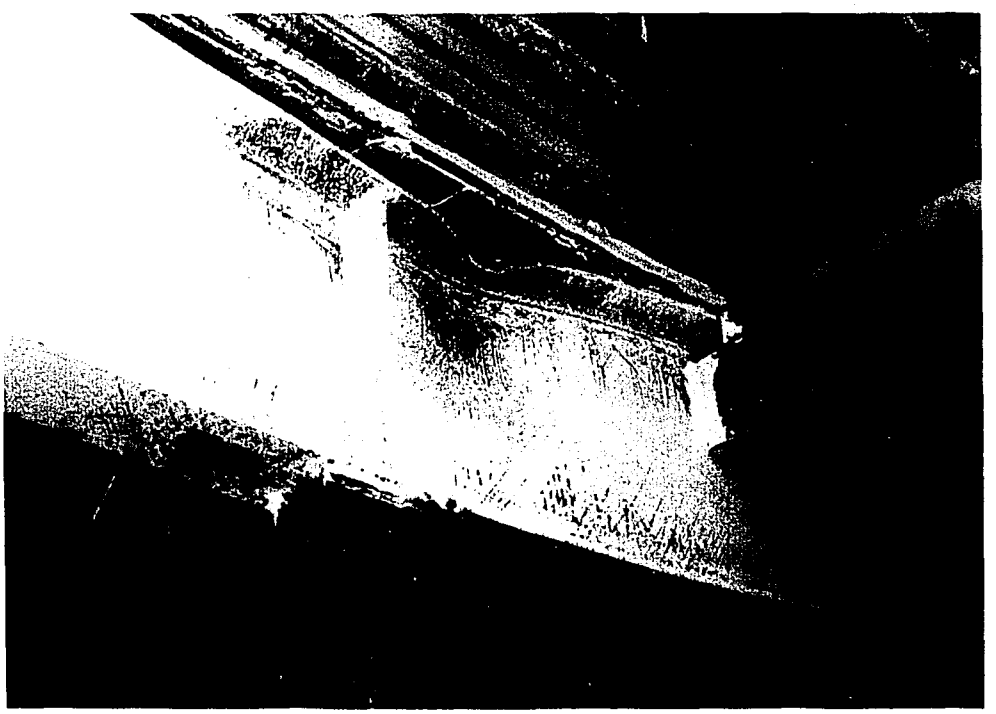

Figure 5.25 West Bay--Plastic Hinge

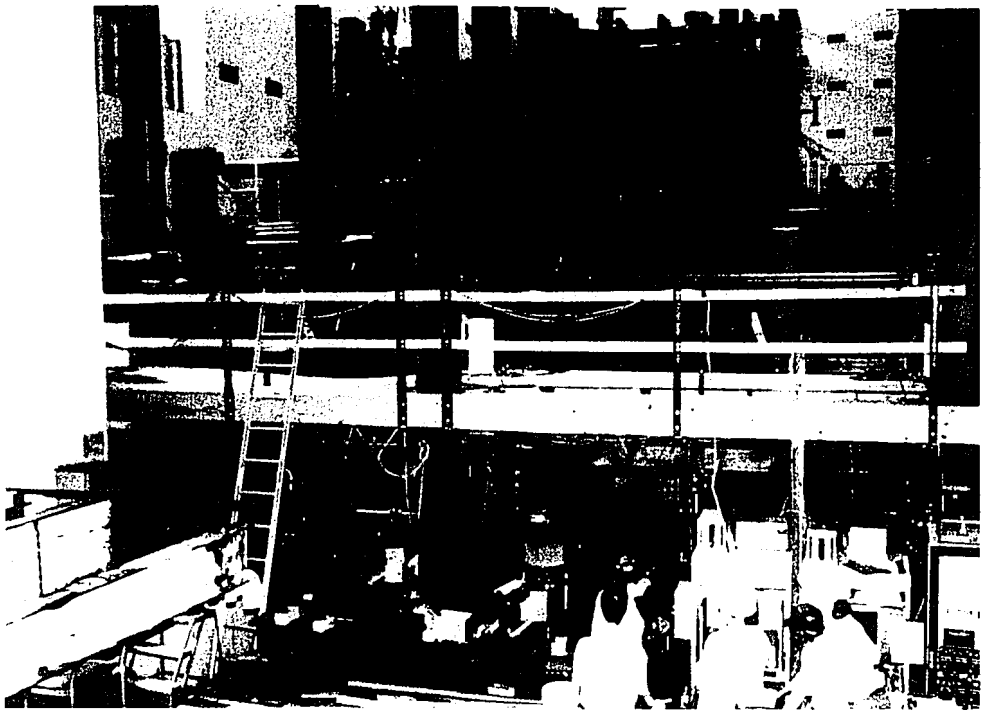

Figure 5.24 During West Bay Test

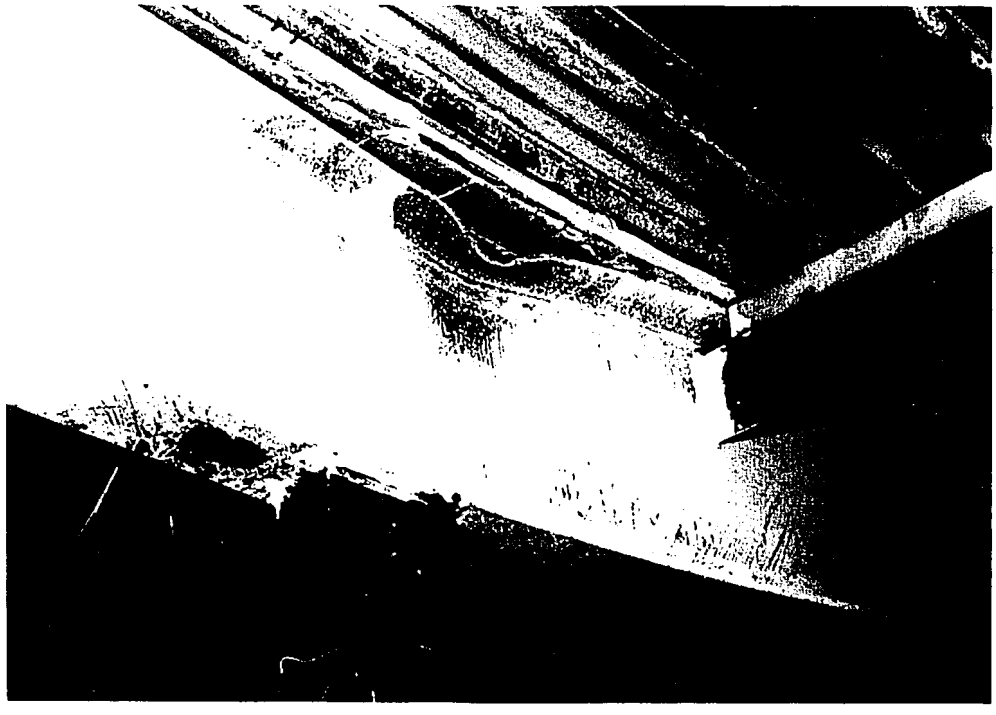

Figure 5.25 West Bay--Plastic Hinge

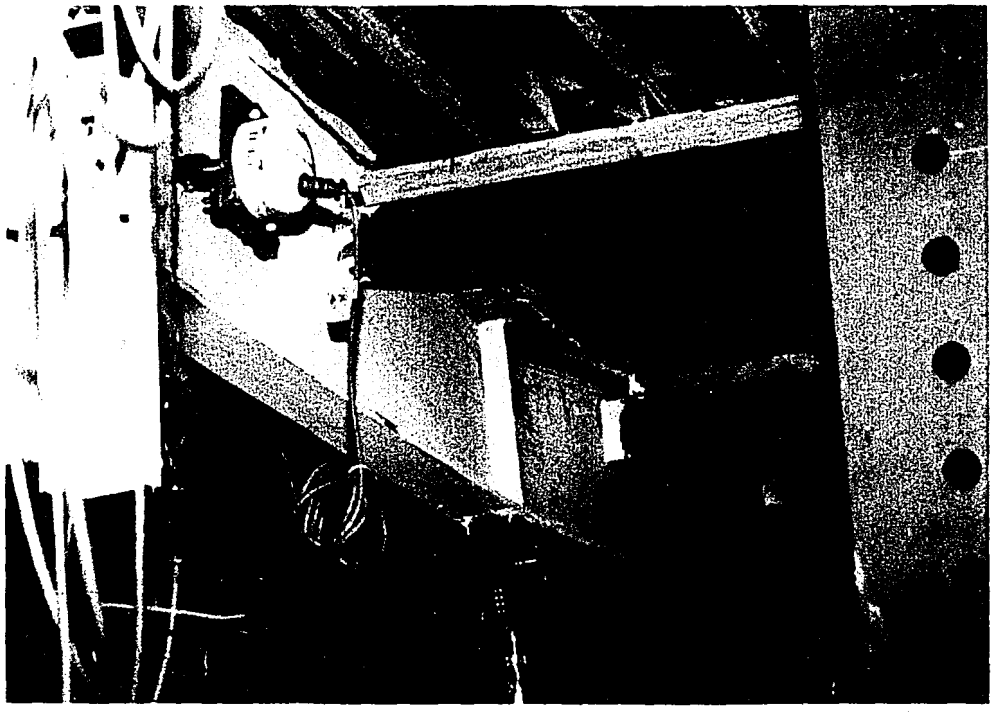

Figure 5.26 West Bay--Plastic Hinge

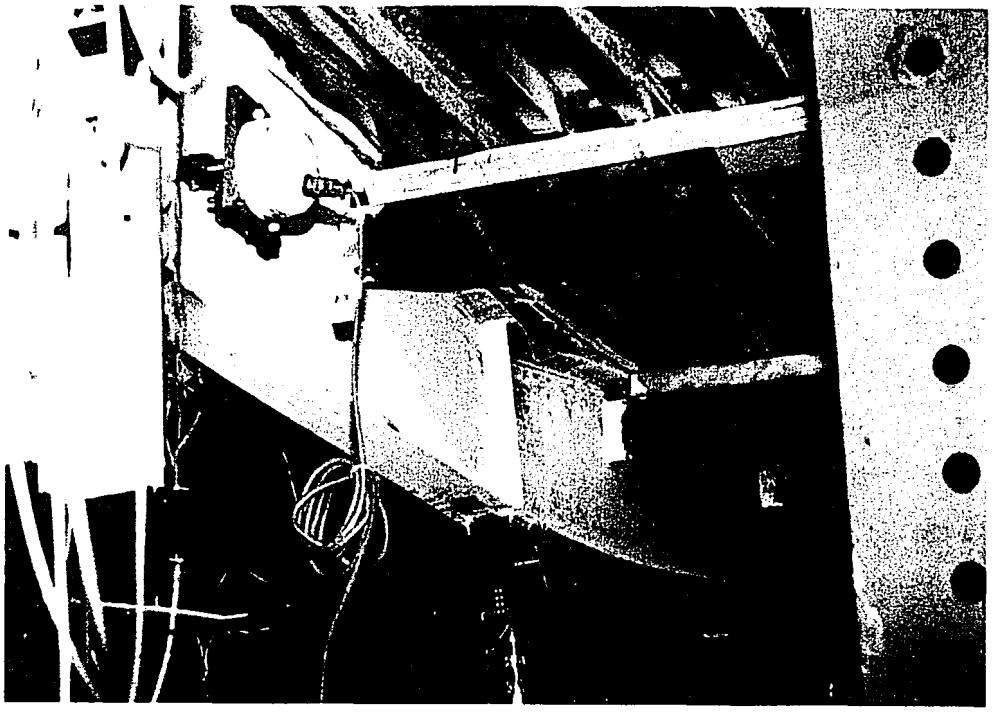

Figure 5.26 West Bay--Plastic Hinge

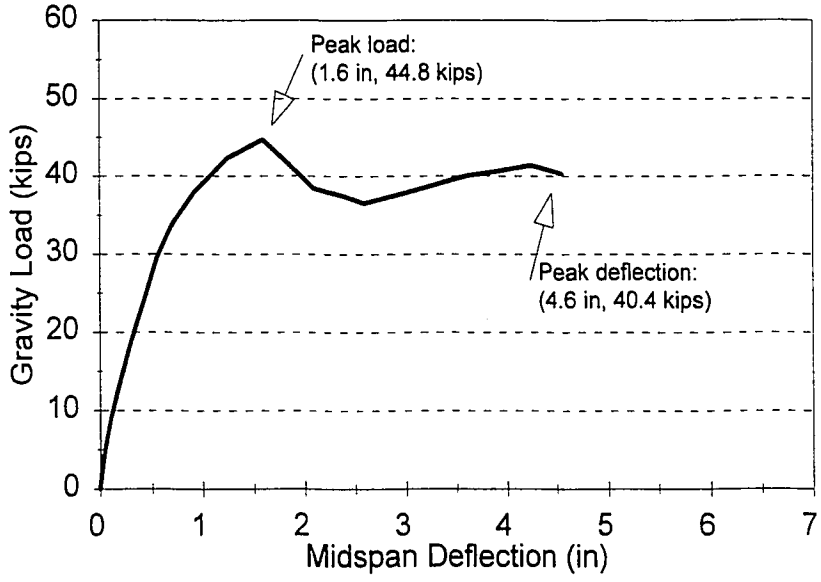

Figure 5.27 East Bay Gravity Load Test Load-Deflection Curve

Figure 5.28 East Bay Concrete Deck Crushing

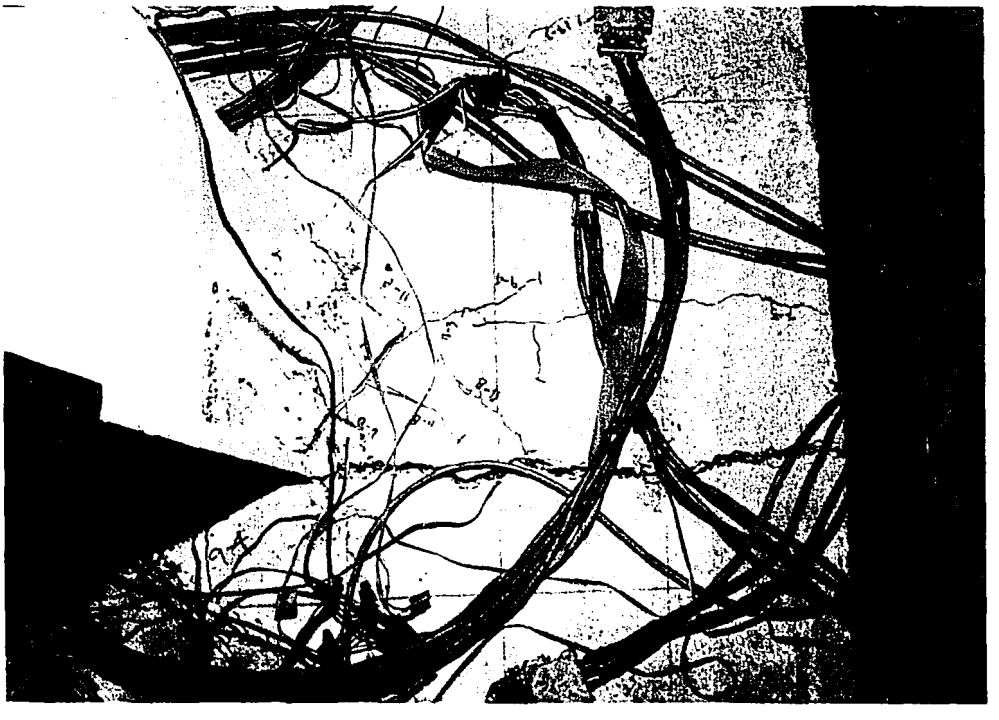

Figure 5.29 Interior Connections after Failure

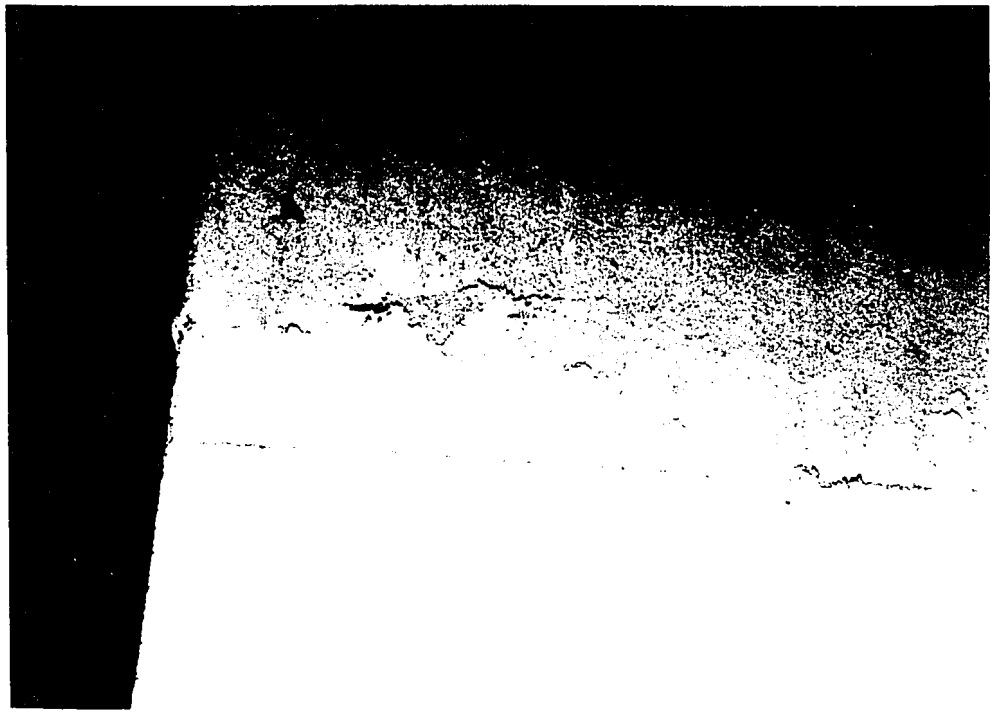

Figure 5.28 East Bay Concrete Deck Crushing

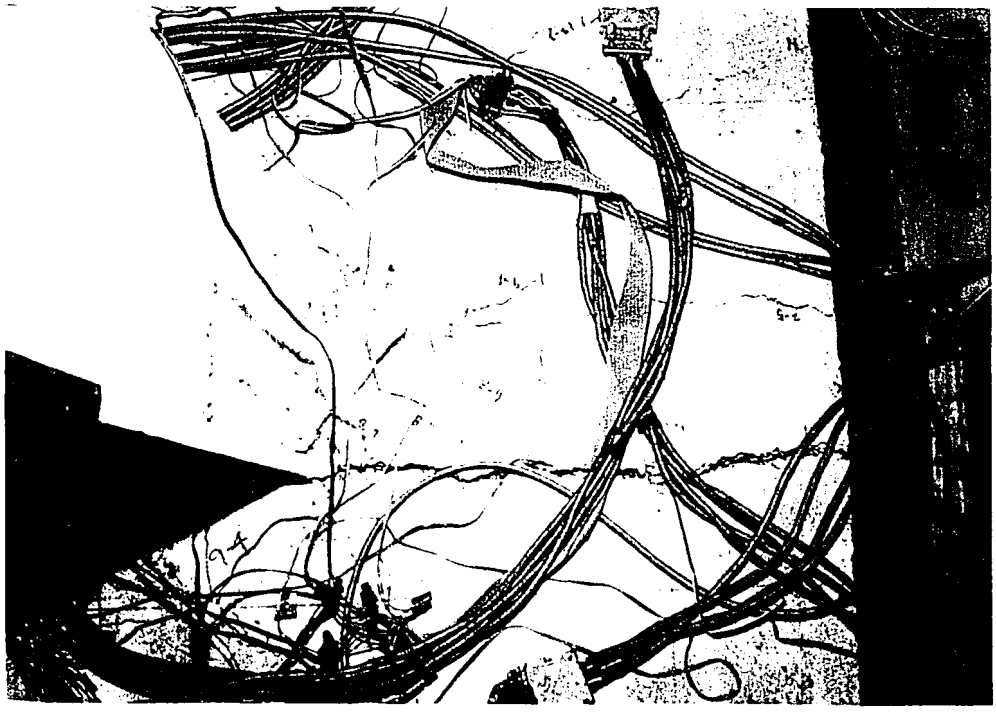

Figure 5.29 Interior Connections after Failure

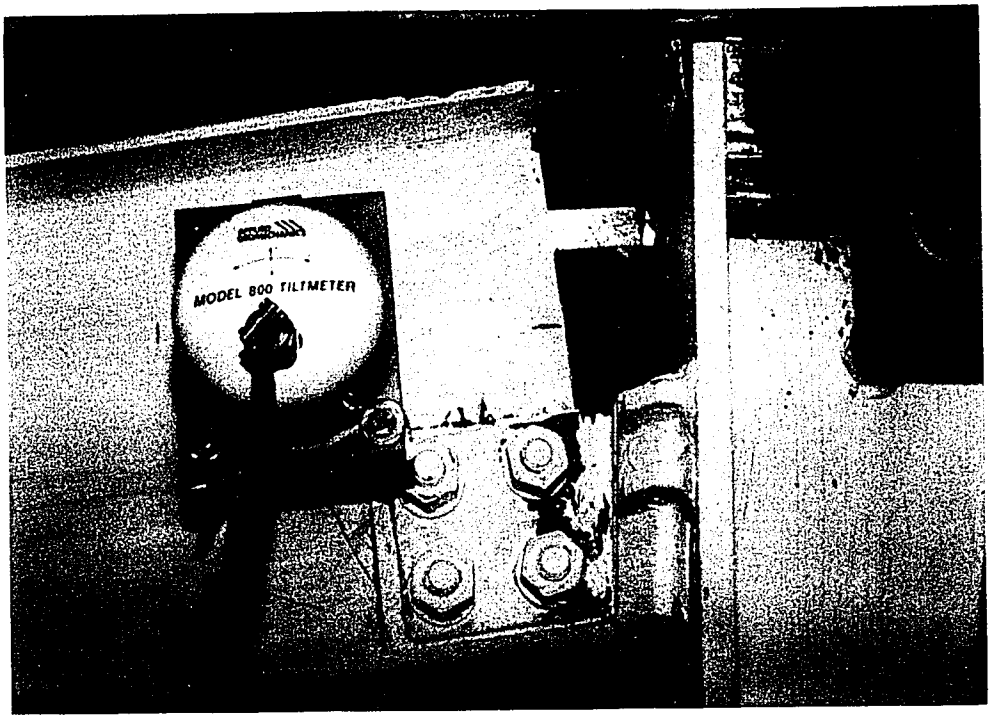

Figure 5.30 Interior Connection 2

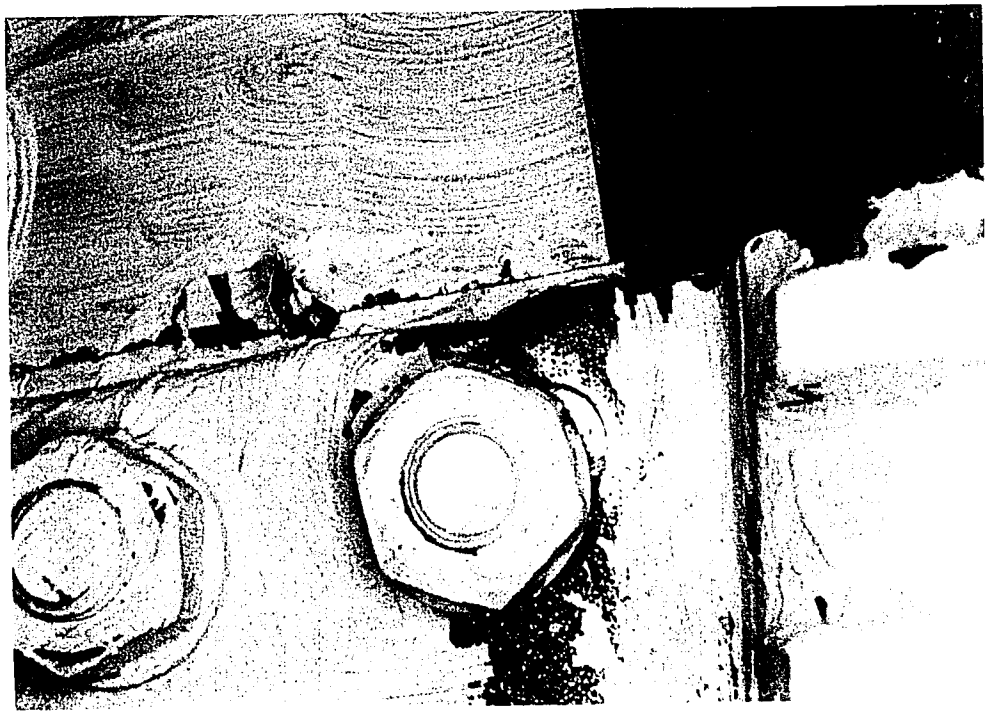

Figure 5.31 ATLSS Connector Fracture

Figure 5.30 Interior Connection 2

Figure 5.31 ATLSS Connector Fracture

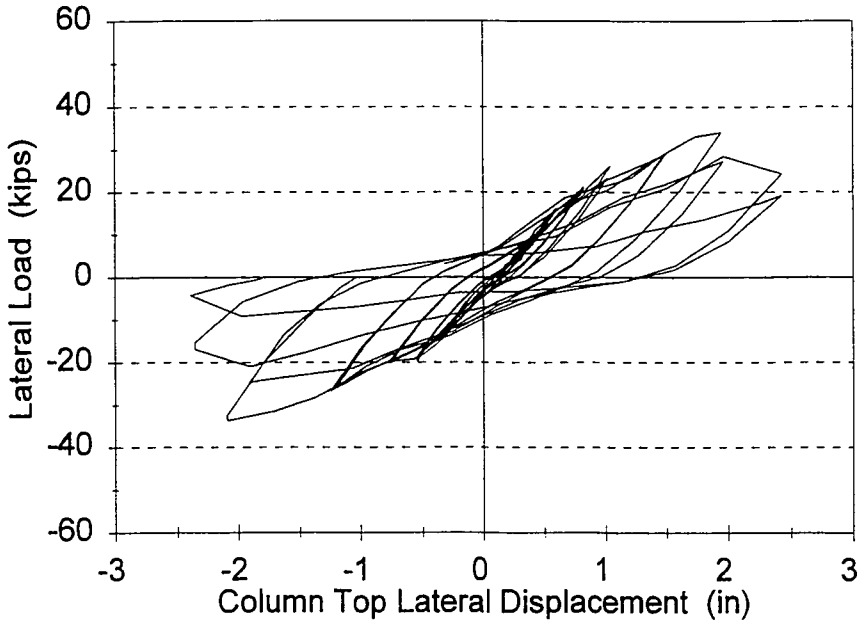

Figure 5.32 Cyclic Frame Lateral Load-Lateral Displacement Curve

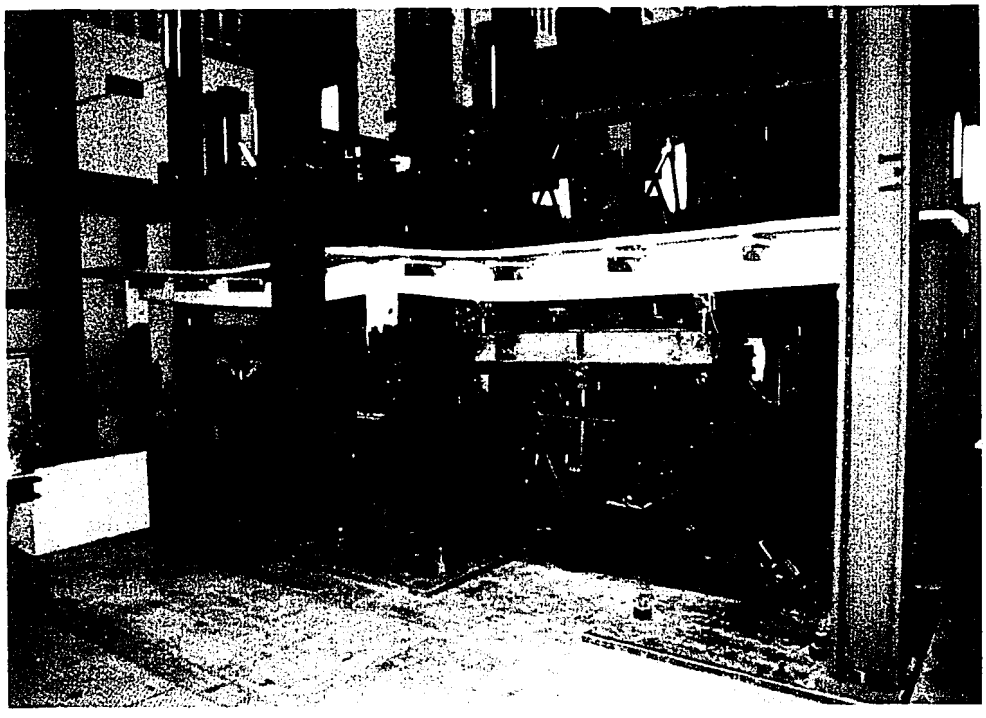

Figure 5.33 Overall Deformation of Frame after Cyclic Test

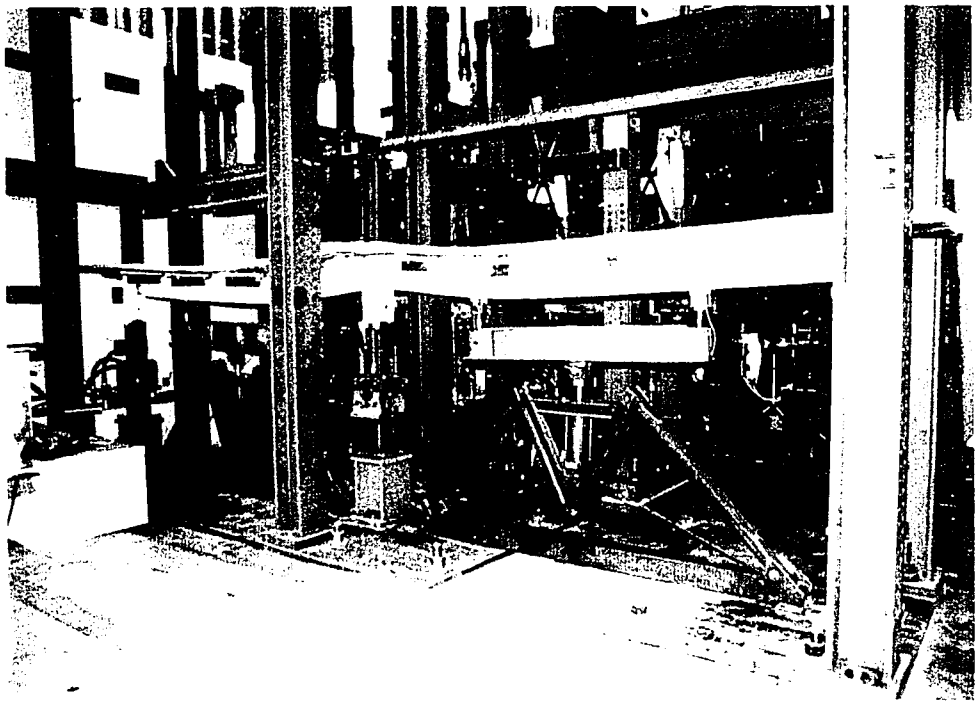

Figure 5.33 Overall Deformation of Frame after Cyclic Test

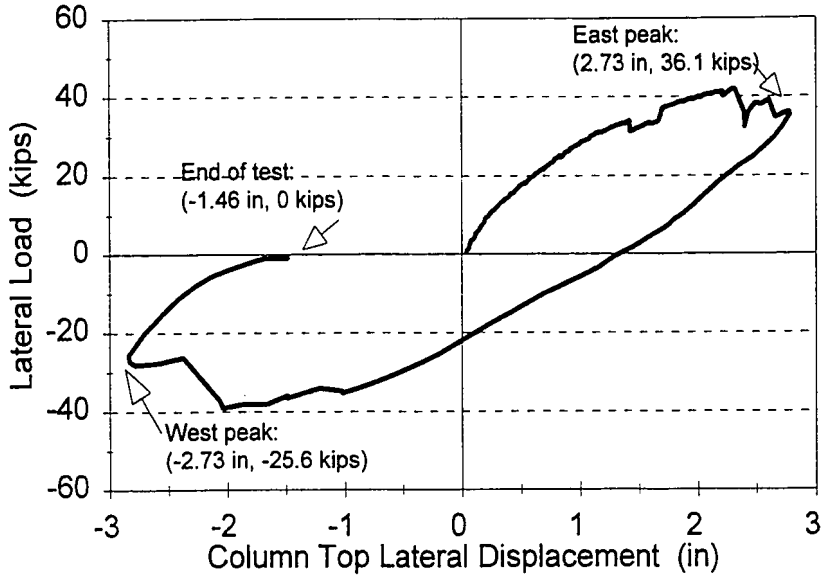

Figure 6.1 Monotonic Frame Lateral Load-Lateral Displacement Curve

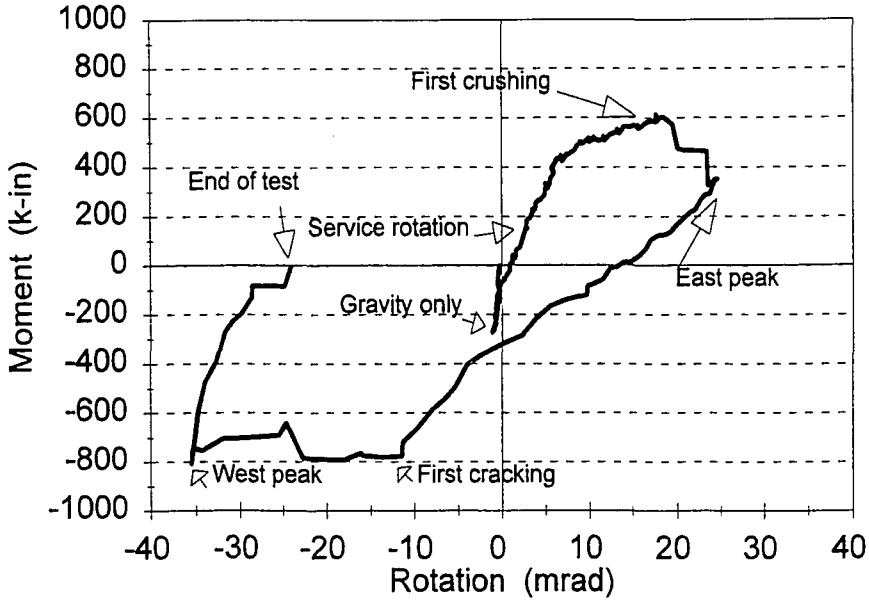

Figure 6.2 Exterior Connection 1 Moment-Rotation Relationship

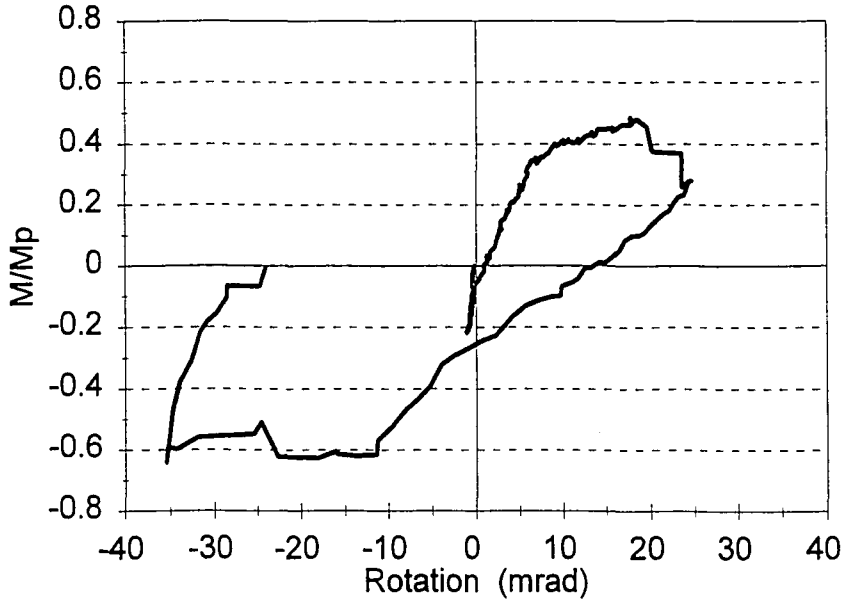

Figure 6.3 Exterior Connection 1 Moment/M_p-Rotation Relationship

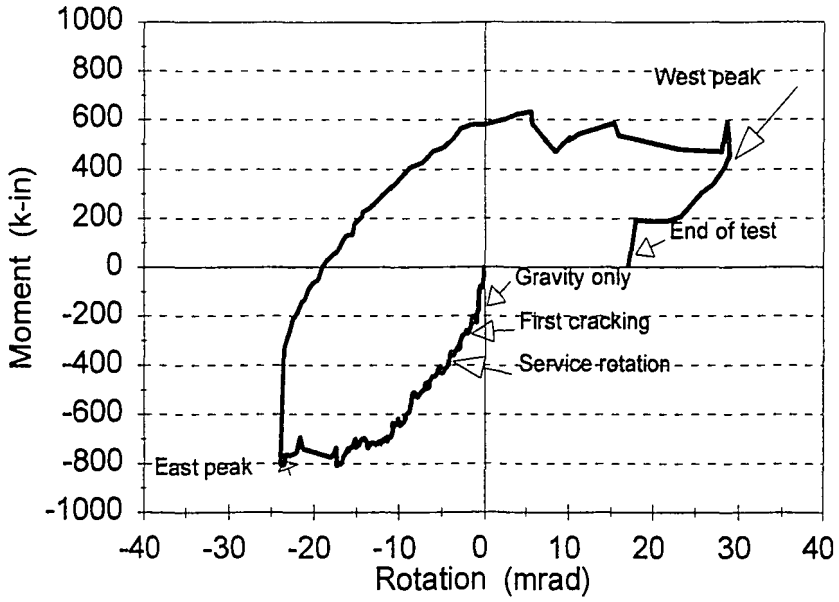

Figure 6.4 Interior Connection 1 Moment-Rotation Relationship

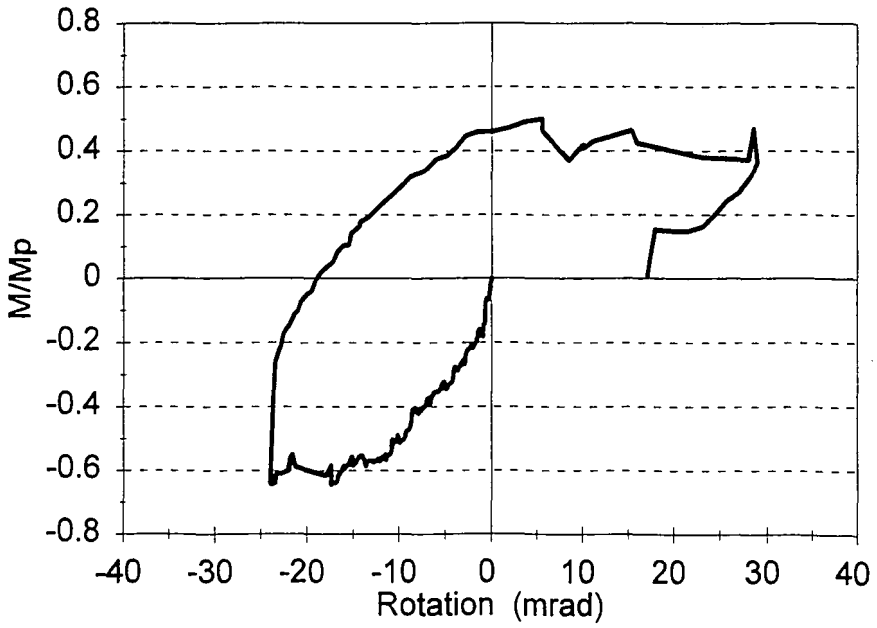

Figure 6.5 Interior Connection 1 Moment/M_p-Rotation Relationship

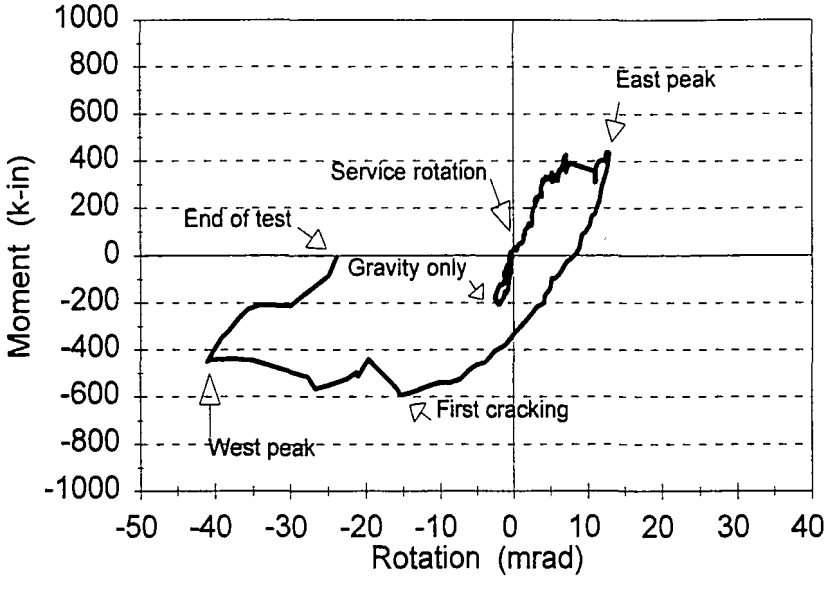

Figure 6.6 Interior Connection 2 Moment-Rotation Relationship

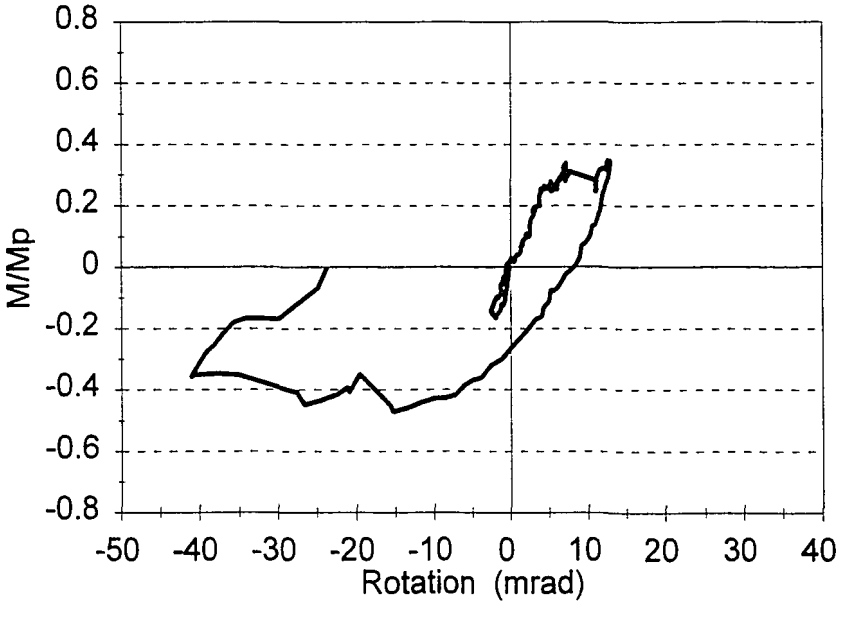

Figure 6.7 Interior Connection 2 Moment/M_p-Rotation Relationship

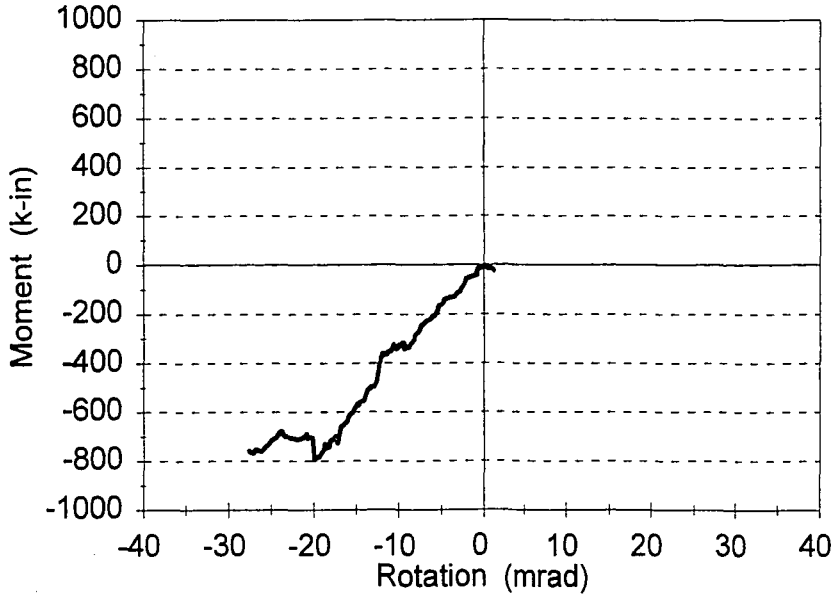

Figure 6.8 Exterior Connection 2 Moment-Rotation Relationship

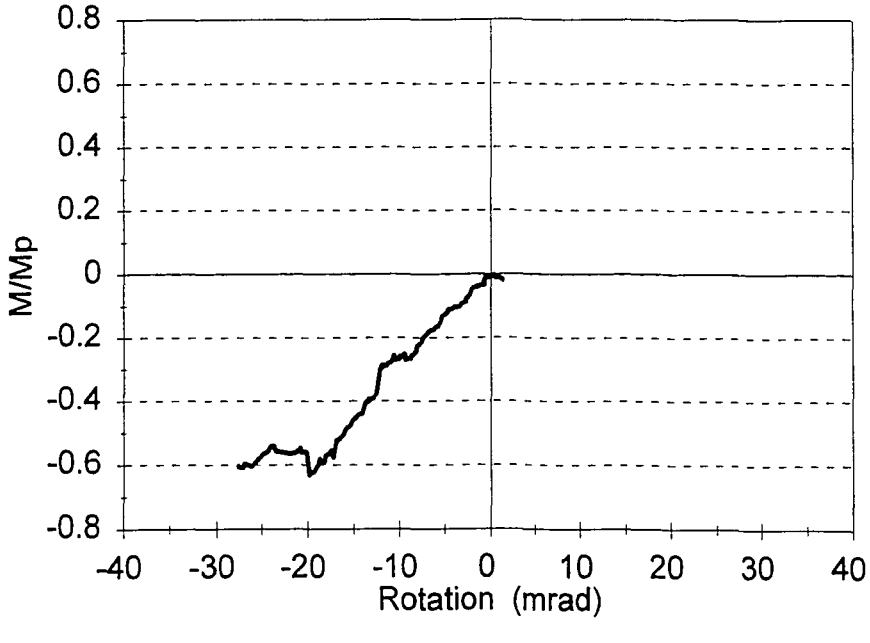

Figure 6.9 Exterior Connection 2 Moment/M_p-Rotation Relationship

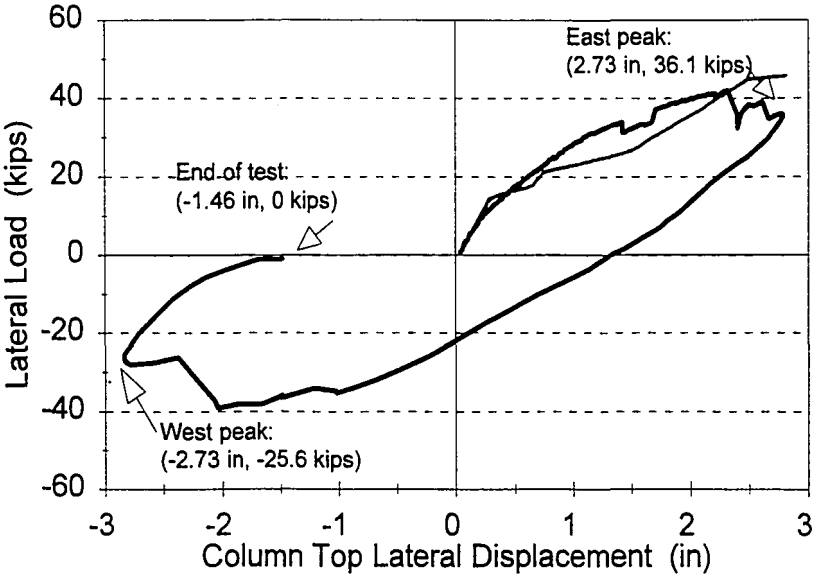

Figure 6.10 Monotonic Frame Lateral Load-Lateral Displacement Prediction

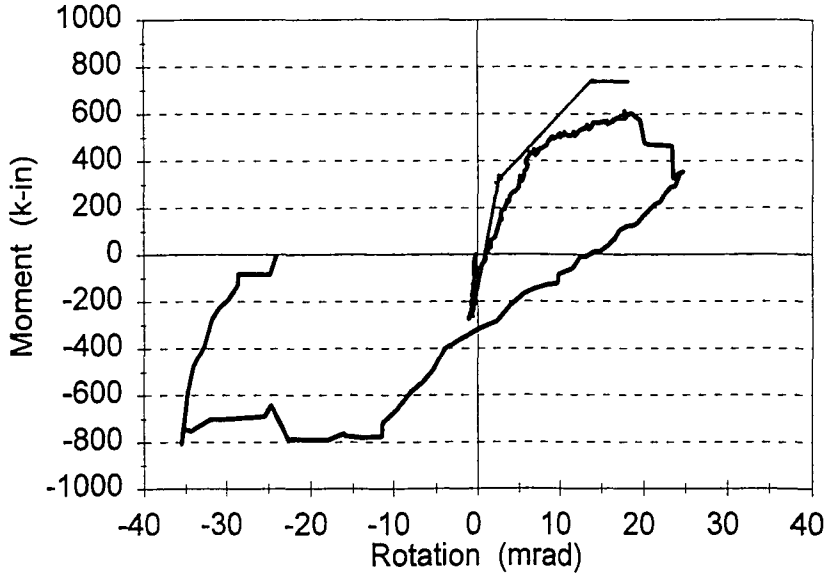

Figure 6.11 Exterior Connection 1 Moment-Rotation Prediction

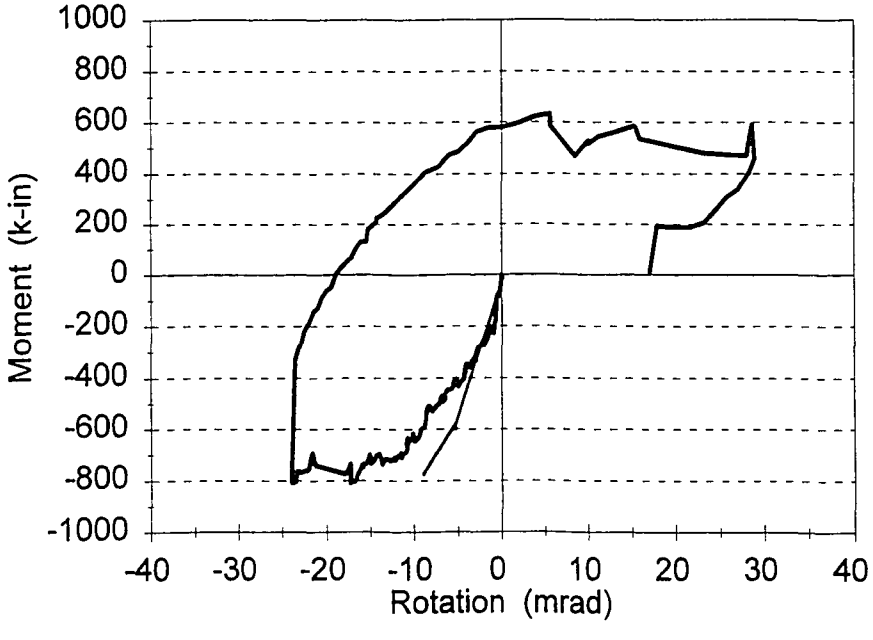

Figure 6.12 Interior Connection 1 Moment-Rotation Prediction

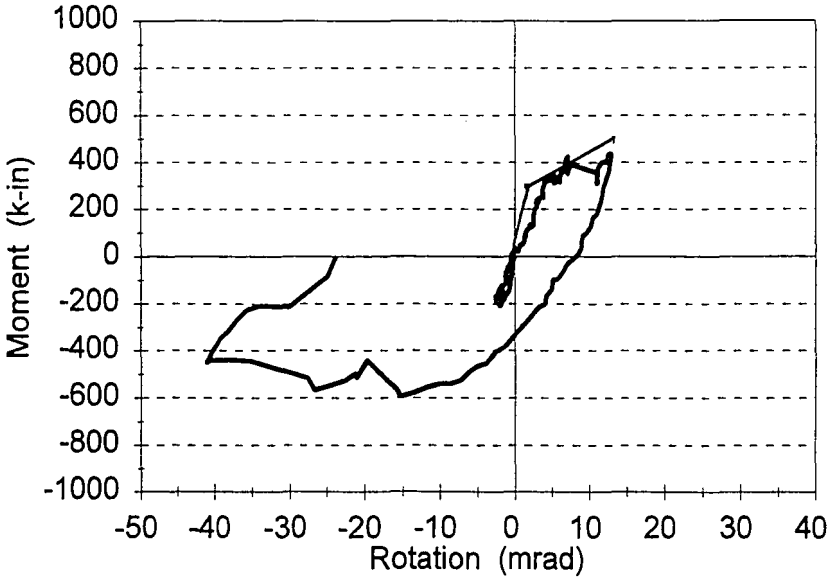

Figure 6.13 Interior Connection 2 Moment-Rotation Prediction

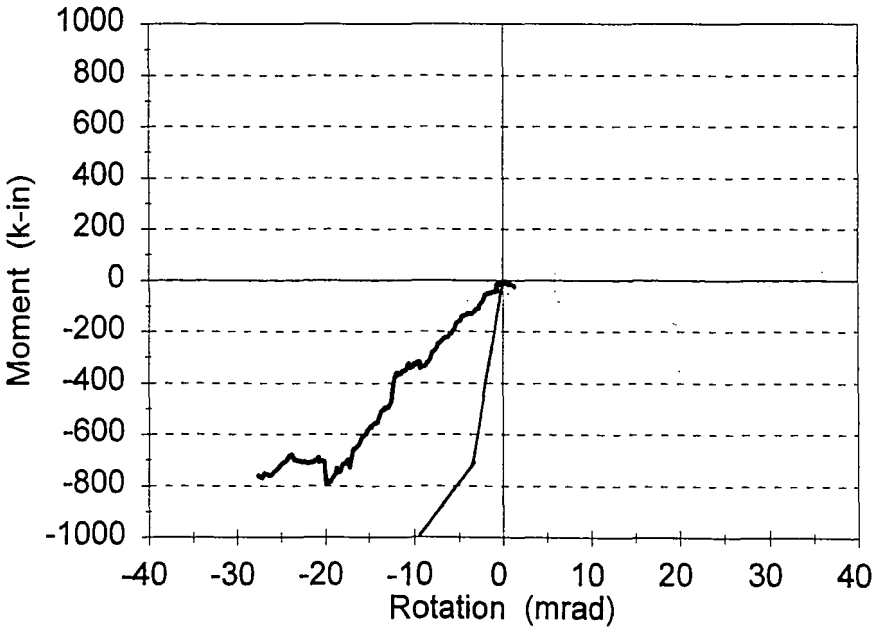

Figure 6.14 Exterior Connection 2 Moment-Rotation Prediction

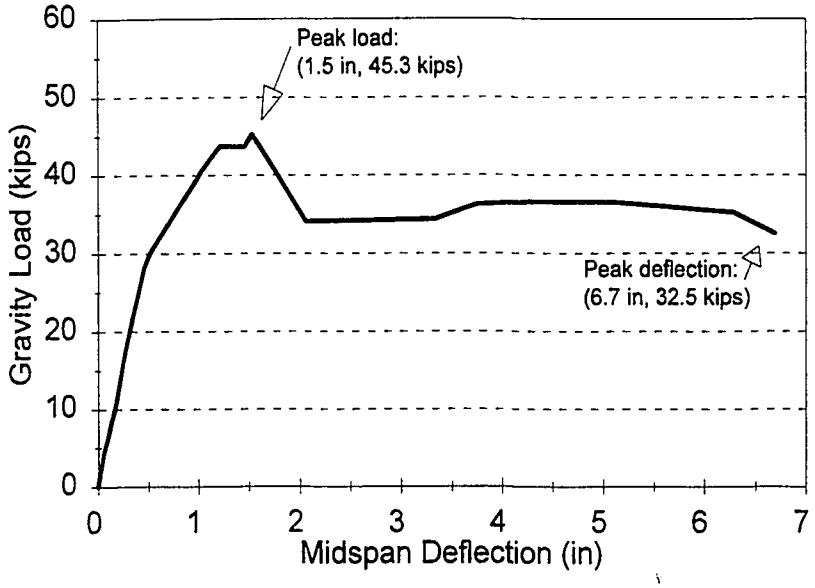

Figure 6.15 West Bay Gravity Load Test Load-Deflection Curve

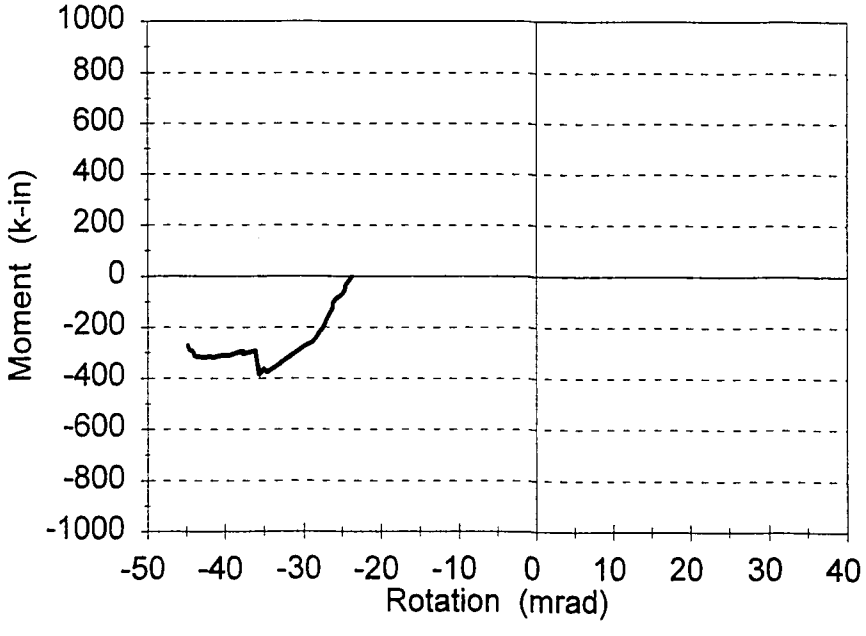

Figure 6.16 Exterior Connection 1 Moment-Rotation Relationship

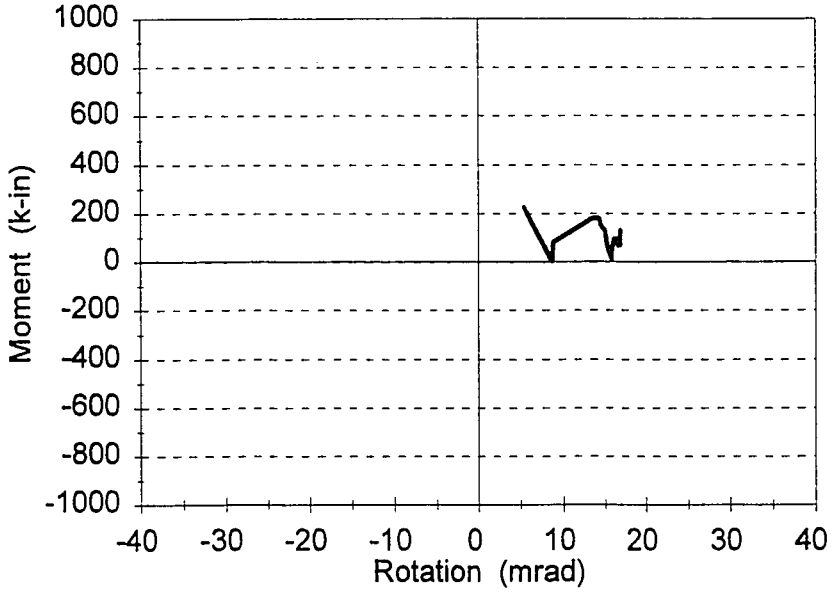

Figure 6.17 Interior Connection 1 Moment-Rotation Relationship

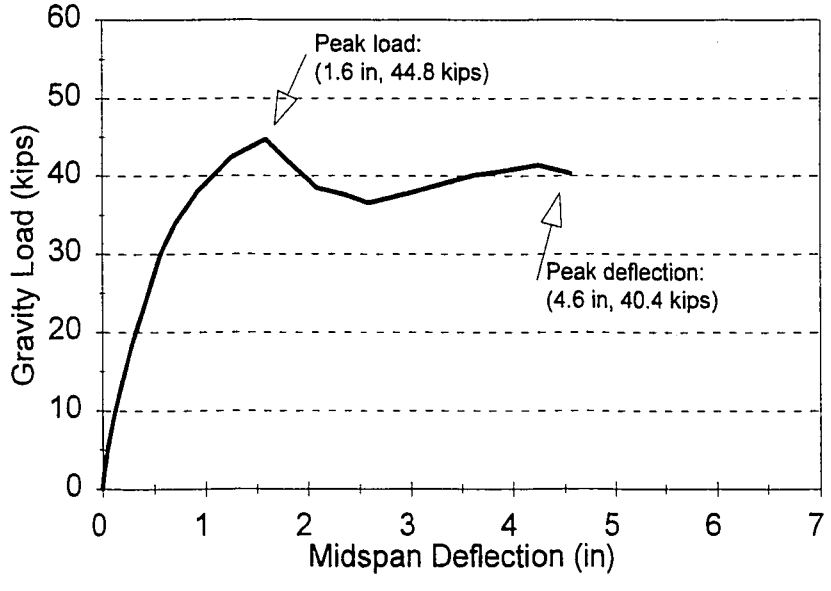

Figure 6.18 East Bay Gravity Load Test Load-Deflection Curve

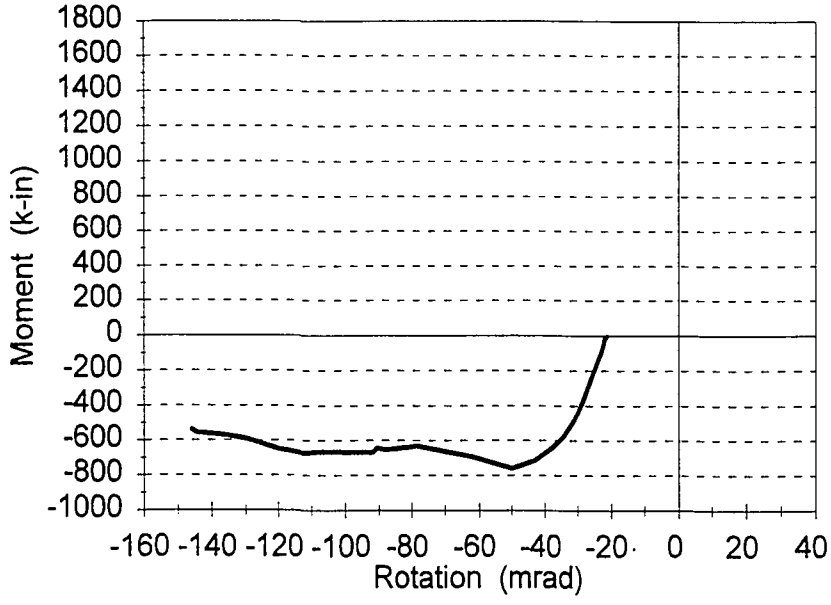

Figure 6.19 Interior Connection 2 Moment-Rotation Relationship

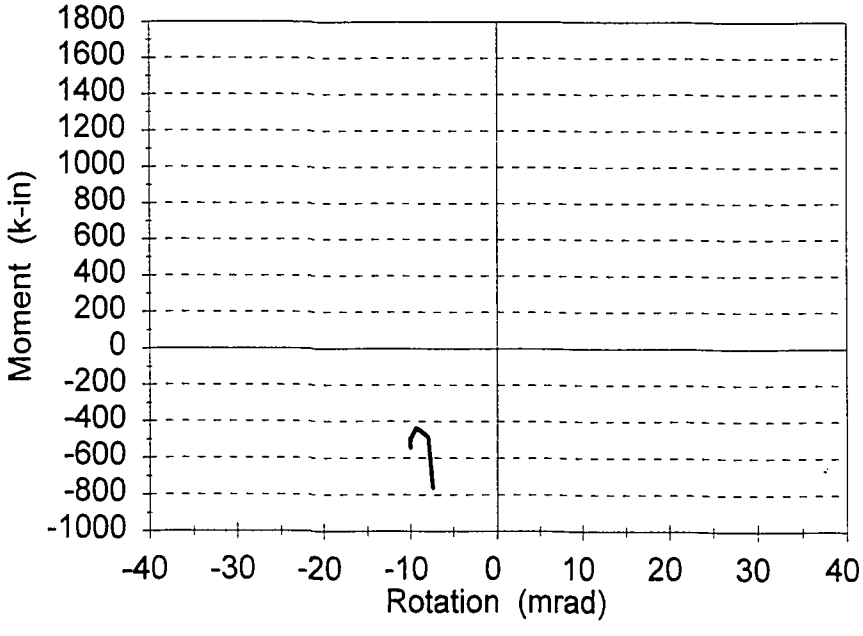

Figure 6.20 Exterior Connection 2 Moment-Rotation Relationship

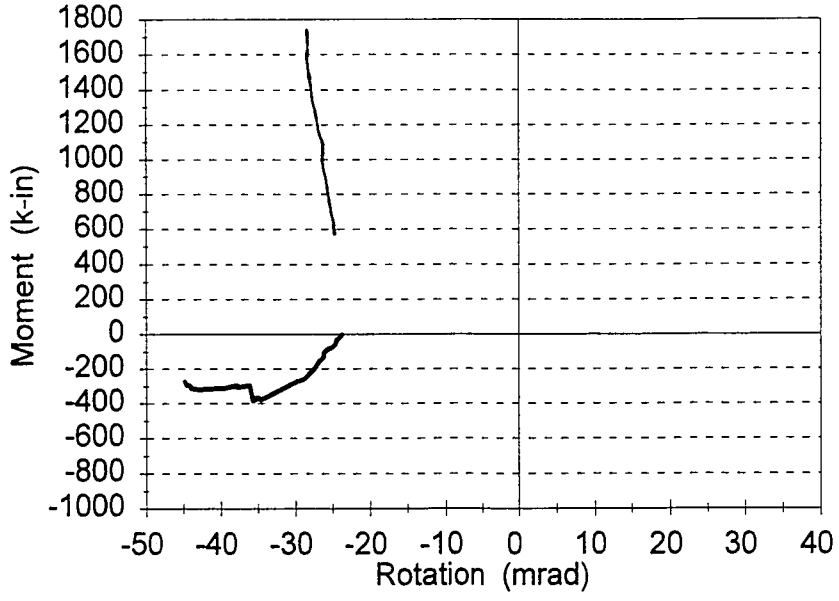

Figure 6.21 West Bay Plastic Hinge Moment with Exterior Connection 1

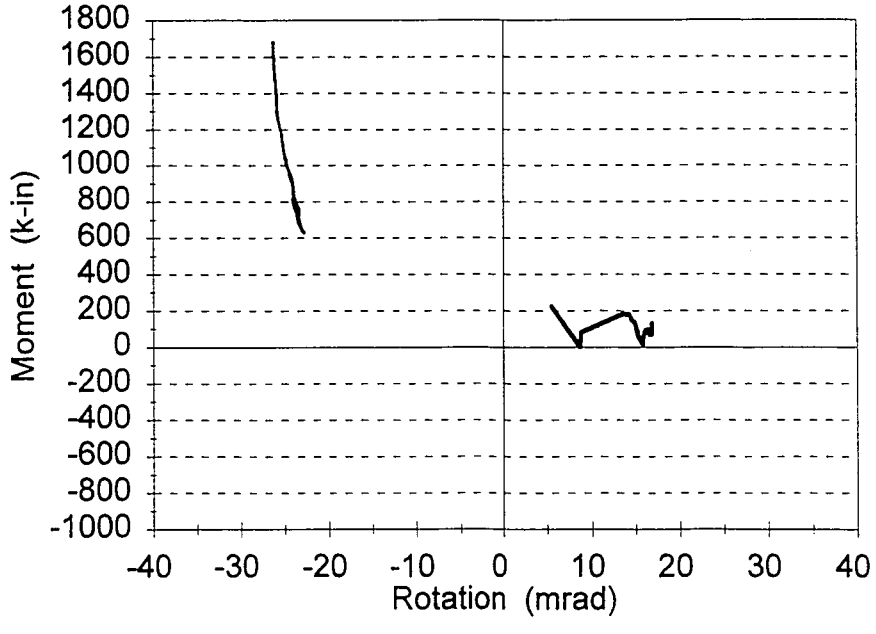

Figure 6.22 West Bay Plastic Hinge Moment with Interior Connection 1

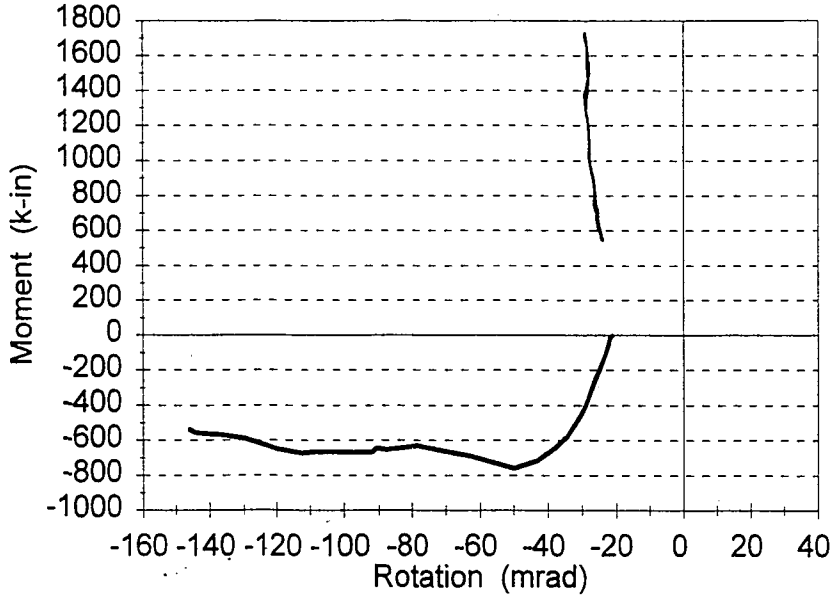

Figure 6.23 East Bay Plastic Hinge Moment with Interior Connection 2

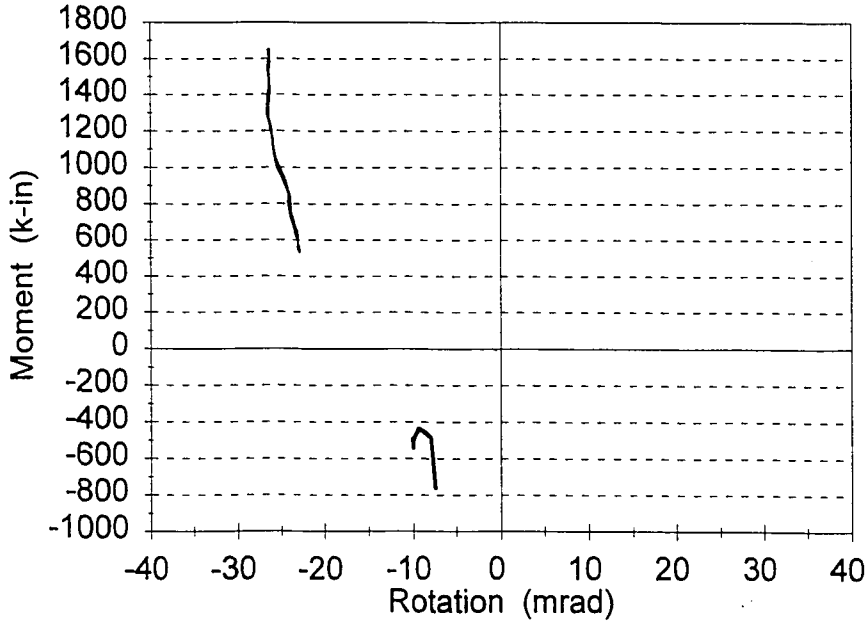

Figure 6.24 East Bay Plastic Hinge Moment with Exterior Connection 2

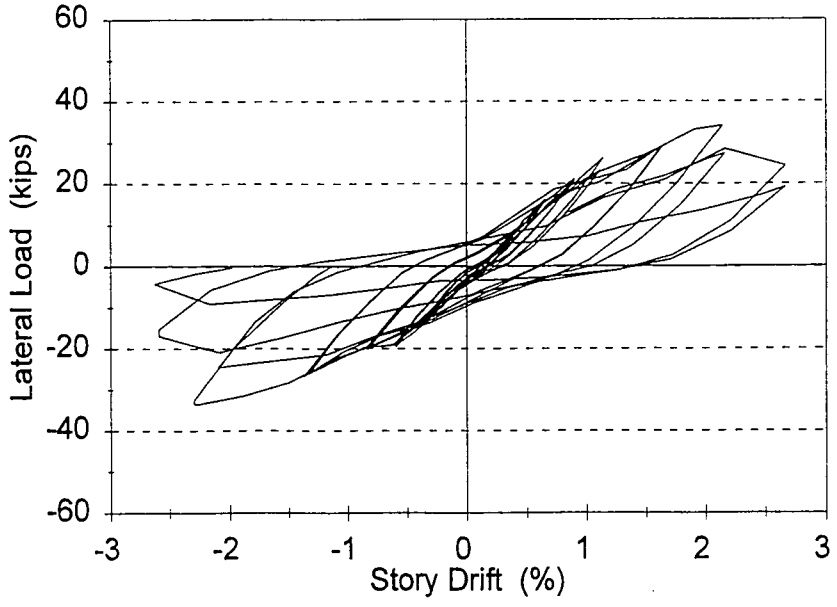

Figure 6.25 Cyclic Test Lateral Load-Story Drift Curve

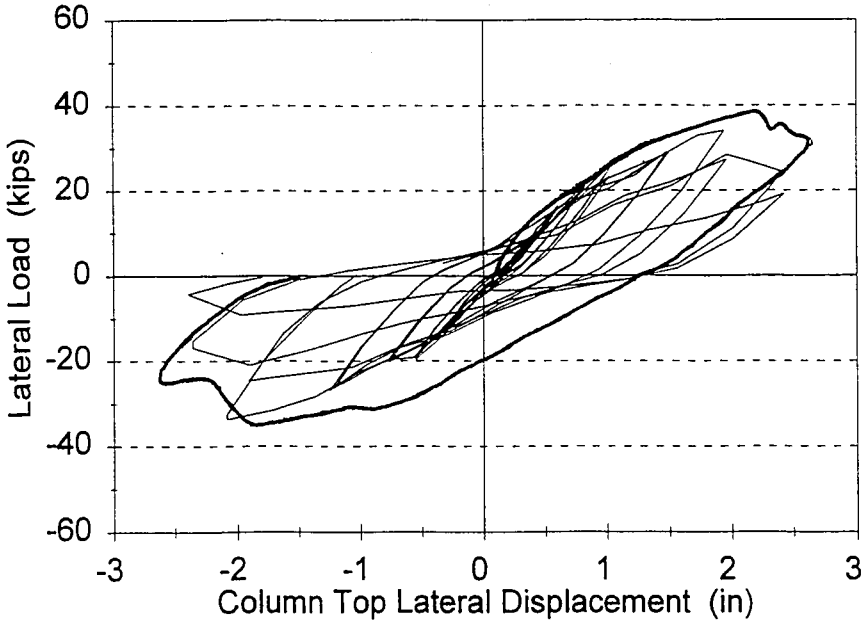

Figure 6.26 Comparison of Monotonic Test Curve with Cyclic Test Curve

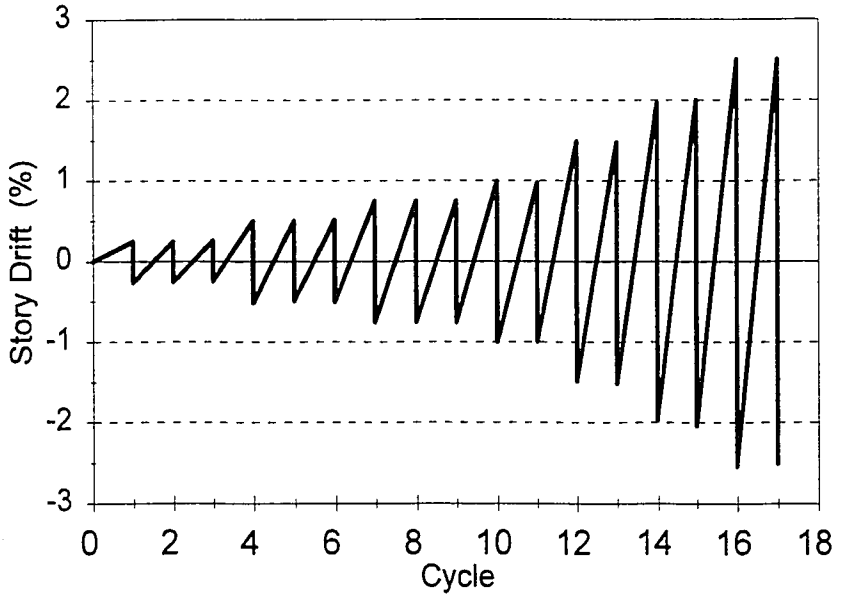

Figure 6.27 Lateral Load History for Cyclic Test

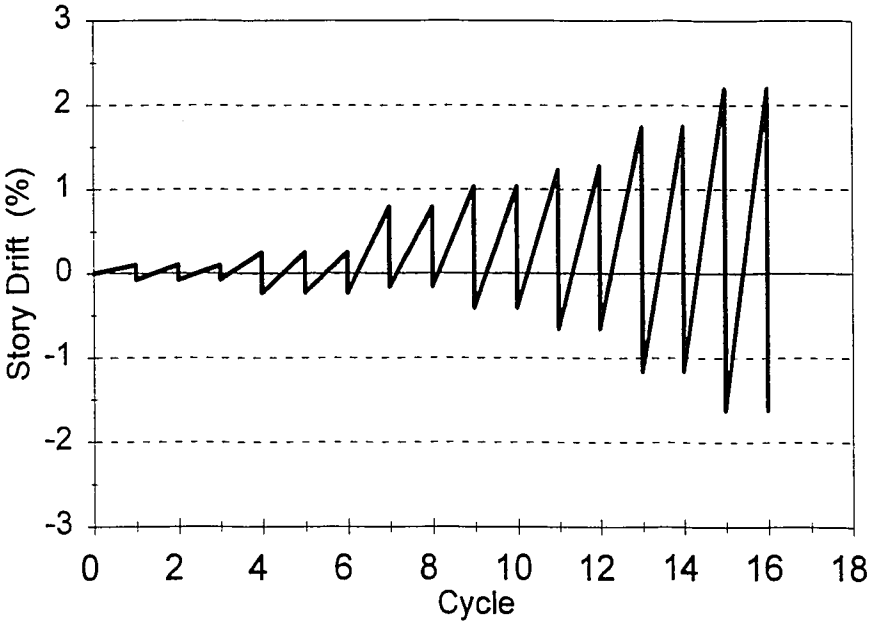

Figure 6.28 Lateral Load History for University of Minnesota Test

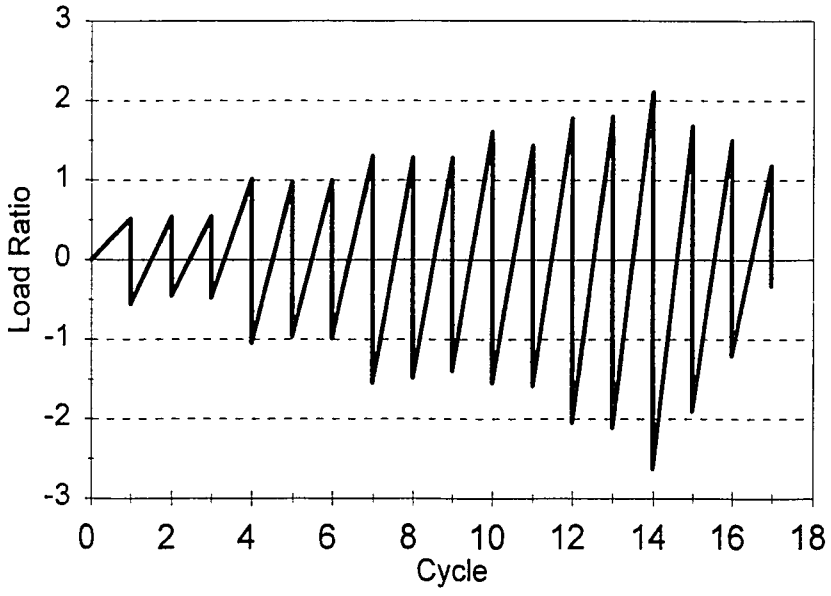

Figure 6.29 Lateral Deflection History for Cyclic Test

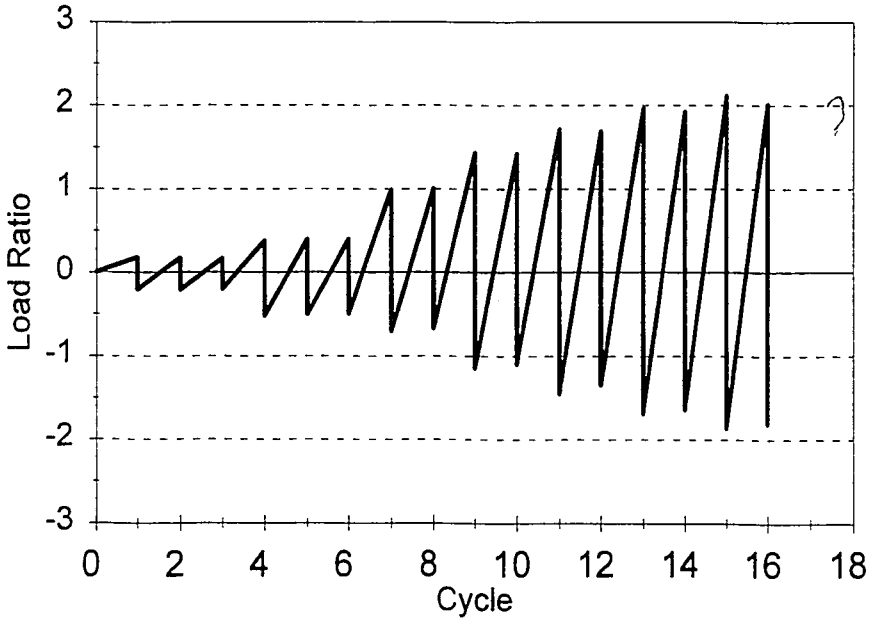

Figure 6.30 Lateral Deflection History for University of Minnesota Test

List of References

ACI Building Code Requirements for Reinforced Concrete (ACI 318-89) and Commentary-ACI 318R-89, 1991. Detroit.

AISC, October 4, 1994. *Semi-Rigid Composite Connections.* Reference material from AISC seminar: Innovative Practices in Structural Steel. Edison, NJ.

AISC Manual of Steel Construction: Load and Resistance Factor Design, 1993. Chicago.

Ammerman, D. J., 1988. *Behavior and Design of Frames with Semi-Rigid Composite Connections.* PhD Dissertation, Department of Civil and Environmental Engineering, University of Minnesota.

Applied Technology Council, 1992. *ATC 24: Guidelines for Cyclic Seismic Testing of Components of Steel Structures.* Stanford, CA.

ASCE Minimum Design Loads for Buildings and Other Structures (ASCE 7-93), 1993. New York.

ATLSS, February 9, 1995. *A Progress and Accomplishment Report to the National Science Foundation (from May 1, 1986 to December 31, 1994).* ATLSS Report No. 95-02, Bethlehem, PA.

AWS 1994 Structural Welding Code-Steel (ANSI/AWS D1.1-94), December 30, 1993. Miami.

Becker, E. P., Chairman, November 17-18, 1991. *Proceedings of the Workshop on Structural Connections: Connections for Building Structures in the 21st Century.* Bethlehem, PA.

Chen, W. F., Ed., 1993. *Semi-Rigid Connections in Steel Frames.* New York: McGraw-Hill, Inc.

Crawley, S. W. and R. M. Dillon, 1984. *Steel Buildings: Analysis and Design.* New York: John Wiley and Sons, Inc., pp. 237-255.

Eraso, M., 1995. *Methodology for the Economic Assessment of Construction Innovations: Simulation of Structural Steel Erection.* M.S. Thesis, Department of Civil and Environmental Engineering, Lehigh University.

Eraso, M. and E. S. Slaughter, November 1994. *Preliminary Simulation Models of the Fabrication and Erection of Steel Structures.* ATLSS Report No. 94-16, Bethlehem, PA.

Fleischman, R. B., 1995. *Analysis and Design of an Innovative Structural Connector.* PhD Dissertation, Department of Civil and Environmental Engineering, Lehigh University.

Fleischman, R. B., B. V. Viscomi and L. W. Lu, April 29-May 1, 1991. "ATLSS Connections: Concept, Development and Study". *Proceedings from ASCE Structures Congress '91.* Indianapolis, IN: pp. 426-429.

Forcier, G. P, 1990. *A Parametric Study of Composite Frame Behavior.* M.S. Thesis, Department of Civil and Environmental Engineering, University of Minnesota.

Gere, J. M., 1963. *Moment Distribution.* New York: D. Van Nostrand Company, Inc., pp. 229-237.

Griffis, L. G., October 1994. "1994 T. R. Higgins Lecture: Composite Frame Construction". *Modern Steel Construction*, pp. 36-47.

Jefferson, T. B. and G. Woods, 1990. *Metals and How to Weld Them.* Cleveland, OH: The James F. Lincoln Arc Welding Foundation, pp. 193, 230-231.

Kaufmann, E. J., 1993-1995. Research Engineer, ATLSS Engineering Research Center, Lehigh University. Private communications.

Koller Concrete, Inc., April 20, 1995 "4000 PSI Concrete Mix Design". Bethlehem, PA.

Larrabee, A. B., W. D. Michalerya and B. V. Viscomi, May 3, 1994. "Initial Economic Assessment for the ATLSS Integrated Building System 'AIBS'". ATLSS and Competitive Technologies, Inc. Report.

Lawrence, W. S., 1994. *Development of a Partially Restrained Composite Connection Utilizing the ATLSS Connector With Tubular Columns.* M.S. Thesis, Department of Civil and Environmental Engineering, Lehigh University.

Lawrence, W. S., L. W. Lu and B. V. Viscomi, December 1993. "Advanced Connections Reduce Costs". *Modern Steel Construction*, pp. 16-21.

Leon, R. T., 1993-1995. Associate Professor of Civil Engineering, University of Minnesota. Private communications.

Leon, R. T., March 1994. "Analysis of Unbraced Frames with Partially Restrained (PR) Connections". *Modern Steel Construction*, pp. 38-41.

Leon, R. T., October 1992. "Composite Semi-Rigid Connections". *Modern Steel Construction*, pp. 18-23.

Leon, R. T., Second Quarter 1994. "Composite Semi-Rigid Construction". *AISC Engineering Journal*, pp. 57-67.

Leon, R. T. and D. J. Ammerman, First Quarter 1990a. "Semi-Rigid Composite Connections for Gravity Loads". *AISC Engineering Journal*, pp. 1-11.

Leon, R. T. and D. J. Ammerman, First Quarter 1990b. "Unbraced Frames with Semi-Rigid Composite Connections". *AISC Engineering Journal*, pp. 12-21.

Lin, J., 1986. *Analytical Study of Semi-Rigid Connection Behavior.* M.S. Project, Department of Civil and Environmental Engineering, University of Minnesota.

Lu, L. W., R. G. Slutter and B. T. Yen, 1980. "Research on Composite Structures for Building and Bridge Applications". *Proceedings of the USA - Japan Seminar on Composite Structures and Mixed Structural Systems.* Tokyo, Japan, pp. 3-18.

Lu, L. W., B. V. Viscomi, R. B. Fleischman, W. S. Lawrence, A. M. Rosa and R. B. Garlock, May 18-20, 1995. "Development and Experimental Investigation of New Types of Connections for Framed Structures Suited for Automated Construction". *Proceedings of the 1st European Conference on Steel Structures.* Athens, Greece, pp. 231-238.

McCormac, J. C., 1995. *Structural Steel Design: LRFD Method.* New York: Harper Collins College Publishers.

Meyer, C., Ed., 1987. *Finite Element Idealization for Linear Elastic Static and Dynamic Analysis of Structures in Engineering Practice.* New York: ASCE.

Michalerya, W. D. and B. V. Viscomi, October 26-28, 1993. "An Advancement in Automated Construction: The ATLSS Integrated Building Systems". *Third International Conference on Fossil Plant Construction.* Palm Beach, FL.

Naeim, F., Ed., 1989. *The Seismic Design Handbook.* New York: Van Nostrand Reinhold, pp. 171-209.

Newman, A., February 1994. "Debating Steel-Connection Design". *Civil Engineering*, pp. 52-55.

Nilson, A. H. and G. Winter, 1991. *Design of Concrete Structures.* New York: McGraw-Hill, Inc.

Rosa, A. M., 1993. *Design, Analysis and Experimentation of a Semi-Rigid Composite Joint Using the ATLSS Shear Connection.* M.S. Thesis, Department of Civil and Environmental Engineering, Lehigh University.

Rosa, A. M., L. W. Lu and B. V. Viscomi, April 24-28, 1994. "ATLSS Connectors in Semi-Rigid Connections". *Proceedings from ASCE Structures Congress XII.* Atlanta, GA: pp. 1149-1154.

Sabnis, G. M., H. G. Harris, R. N. White and M. S. Mirza, 1983. *Structural Modeling and Experimental Techniques.* Englewood Cliffs, NJ: Prentice-Hall, Inc., Chapter 2.

Salmon, C. G. and J. E. Johnson, 1990. *Steel Structures: Design and Behavior.* New York: Harper Collins Publishers.

Slaughter, E. S. and M. Eraso, June 1995. "Dynamic Simulation Methodology to Assess Structural Steel Erection Innovations". Submitted to the *Journal of Construction Engineering and Management.*

Structural Optimization Design and Analysis Software for Structural Engineering (SODA), 1993. Version 3.2.5. Waterloo, Ontario, Canada: Waterloo Engineering Software.

Swenson, K., October 1992. "Unlocking the Inherent Stiffness of Low-Rise Buildings". *Modern Steel Construction*, pp. 24-29.

TRW Nelson Stud Welding Division, 1977. *Construction-Design Data: Nelson Embedment Properties of Headed Studs.* Elyria, Ohio, p. 6.

Uniform Building Code--1988 Edition, May 1, 1991. Whittier, CA.

Viscomi, B. V., L. W. Lu, N. D. Perreira, W. D. Michalerya and A. B. Larrabee, September 1995. "Automated Erection of Structures Utilizing ATLSS Connections and a Robotic Crane". *Microcomputers in Civil Engineering*, pp. 309-323.

Wenk, T. and J. H. Daniels, May 1977. *Composite Assemblage Experiments.* Fritz Engineering Laboratory Report No. 403.2, Bethlehem, PA.

Yarimci, E., J. A. Yura and L. W. Lu, May 1966. *Techniques for Testing Structures Permitted to Sway.* Fritz Engineering Laboratory Report No. 273.40, Bethlehem, PA.

Young, W. C., 1989. *Roark's Formulas for Stress and Strain.* New York: McGraw-Hill, Inc.

Nomenclature

A_a Effective peak acceleration
A_r Area of reinforcing bars (in^2)
A_s Area of steel cross section (in^2)
A_{sc} Cross-sectional area of stud shear connector (in^2)
A_v Effective peak velocity-related acceleration
A_w Effective area of weld (in^2)
A_1 Area of seat angle (in^2)
C_{eq} Carbon equivalence
D Dead load (ksf)
E Earthquake load
E_c Modulus of elasticity of concrete (ksi)
E_s Modulus of elasticity of steel (ksi)
F_y Yield stress of seat angle (ksi)
F_{yf} Yield stress of flange (ksi)
F_{yr} Yield stress of reinforcing bars (ksi)
F_{yw} Yield stress of web (ksi)
H Average story height (ft)
I Importance factor for wind loads
I_B Weighted moment of inertia (in^4)
I_{LBp} Lower bound moment of inertia for composite section (in^4)
I_{LBn} Negative bending moment of inertia for a steel section (in^4)
K_i Initial stiffness (k-in/mrad)
K_{sec} Secant stiffness (k-in/mrad)
L Total live load (ksf)
L_r Roof live load (ksf)
M_n Nominal flexural strength (k-in)
M_p Plastic bending moment (k-in)
M_u Required flexural strength (k-in)
M_y Initial yield bending moment (k-in)
N_b Number of bolts in a joint
P Concentrated load (k)
P_u Factored concentrated beam load (k)
P_y Yield strength (k)
PNA Plastic neutral axis
Q_n Nominal strength of one stud shear connector (k)
Q_y Cyclic test (yield) force control parameter (k)
R Nominal reaction (k)
R Maximum strength ratio
R_n Nominal resistance or strength (k)

R_s Nominal slip resistance of a bolt (k)
R_u Required strength determined from factored loads (k)
S Snow load (ksf)
S_E Elasticity scale factor
S_l Length scale factor
S_x Elastic section modulus about major axis (in^3)
V Shear force (k)
W Wind load (ksf)
Y_3 Distance from top of steel beam to centroid of reinforcing bars (in)
Z Plastic section modulus (in^3)
b_{eff} Effective width of composite slab (in)
b_f Flange width of rolled beam (in)
d Overall depth of member (in)
d_b Nominal bolt diameter (in^2)
d_c Column depth (in)
d_h Hole diameter (in)
d_z Overall panel-zone depth (in)
f'_c 28-day concrete design compressive strength (psi)
$g_{1,2,3}$ Usual gages in angle legs (in)
h_r Nominal rib height (in)
k Distance from outer face of flange to web toe of fillet (in)
l Span length (in)
l Length of weld (in)
n Number of bolts in a vertical row
r_n Nominal strength per bolt from LRFD Specification
s Bolt spacing (in)
t_f Flange thickness of rolled beam (in)
t_w Web thickness (in)
w Uniformly distributed load per unit of length (k/in)
w Fillet weld size (in)
w Unit weight of concrete (pcf)
w_r Average width of concrete rib or haunch (in)
w_z Panel zone width (in)
x Horizontal distance (in)
y Moment arm between centroid of tensile/compressive forces (in)
Δ Deflection (in)
δ Deflection (in)
δ_y Cyclic test (yield) deformation control parameter (in)
μ Coefficient of friction
μ_θ Rotational ductility ratio
ϕ_b Resistance factor for flexure
ϕ_v Resistance factor for shear
ϕ_w Resistance factor for welds

ϕR_n Design strength from LRFD Specification
ϕr_n Design strength per bolt or per inch of weld from LRFD Specification
θ Beam rotation (mrad)
θ_{max} Rotation at M_{max} (mrad)
θ_y Rotation at M_y (mrad)

Vita

Kali Elizabeth Wyncott was born in Lafayette, Indiana on April 1, 1970, to Marlaya E. (Hirsch) Wyncott and George F. Wyncott, Jr. She attended Purdue University and graduated with a B.S.C.E. in May 1993. During her undergraduate program, Kali worked as an engineering co-op with Bechtel Corporation. She began work on an M.S.C.E. at Lehigh University in August 1993 and received her degree in January 1996. After graduation she went to work as a structural engineer for S & B Engineers and Constructors, Ltd. in Houston, Texas.

END OF TITLE